LEVEL II

FURTHER ANALYSIS OF TROPICAL CYCLONE CHARACTERISTICS FROM RAWINSONDE COMPOSITING TECHNIQUES

Prepared By:

William M. Gray

Colorado State University
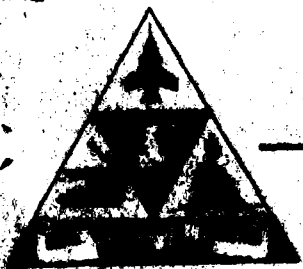Fort Collins, Colorado 80523

Contract No. N00228-78-C-2129

MARCH 1981

Prepared for:

NAVAL ENVIRONMENTAL

REPORT DOCUMENTATION PAGE		READ INSTRUCTIONS BEFORE COMPLETING FORM
1. REPORT NUMBER NAVENVPREDRSCHFAC Contractor Report No. CR 81-02	2. GOVT ACCESSION NO. AD-A102053	3. RECIPIENT'S CATALOG NUMBER
4. TITLE (and Subtitle) Further Analysis of Tropical Cyclone Characteristics from Rawinsonde Compositing Techniques.		5. TYPE OF REPORT & PERIOD COVERED Final rept.
		6. PERFORMING ORG. REPORT NUMBER
7. AUTHOR(s) William M. Gray		8. CONTRACT OR GRANT NUMBER(s) N00228-76-C-2129
9. PERFORMING ORGANIZATION NAME AND ADDRESS Colorado State University Fort Collins, Colorado 80523		10. PROGRAM ELEMENT. PROJECT. TASK AREA & WORK UNIT NUMBERS W.U. 6.2-14 PE 62759N PNSF 59-551
11. CONTROLLING OFFICE NAME AND ADDRESS Naval Air Systems Command Department of the Navy Washington, DC 20361		12. REPORT DATE March 1981
		13. NUMBER OF PAGES 132
14. MONITORING AGENCY NAME & ADDRESS(if different from Controlling Office) Naval Environmental Prediction Research Fac. Monterey, CA 93940		15. SECURITY CLASS. (of this report) UNCLASSIFIED
		15a. DECLASSIFICATION DOWNGRADING SCHEDULE

16. DISTRIBUTION STATEMENT (of this Report)

Approved for public release; distribution unlimited.

CR 81-02

17. DISTRIBUTION STATEMENT (of the abstract entered in Block 20, if different from Report)

19. KEY WORDS (Continue on reverse side if necessary and identify by block number)
Tropical Cyclones
Typhoons
Hurricanes
Data Compositing
Tropical Cyclone Observational Studies

20. ABSTRACT (Continue on reverse side if necessary and identify by block number)
Up-to-date results of recent tropical cyclone research at Colorado State
University are presented. Particular attention is paid to new findings
which impact on tropical cyclone analysis and forecasting efforts. Obser-
vational studies using large amounts of composited rawinsonde, satellite,
and aircraft flight data have been performed to analyze tropical cyclone
formation, diurnal variability of tropical cyclones, tropical cyclone
intensity change, statistical validity of rawinsonde compositing philosophy,
and tropical cyclone looping motion.

DD FORM 1473 EDITION OF 1 NOV 65 IS OBSOLETE
S N 0102-014-6601

TABLE OF CONTENTS

ACKNOWLEDGEMENTS

1. INTRODUCTION

Over the last decade the author's research project has undertaken a comprehensive study of the origins and characteristics of tropical cyclones. Many of these results are believed to be relevant to the U.S. Navy for forecasting and numerical simulations of these storms, and this report is issued to disseminate this information. This is the fourth report on this subject. Previous reports by Gray and Frank (1977, 1978) and Gray (1979) give additional information. This research includes composite studies of large amounts of rawinsonde and satellite data.

Section 2 presents information on tropical cyclone development. Section 3 discusses tropical cyclone diurnal variability. Section 4 gives new information on the intensity change of tropical cyclones. Section 5 gives information on new statistical analysis supporting the validity of the rawinsonde composite methodology. Section 6 gives information on tropical cyclone looping motion. Other tropical cyclone information is also presented and discussed.

More detailed information is contained in the Colorado State University Department of Atmospheric Science tropical cyclone project reports of Gray, 1975a, 1975b; George, 1975; Frank, 1976; Zehr, 1976; S. Erickson, 1977; Arnold, 1977; and other papers by Frank, 1977a, b, c; Gray, 1975a, b; Gray, 1977a, b, c; Núñez and Gray, 1977; McBride and Gray, 1978; Gray, 1979; McBride, 1979; and Chan, Gray and Kidder, 1979; and Núñez, 1981.

2. TROPICAL CYCLONE FORMATION

At locations and in seasons in which tropical cyclone genesis regularly occurs, such as around Guam during the summer, seasonal climatological factors such as depth of warm water, θ_e gradient in lower troposphere, middle-level humidity, etc. are always positive and large. Consideration must be given to the day to day variations of dynamic factors. Hundreds of individual case data sets of developing and non-developing disturbances in the western Pacific and western Atlantic have been assembled at Colorado State University (CSU) to try to better understand the day by day factors which are associated with tropical cyclone genesis. These new data sets have been extensively analyzed by the rawinsonde data compositing techniques that have been developed at CSU and discussed in reports of Gray (1967), Zehr (1976), Erickson (1977), Arnold (1977), McBride (1979) and Núñez (1981). The papers by McBride and Núñez have reviews of our most recent observational results on tropical cyclone genesis.

To understand cyclone genesis one must be able to explain not just the processes which bring about cyclone genesis, but also the conditions which, in the majority of cases, inhibit genesis. Non-genesis cloud cluster disturbances have also been extensively studied.

Analysis of the moisture, vertical stability, and cloud fields between the developing and non-developing cloud cluster systems in both the west Pacific and the west Atlantic do not show significant differences between the composite fields. Major differences occur only in the surrounding environmental tangential wind fields and the tropospheric vertical wind shears. Vertical cross-sections of the tangential wind of developing (D1, D2) and non-developing cloud cluster systems (N1, N2)
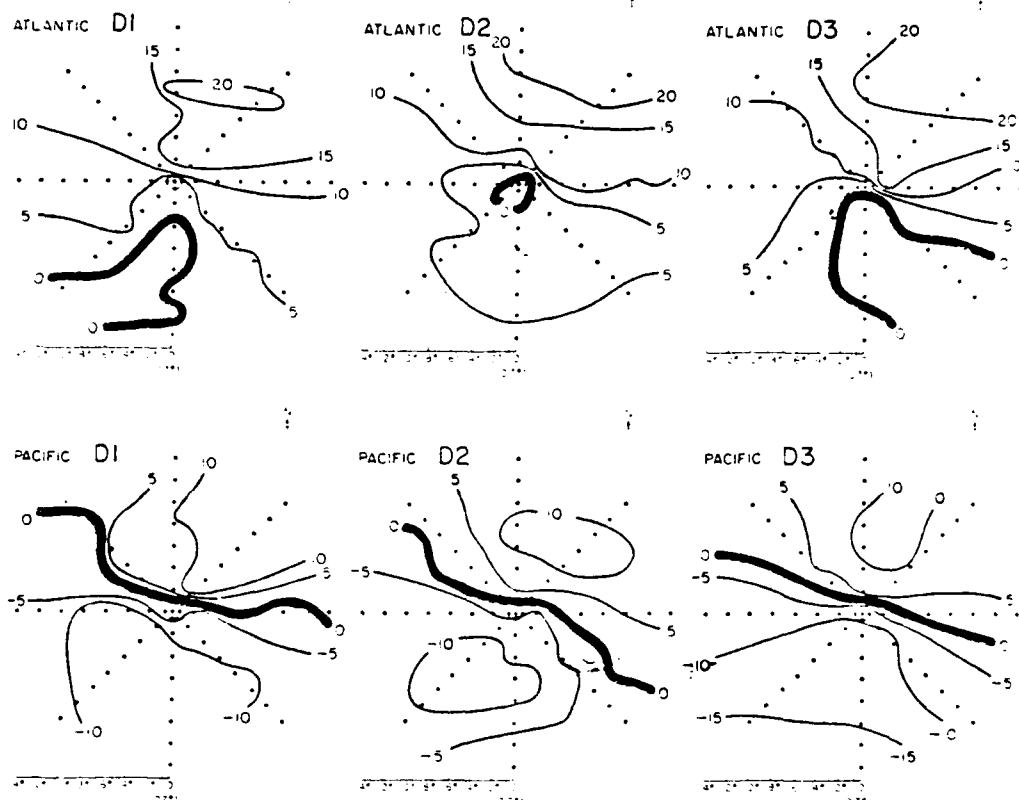
Fig. 3. Plan views of zonal shear, $U_{200\ mb} - U_{900\ mb}$ $(m\ s^{-1})$ for the Atlantic (top diagram) and Pacific (bottom diagram) developing disturbances (from McBride, 1979).

genesis. The above data shows that there is a requirement not only for very small vertical wind shear near the system center but also for two adjoining regions of strong 200-900 mb vertical shear of opposite sign on either side of the developing system. It is necessary that most of this vertical wind shear be in the upper troposphere, however. Such requirements are met when a strong anticyclone is located over a low level disturbance.

The vertical shear pattern for the developing systems is a function of both the upper level and the lower level flow and extends over a large region of the tropics, often as far as 10° latitude distance from the center of the system. These ideas correspond well to the results of
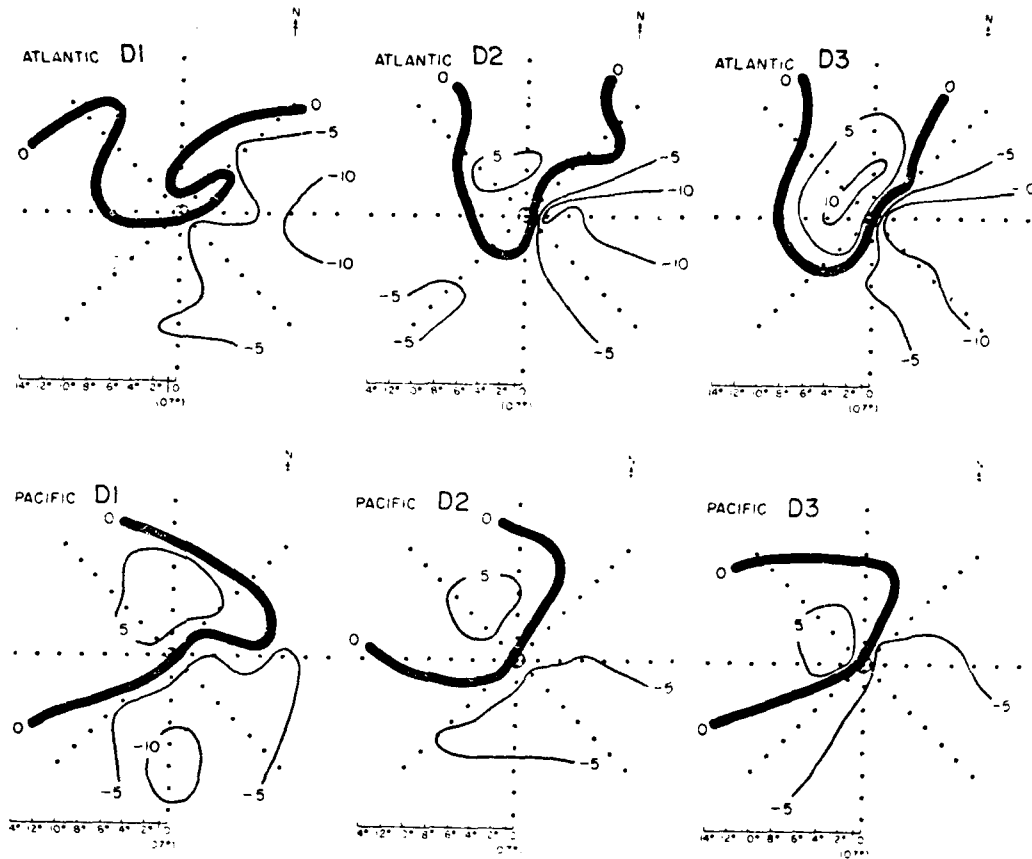
Fig. 4. Plan views of meridional shear, $V_{200\ mb} - V_{900\ mb}$ $(m\ s^{-1})$ for the Atlantic (top figure) and the Pacific (bottom figure) data sets (from McBride, 1979).

a number of previous researchers who have emphasized the requirement for a superposition of favorable upper level and lower level large scale flow features prior to disturbance intensification (Riehl, 1954; Yanai, 1961, 1968; Sadler, 1967, 1976a, 1976b).

More specifically, V. Dvorak (1975) states that development will not take place underneath a unidirectional upper tropospheric flow pattern. Such a flow pattern is inconsistent with a large north-south gradient of $\partial U/\partial p$. Dvorak (personal communication) also states that development in the Atlantic is inhibited by upper level northerly flow
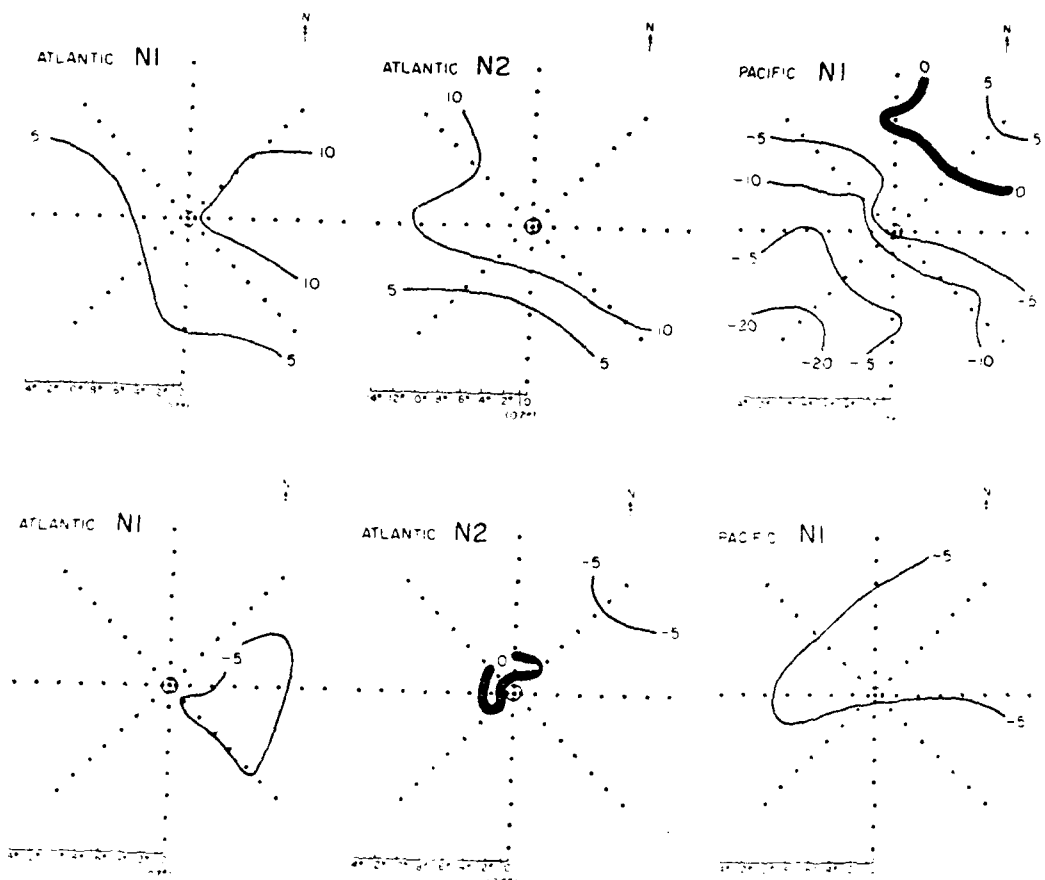
Fig. 5. Plan views of zonal $U_{200 mb} - U_{900 mb}$ wind shear (top figures) and meridional shear $V_{200 mb} - V_{900 mb}$ wind shear (bottom figures) for different non-developing west Atlantic tropical cloud clusters and easterly waves. Units: m s^{-1} (from McBride, 1979).

to the west of a disturbance. This is consistent with the requirement

for a large value of $\partial/\partial x(\partial V/\partial p)$ shear.

McBride (1979) has shown that at 6° radius 900 mb minus 200 mb vorticity

differences are about three times greater for the developing systems than

for the non-developing systems (see Table 1). Thus, in the beginning

or cluster stage of development, there is already quite a large amount of

positive relative vorticity which extends over such a large scale that

its origin must be external to the cluster or incipient cyclone system

SOUTH PACIFIC
VERTICAL SHEAR OF ZONAL WIND
$(U_{200mb} - U_{850mb})$ Knots
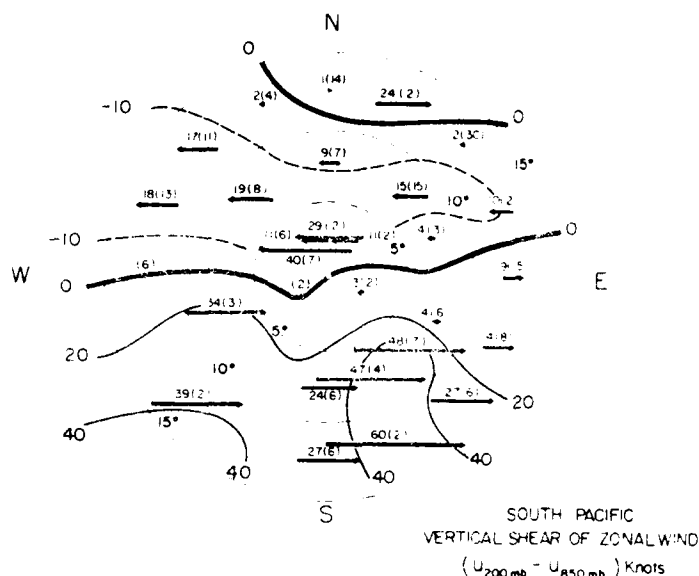
Fig. 6.   Composite zonal vertical wind shear for average rawin informa-
tion in each area relative to the center of 84 tropical dis-
turbances in the South Pacific which later developed into
tropical storms.   Length of arrows proportional to wind shear
in knots (at left).   Values in parentheses are number of wind
reports in each area average.   Distance from the center is
given by the lightly dashed circular lines at 5° latitude incre-
ments (from Gray, 1968).

N INDIAN OCEAN
VERTICAL SHEAR OF ZONAL WIND
$(U_{200mb} - U_{850mb})$ - Knots
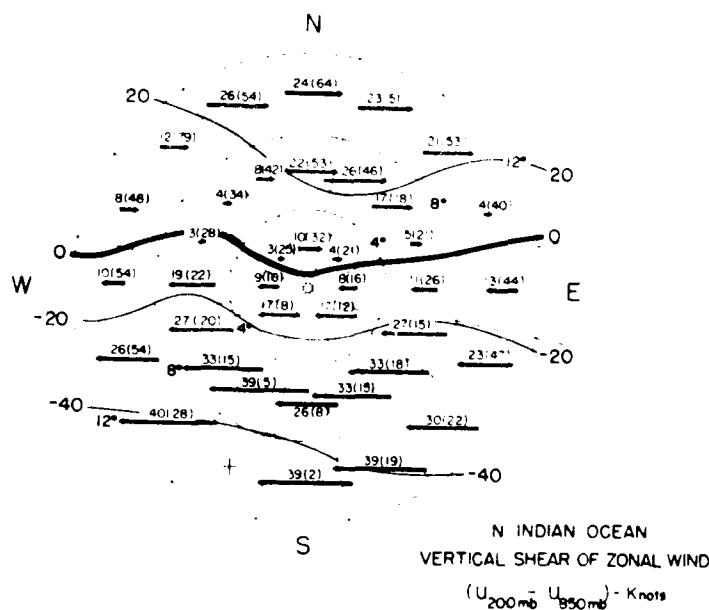
Fig. 7.   Same as Fig. 6 but for 54 tropical disturbances in the North
Indian Ocean which later developed into tropical storms (Gray,
1968).

and likely dependent on the characteristics of the tropical ITCZ and the middle latitude westerly wind belts of both hemispheres. The establishment of these favorable middle latitude conditions which allow for a favorable cyclone genesis environment is not very frequent. When these conditions occur a multiple of cyclones often form.

Cyclone genesis may be viewed in terms of a vertical gradient of vorticity: a large north-south gradient of $-\partial U/\partial p$ in combination with a large east-west gradient of $\partial V/\partial p$.

$$= \frac{\partial}{\partial y}\left(-\frac{\partial U}{\partial p}\right) + \frac{\partial}{\partial x}\left(\frac{\partial V}{\partial p}\right)$$

$$= \frac{\partial}{\partial p}\left(-\frac{\partial U}{\partial y} + \frac{\partial V}{\partial x}\right) = \frac{\partial \zeta_r}{\partial p}, \text{ or } \zeta_{r_{900mb}} - \zeta_{r_{200 mb}}$$

TABLE 1

Mean relative vorticity differences between 900 and 200 mb for the average of developing and non-developing data sets $(10^{-5}s^{-1})$ (from McBride, 1979).

	$0-2°$	$0-4°$	$0-6°$
Average NON-DEVELOPING (Pacific N1; Atlantic N1, N2, N3)	2.3	1.1	0.7
Average DEVELOPING weak systems (D1, D2)	5.2	3.1	2.0

2.1 The Concept of Condensation Warming

Our conceptual view of the basic causes of the hurricane are inexorably tied up in the condensation energy release process associated with cumulus convection. A rainfall of 1 cm can produce an energy equivalent of about $2.5°C$ mean troposphere temperature increase. Hurricanes have large positive interior temperature anomalies. These temperature anomalies seem to occur where condensation energy release is large. The general view has been that condensation from inward advection of water vapor brings about tropospheric temperature increase, surface pressure fall, and strong winds through a wind to pressure adjustment. This view has implied that temperature and pressure changes occur first and wind responds to them. Figure 8 is a typical example of this type of "in-up-out" hurricane circulation which has been viewed as typical. Inflowing water vapor condenses and acts to warm the interior of the storm system and lower the interior pressure. The wind increases in response to the pressure drop.

This generally held conceptual view of the basic process of the hurricane is not so well supported by the observations. Although condensation energy release is a fundamental ingredient of the hurricane, its existence in large amounts does not necessarily insure the hurricane's formation or maintenance.

In general, cloud cluster cumulus convection brings about no significant net tropospheric temperature change at the time and place it occurs. Rain area upper tropospheric temperature increase is typically balanced by a lower tropospheric temperature decrease. Almost no tropospheric warming occurs. The wind response to such lower and upper tropospheric temperature change is to bring about vertical motion change which act to wipe the temperature change away - see Fig. 9.
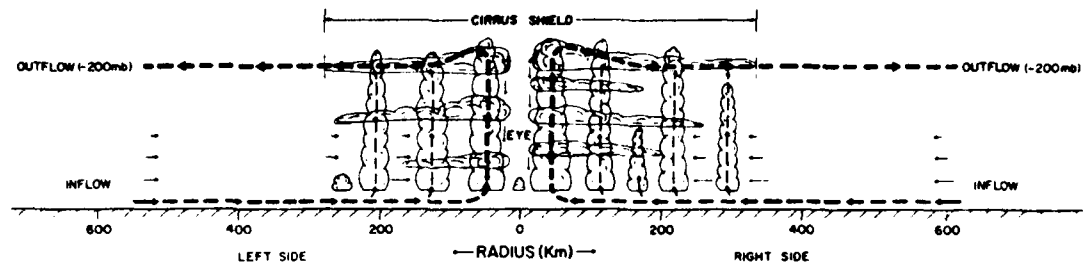
Fig. 8.   Idealized view of the hurricanes mean radial circulation which is just "in-up-out" without vertical mass recycling.
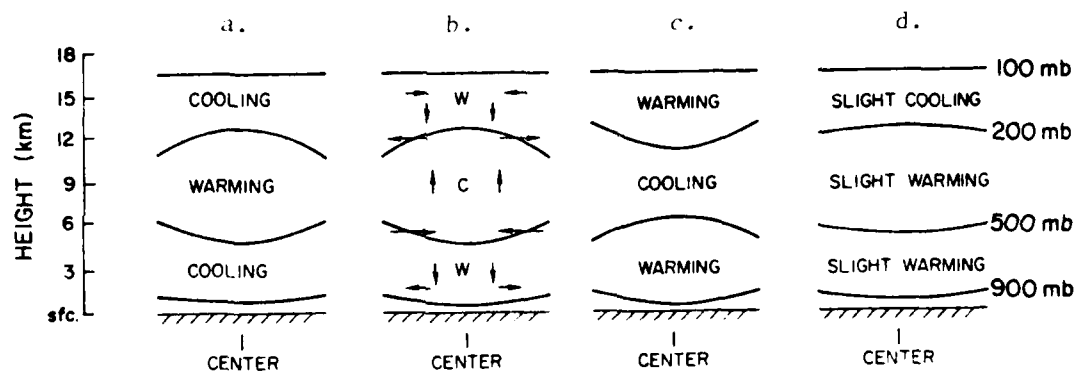
Fig. 9.   Idealized vertical cross-section portrayal of how the atmosphere will respond to direct meso-scale cloud cluster warming (in diagram a) to induce a vertical motion response (diagram b) which cause an opposite warming influence (diagram c) that acts to nearly cancel the original cloud cluster warming (diagram d).

Warming as a Pressure to Wind Adjustment Process.   Recent CSU studies of wind-pressure adjustment by W. Schubert and his group and W. Fingerhut indicate that at tropical locations where f and $\not{\chi}_{r}$ are small that the mass field will adjust to the wind and not vice-versa for scales smaller than the Rossby radius of deformation.   Temperature increase on the meso or smaller-scale occurs only when the mass field sinks and

warms in adjustment response to a stronger momentum field. Thus, in

a general sense, the influence of cloud convection on meso-scale tem-

perature increase appears to be primarily that of the convective cloud's

role in altering the momentum field and a consequence mass adjustment

to such altered momentum fields. The degree of momentum field altera-

tion by convection depends upon the momentum field itself and its

latitude.

Vertical Mass Recycling. In the last 10-12 years a general belief

has begun to emerge among a number of tropical meteorologists that there

exists in tropical cloud clusters and hurricanes (except in the inner

core region, $r < 1^\circ$) a substantially greater amount of mass going up-

and-down within the system than that specified by the mean vertical

circulation. The hurricane circulation is not just "in-up-out" as

has been generally envisaged (and as portrayed in Fig. 8) but rather is

more typical of an "in, down-up, down-up, down-up, out" transverse cir-

culation. Recycling is largest at cloud base and decreases to zero in

the upper troposphere (see Fig. 10). This means that a high degree of

vertical exchange of energy, moisture, and momentum can occur in the

lower two-thirds of the troposphere. Such vertical recycling mass

exchange is indespensable for:

1) the maintenance of the hurricane's convection. Cloud models
   show that for the typical lapse rate of these tropical systems
   Cb convection requires large boundary layer downdraft mass
   forcing,

2) raising evaporated vapor out of the planetary boundary layer,

3) allowing the greater tapping of the ocean energy source through
   downdraft drying and cooling of the boundary layer. This
   allows the maintenance of the transverse circulation against
   its normal energy loss (as discussed later),

4) maintaining the sensible temperature of the hurricane's bound-
   ary layer inflow at close-in radii against expansion cooling.
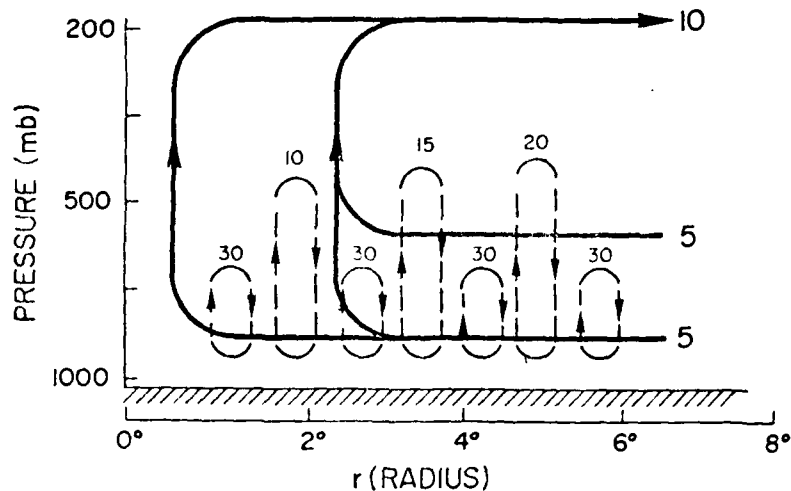
Fig. 10. Idealized x-section view of the hurricane's mean radial
circulation with superimposed mass recycling. Units are
arbitrary and represent mass transport.

This is to a substantial degree accomplished by expansion
warming of downdraft circulations. A number of models are now
producing this effect and

5) balance hurricane circulation against radiational cooling.

Thus, the hurricane's transverse circulation is not just an "in-up-out"

circulation but rather an in-up-out circulation with a great deal of

extra superimposed vertical mass circulation. It is rather an "in-down-

up, down-up, down-up, out" circulation.

Convection Induced Temperature Change in the Vertical. Nearly all

tropical cloud cluster systems develop 500-200 mb positive temperature

anomaly and small negative temperature anomalies at 900 to 500 mb and

200-100 mb levels. These temperature anomalies are a consequence of

the large amounts of upward-and-downward vertical mass recycling which is

occurring in the tropical weather system and the consequent buoyancy

requirements to maintain such vertical mass recycling. Downdraft

evaporation leads to cooling at lower levels and overshoot Cb tops lead

to cooling above 200 ___. The correlation of vertical motion (w') with ___ ___ure anomaly ___ is such that significant upward-and-downward ___ ___ of sensible temperature (w'T') results. The vertical gradient ___ ___ transport $(-\partial \overline{w'T'}/\partial z)$ and the resulting temperature changes ___ tropical disturbance cumulus convection directly induce upon the ___ ___ is thus one of surface-500 mb cooling, 500-200 mb warming, ___ 200-100 mb cooling. How such temperature changes occur is idealized in Fig. 11.

A continuation and progressive accumulation of such convectively induced sensible temperature changes (as shown is the left diagram of ___ 12) can never by itself bring about the observed low level temperature gains and progressive low level wind maximum increases which occur with tropical cyclone genesis and intensification. The progressive upper level positive temperature anomaly going from 1 to 3 and low level negative temperature anomaly of convectively induced temperature change lead to middle level wind maxima and only weak surface winds (as the left diagram of Fig. 13 indicates). Such wind regimes are not conducive to low level frictionally driven inflow and vortex spin-up and lower tropospheric positive temperature anomaly will not occur.

There must be other physical processes operating within the tropical disturbance which act to oppose these convectively induced temperature changes and vertically redistribute the temperature anomalies. These other physical processes are indicated by the center diagrams of Figs. 12 and 13.

It is hypothesized that the vertical momentum rearrangement by cumulus convection and its associated mass recycling can act as a mechanism to oppose and redistribute cumulus heating in the vertical
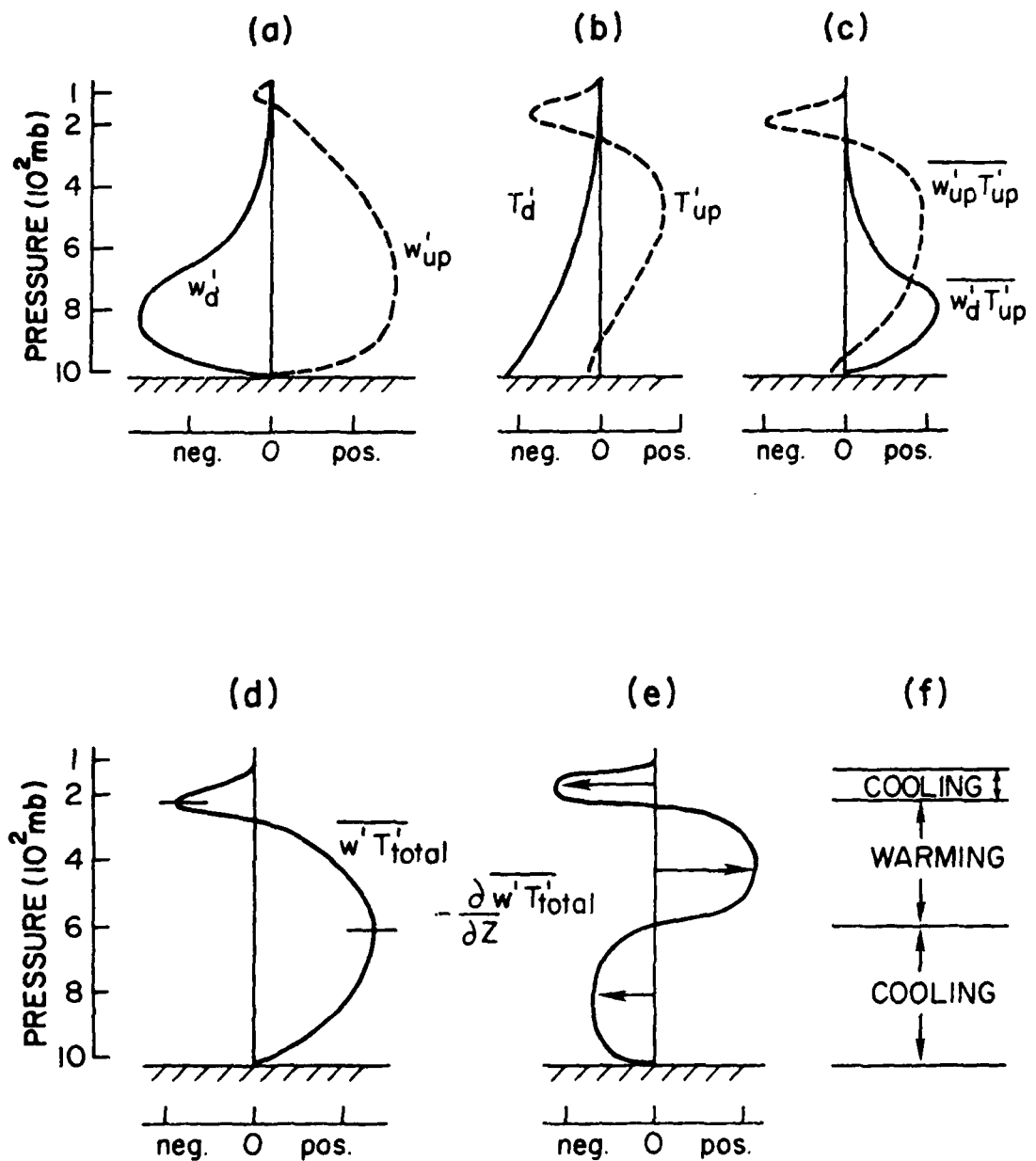
Fig. 11. Vertical cross-section portrayal of the typical up-and-
downdraft vertical motion occurring in the usual strong tro-
pical cloud cluster (diagram a) and the needed temperature
anomaly (diagram b) within such vertical up-and-downdraft
motion for buoyancy. The resulting w'T' correlations (dia-
grams c and d) within the up-and-downdrafts which lead to a
lower tropospheric cooling and upper tropospheric warming are
shown in diagrams (e) and (f).

(a) CUMULUS INDUCED DIRECT TEMP. CHANGE
(b) TEMPERATURE CHANGE FROM CUMULUS REARRANGMENT
(c) NET CUMULUS INDUCED TEMP. CHANGE

TEMPERATURE DEVIATION
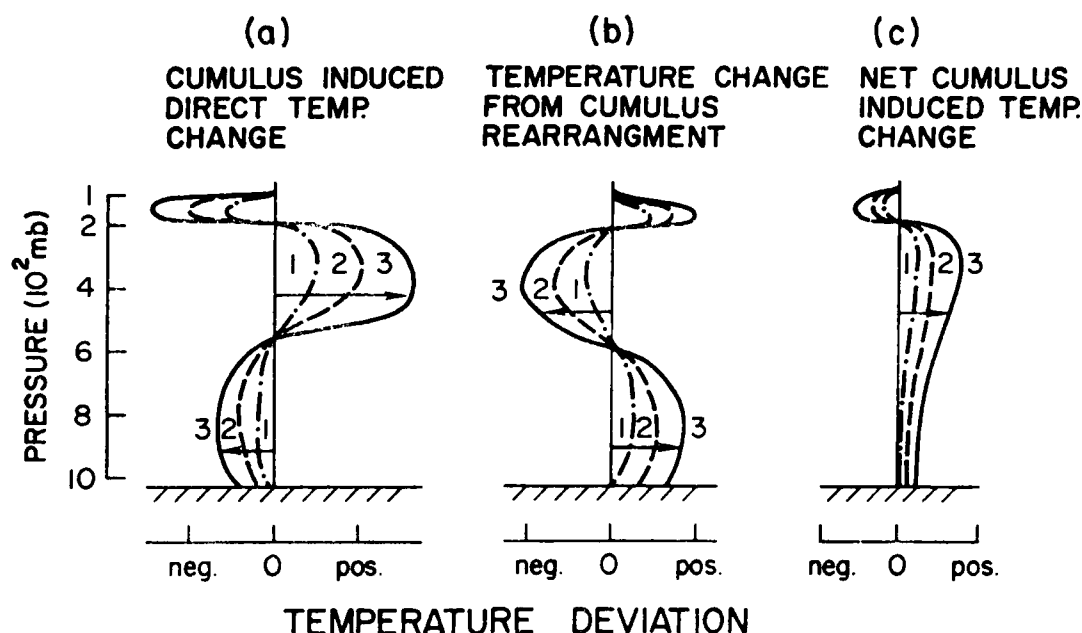
Fig. 12. Idealized portrayal of the vertical x-section of progressive temperature anomaly (T') with time to be expected for direct cumulus warming (diagram a) and the needed progressive temperature anomaly which is required from cumulus rearrangement of horizontal momentum (diagram b) such that the net temperature anomaly pattern at the right (required for cyclone development) can result.

to bring about the required surface to 500 mb positive temperature anomaly. This is indicated by the right diagram of Fig. 13. But such momentum rearrangement influences will occur only in proportion to the disturbance's already existing 2-8° radius surrounding vertical wind shear. If such vertical wind shears are large, as occurs when the lower (900 mb) minus upper level (200 mb) tangential wind differences are large, then the influence of cumulus horizontal momentum rearrangement influences will be large. The progressive vertical temperature and tangential wind profiles - indicated in the right diagram of Figs. 12 and 13 (which are required for cyclone development) can then result. If such vertical wind shears are small, as is normally the

PROGRESSIVE ALTERATIONS OF
TANGENTIAL WIND

FROM CUMULUS   FROM CUMULUS   <u>NET</u> INFLUENCE
DIRECT TEMP.   MOMENTUM
CHANGE   REARRANGEMENT
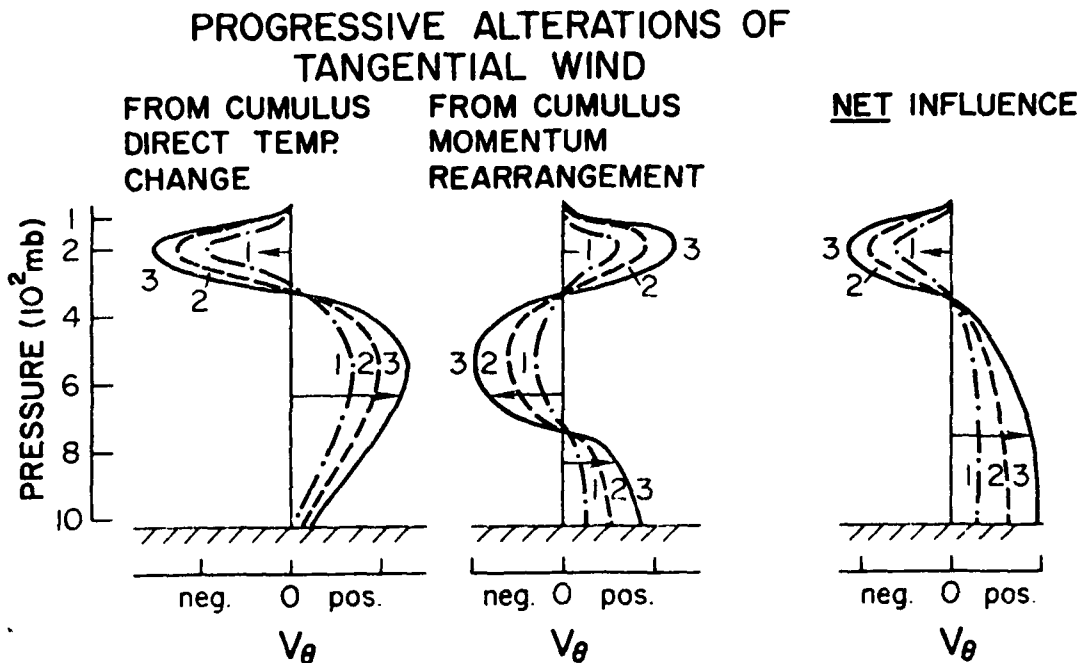
Fig. 13. Idealized portrayal of the vertical x-section of progressive
tangential wind (V_θ) variation with time to be expected for
wind-pressure balance associated with the progressive tempera-
ture anomalies of Fig. 12. Low level cooling leads to max-
imum winds at middle levels (diagram on left), progressive
cumulus momentum rearrangement leads to the V_θ profile of the
middle diagram, and the net influence of both to the profile
on the right - that needed for cyclone development.

case with most tropical disturbances, then the vertical recycling momen-
tum rearrangement influences will be too small to offset the direct
convective condensation temperature changes and lower tropospheric posi-
tive temperature anomaly will not occur. Núñez (1981) has solved for
this type of momentum rearrangement by cumulus. An idealized model of
such horizontal wind changes is portrayed in Fig. 14.

The direct association of strong surrounding disturbance vertical
wind shear and tropical cyclone genesis thus appears to be linked through
the feed-back mechanism of the convectively induced vertical momentum
rearrangement.
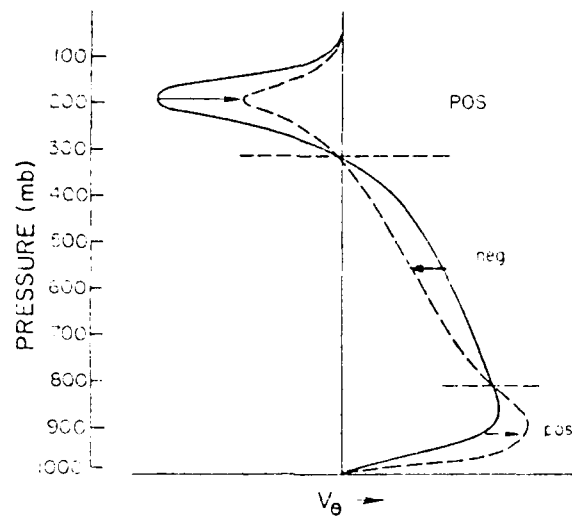
Fig. 14. Idealized portrayal of how horizontal momentum rearrangement within Cb cloud lines may act to bring about a change in the tangential wind (V_θ) from the solid to the dashed line. This alteration increases the wind shear in the 900-500 mb layer but decreases the wind shear at layers above 500 mb.

2.2 Tropical Disturbance Energy Budget

Moist-static (or total) energy (h) can increase or decrease in the tropical pre-cyclone disturbance through transfer from the sea by latent and sensible exchange (E_o), by radiation (R), or through horizontal transports on the boundaries ($\nabla \cdot \mathbf{V}h$). This energy balance may be expressed as:

$$\frac{\partial h}{\partial t} = (E_o + R) - (\nabla \cdot \mathbf{V}h) \tag{1}$$

where $h = gz + C_p T + Lq$.

Each term has been integrated through the depth of the troposphere. Calculations of the $\nabla \cdot \mathbf{V}h$ term and estimates of R for western ocean tropical systems indicate that there is horizontal advection of energy out of these systems ($\nabla \cdot \mathbf{V}h$ is positive) and $E_o + R$ is positive. Western ocean summertime sea surface energy flux is usually larger

than tropospheric radiational cooling. Steady state conditions
($\partial h/\partial t = 0$) are accomplished only through a higher radial export of
energy in the upper level outflow than that imported at lower levels.
An idealized h-budget for the summertime pre-cyclone disturbance
(diagram a) and the hurricane (diagram b) is shown in Fig. 15.
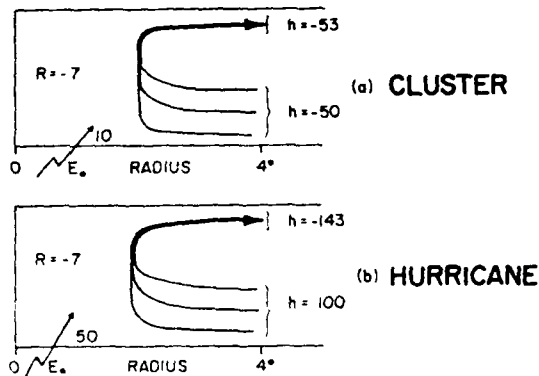
Fig. 15. Schematic representation of the typical h budget within 4°
radius of the steady-state cloud cluster, (a), and of the
steady-state hurricane, (b). Units are arbitrary. R = net
tropospheric radiation, E_o = surface energy flux, and h is
moist-static energy.

It is seen that the usual vertical circulation through the organ-
ized tropical weather system or cyclone typically produce an energy
depletion of the system. The tropical system maintains itself only
through energy received from the ocean.

Cumulus parameterization schemes which show energy accumulation
depending on the magnitude of the mean upward circulation alone are not
valid. Energy received from the low-level inflow goes to enhance deep
Cb convection. These Cb clouds rise to great heights and induce out-
flow at levels ($\sim$12-14 km) where h is larger than that of the inflow

air. Therefore, the transverse circulation of the tropical disturbance
and cyclone is typically acting to decrease the energy of the system as
Fig. 16 shows.

Thus, the paradox of the hurricane's radial circulation. The in-
up-out mean radial circulation needed in a mechanical sense to spin-up
the vortex also acts in an opposite sense to export net energy from
the vortex and weaken it. This paradox has also been noted and dis-
cussed by Pearce (1981). Hurricane development and maintenance from
the energy point of view requires that the storm's surface energy flux
(E_o) be as large as the energy loss of the storm through its radial
circulation and radiational loss. Thus, the temperature change in the
tropical cyclone may be represented as:

$$\frac{\partial T}{\partial t} = -\mathbf{V} \cdot \nabla T + \begin{pmatrix} \text{All Vertical} \\ \text{Motion Processes} \end{pmatrix} + R \tag{2}$$

$-\mathbf{V} \cdot \nabla T$ is horizontal advection which is very small and can be neglected,
R is radiation. This equation may also be written as:

$$\frac{\partial T}{\partial t} = Q_{TOTAL} + \omega(\Gamma_d - \Gamma_a) + R \tag{3}$$

where Q_{TOTAL} represents the diabatic energy gains to the system, ω is
vertical p-velocity, and Γ_d and Γ_a are the dry and actual lapse rates.

Q_{TOTAL} may be transformed as:
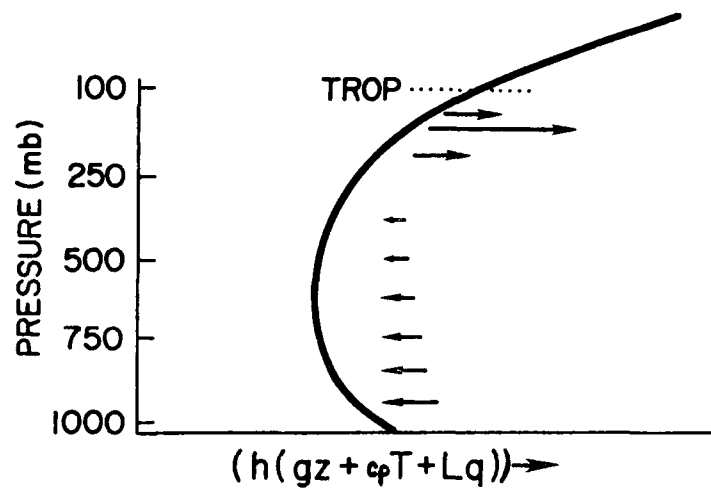
Fig. 16. Moist-static energy (h) curve of western ocean tropical weather systems and how the storm outflow occurs at a higher value of h than the inflow.
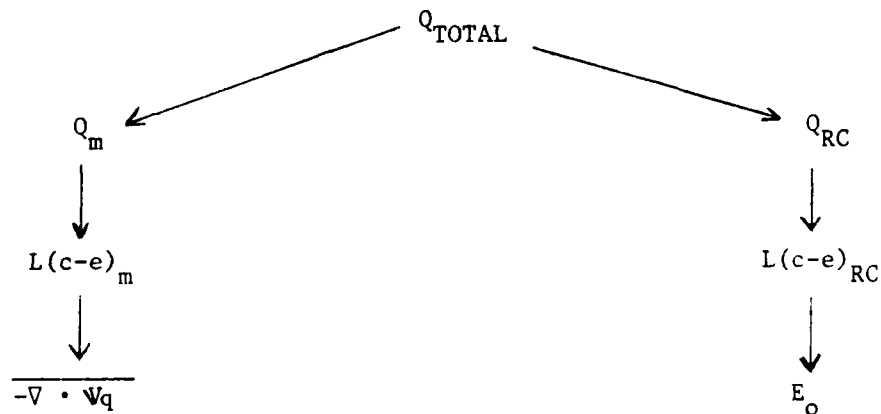
where Q_m and Q_{RC} are the diabatic energy sources from the mean radial circulation and the up-moist and down-dry vertical mass recycling (RC) circulation. This diabatic energy source comes from net condensation (c) minus evaporation (e) energy release or $L(c-e)_m$ and $L(c-e)_{RC}$. $L(c-e)_m$ and $L(c-e)_{RC}$ can be equated with mean inward horizontal moisture advection and surface energy flux, respectively.

Equation (3) then reduces to:

$$\frac{\partial T}{\partial t} = E_o + [-\nabla \cdot \psi q + \bar{\omega} (\Gamma_d - \Gamma_a)] + R \qquad (4)$$

$$\text{(a)} \qquad \qquad \text{(b)} \qquad \qquad \text{(c)}$$

Terms (b) and (c) are negative. Temperature increase can occur only if:

$$E_o \geq [-\cdot \psi q + \bar{\omega}(\Gamma_d - \Gamma_a)] + R \qquad (5)$$

As radiation does not vary much in time, hurricane development requires that the rate of change of $\nabla \cdot \psi h$ or radial circulation be no larger than the rate of change of surface energy flux or

$$\partial E_o / \partial t \geq \partial \nabla \cdot \psi h / \partial t.$$

Systems which do not extract enough energy from the ocean must weaken. The rapidly weakening of cyclones as they come ashore and lose most of their surface energy source is well known.

What processes act to enhance the extraction of energy from the ocean? The most important process is vertical mass recycling. The more the storm's boundary layer can be ventilated from above by down-draft air which is dryer, stronger in velocity, and colder than the average boundary layer air the larger will be the surface to air energy flux. The larger the mean mass circulation through the storm system, the larger will be its momentum spin-up and intensity increase. Boundary layer energy flux is especially favored with Cb line and squall convection typical of outer rainband cloudiness (as in Fig. 17). Such cloudiness requires the existence of large upper tropospheric vertical wind shear. Rainband air penetrates the storm's boundary layer at high wind speeds and low moisture contents. Wind velocities (V_o) and ocean-air moisture differences $(q_s - q)$ at 10m are substantially raised. This

results in an exponential increase in the bulk aerodynamic formula for evaporation $[E = \rho\ C_E\ V_o\ (q_s - q)]$. Figure 18 shows how line convective downdraft action can enhance boundary layer winds and drying. Such squall-line convection which brings about a larger than normal extraction of energy from the ocean is dependent upon favorable tropospheric vertical wind shears between 900 mb and 200 mb. It is interesting to note that cloud clusters which develop into tropical storms typically have substantially larger 900 to 200 mb vertical wind shears at radii of 2-8° than cloud clusters which do not develop into cyclones. Without sizable up-and-downdraft vertical mass recycling, a tropical weather system's boundary layer is typically not ventilated enough to permit sufficient energy extraction for maintenance of the storm's energy depleting radial circulation.

The very crucial role of the boundary layer in providing enough energy flux to maintain the storm's radial circulation has not, in general, been fully appreciated!

The type of cyclone development, the author envisages, is portrayed in Fig. 19. Required prerequisite genesis conditions are given at the top. These include strong vertical wind shear around the cluster which allow Cb rainbands to form and enhance surface to air energy flux, such that the condition of the right is always valid ($E_o \geq \overline{\nabla \cdot\ Vh} - R$). If this is accomplished, then the spin-up portrayal in loop C can recycle many times and cause momentum spin-up and development of the system.

2.3 Evidence for Outer Radii Convection, Cloud Lines, and Cumulus Rearrangement of Horizontal Momentum

Satellite pictures of pre-cyclone disturbances often reveal significant amounts of line convection at outer radii as indicated in Fig. 20.
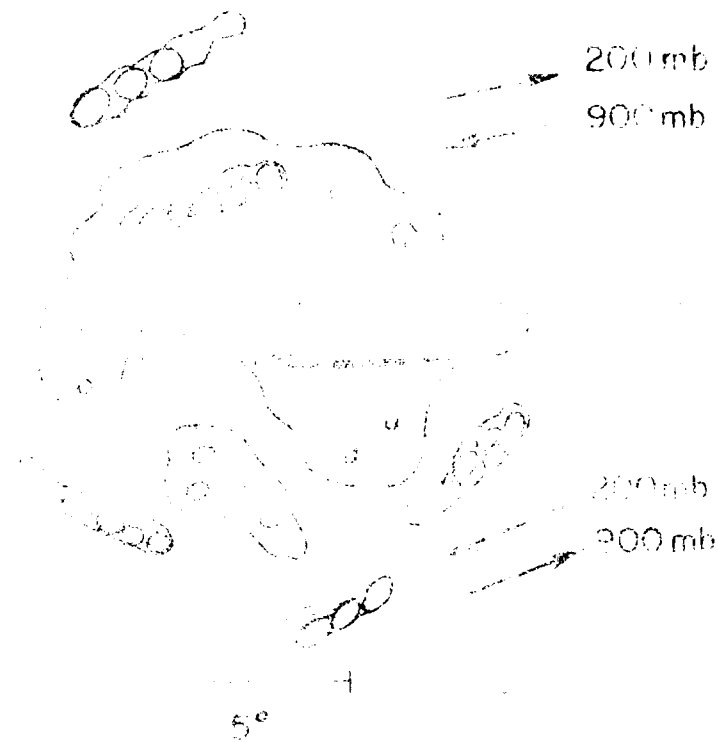
200 mb

900 mb

200 mb

900 mb

5°

Fig. 18. Idealized vertical cross-section of downdrafts from line
convection which brings high momentum and dry air into the
boundary layer. This enhances ocean energy extraction.

INITIAL CONDITIONS

6° RADIUS
900 mb POS. V_θ
200 mb NEG. V_θ
$\therefore$ LARGE $\dfrac{\partial V_\theta}{\partial p}$

CLOUD CLUSTER
SIGNIFICANT
VERTICAL MASS
RECYCLING
$\therefore$ SIZABLE E_o

LINE CONVECTION
LARGE VENTILATION
OF B.L.
$\dfrac{\partial E_o}{\partial t} > \dfrac{\partial V_\theta}{\partial t}$

DEEP LAYER
INFLOW
UPPER LAYER
OUTFLOW

IF →

$\dfrac{\partial V_\theta}{\partial t}$ POS. IN
LOW LEVELS
NEG. ALOFT

IF →

C

$E_o \geq \overline{\nabla \cdot \nabla h} - R$

P. AND TEMP.
ADJUST TO
V_θ CHANGES

IF →
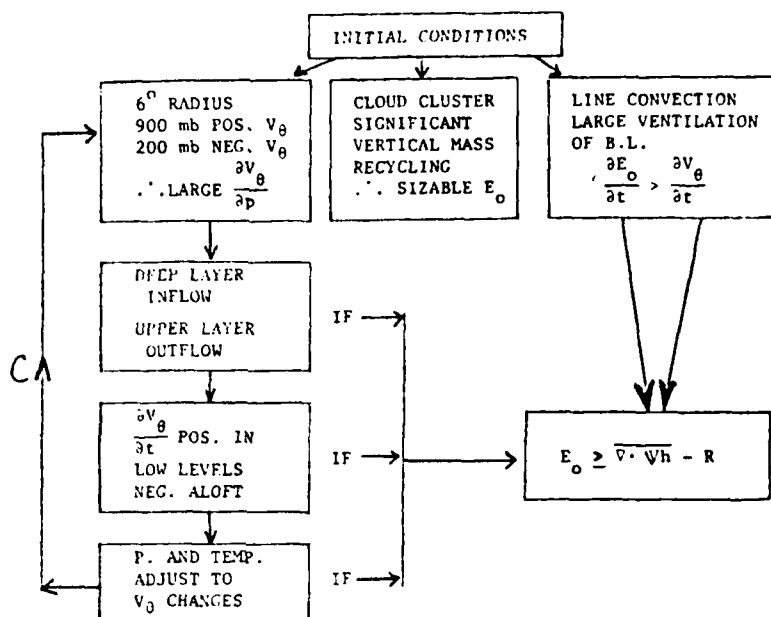
Fig. 19. Idealized portrayal of how hurricane development can occur
from the mean radial in-up-out circulation (left loop C) pro-
vided favorable initial conditions are present and sea to air
energy exchange E_o remains greater than h-budget and radia-
tion energy loss as indicated on the right portion of the
figure.

Figures 21-23 portray radar picture composites of the convective

patterns of three west Atlantic tropical systems of different intensity.

Note how the convection, much of it of Cb intensity, tends to organize

itself into cloud lines. These cloud lines tend to arrange themselves

parallel with the tropospheric vertical wind shear and produce, through

their downdraft action, an enhancement of boundary layer ventilation and

energy extraction from the ocean.

Figure 24 gives a composite of the vertical zonal profiles before

and after the passage of 4 line type convective storms which passed

through Venezuela during the summer of 1972. Note how the convective

storms tended to increase the low level (surface-700 mb) zonal wind

but decrease the wind above 700 mb. These wind differences are very
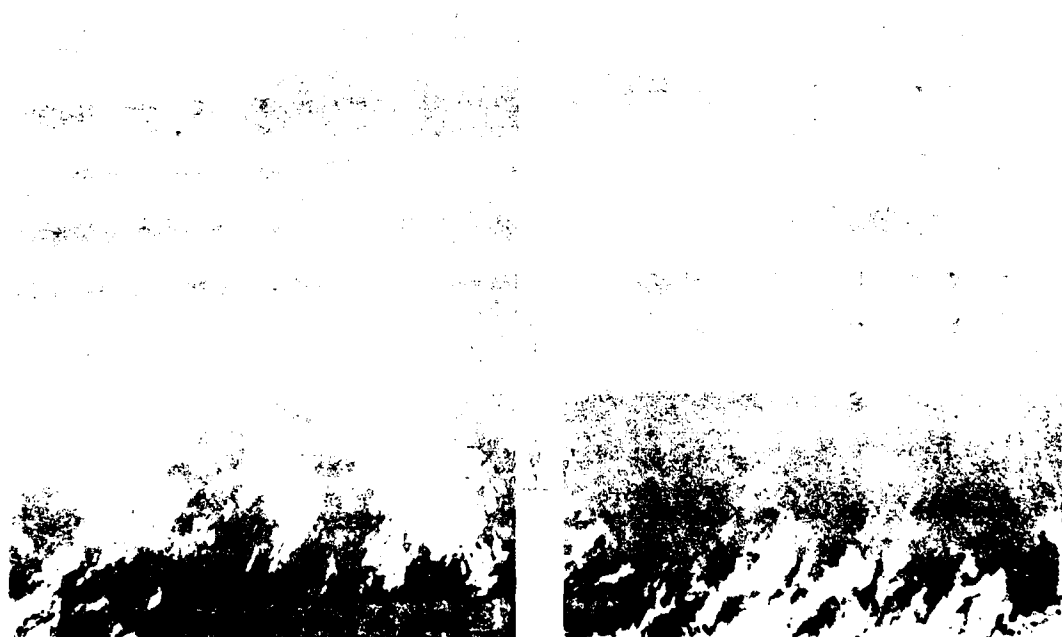
Fig. 20. DMSP satellite visual (left) and infrared, shading reversed (right) of three western North Pacific pre-typhoon cloud clusters in early stage development. Maximum sustained winds are less than 10 m/s. The circle indicates where the center of the forming circulation is. Note the surrounding outer cloud bands (from Arnold, 1977).

CLOUD RADAR COMPOSITE
14 AUG. 1961 (1340-2300 GMT)
FLIGHT ALTITUDE 1,700 FT.
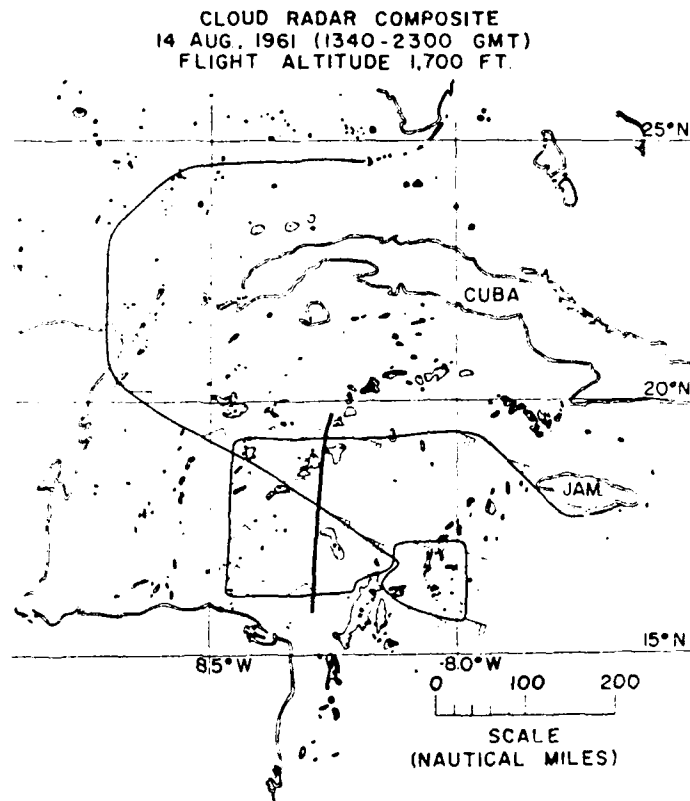
Fig. 21. Radar composite of cumulus rain echoes in an easterly wave that did not quite develop into a tropical cyclone (August 14, 1961). Note the tendency for the rain areas to arrange themselves in lines.

analogous in level and magnitude to our residual calculations on the influence of convective rearrangement of horizontal momentum in our composite data sets previously discussed.

It is important that one distinguish between the tropical cyclone outer radii squall or convection cloud line and the typical middle latitude severe weather squall line. The tropical cyclone squall line is typically oriented parallel with the vertical wind shear vector

CLOUD RADAR COMPOSITE
6 SEPT. 1961 (1640-2240 GMT)
FLIGHT ALTITUDE 3240 FT

25° N

CUBA

YUCATAN

20° N

0   100   200

SCALE
(NAUTICAL MILES)

90° W   85° W   80° W
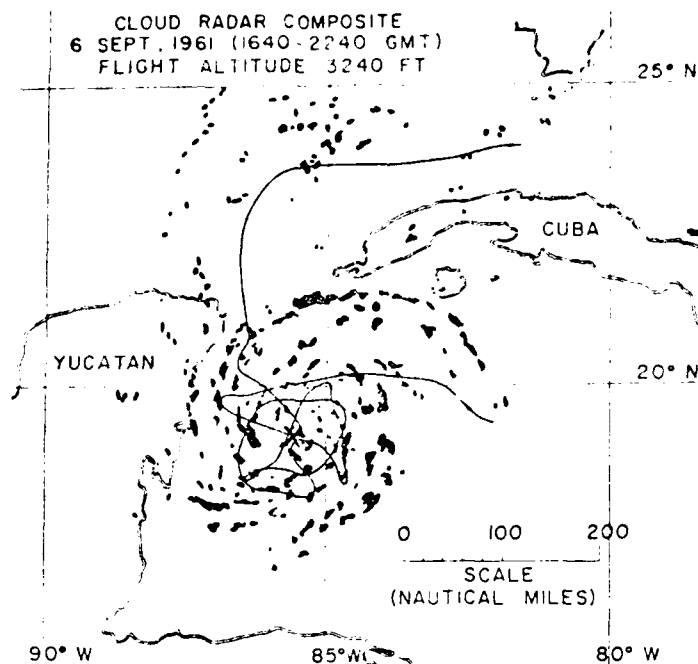
Fig. 22. Radar composite of cumulus rain echoes for September 6, 1961.
Maximum sustained surface winds and minimum sea-level pressure
at this time are 50 knots and 1000 mb respectively. The x
marks the center of the system.

CLOUD RADAR COMPOSITE

From B-47 Flight into
Hurricane DAISY
Altitude 35,000 ft. (237mb)
25 Aug. 1958
1800-2300 GCT

■ Intense Radar Echoes
☐ Radar Echoes of lesser
intensity

0   30   50

Scale Nautical Miles

end of
radar

start of
radar
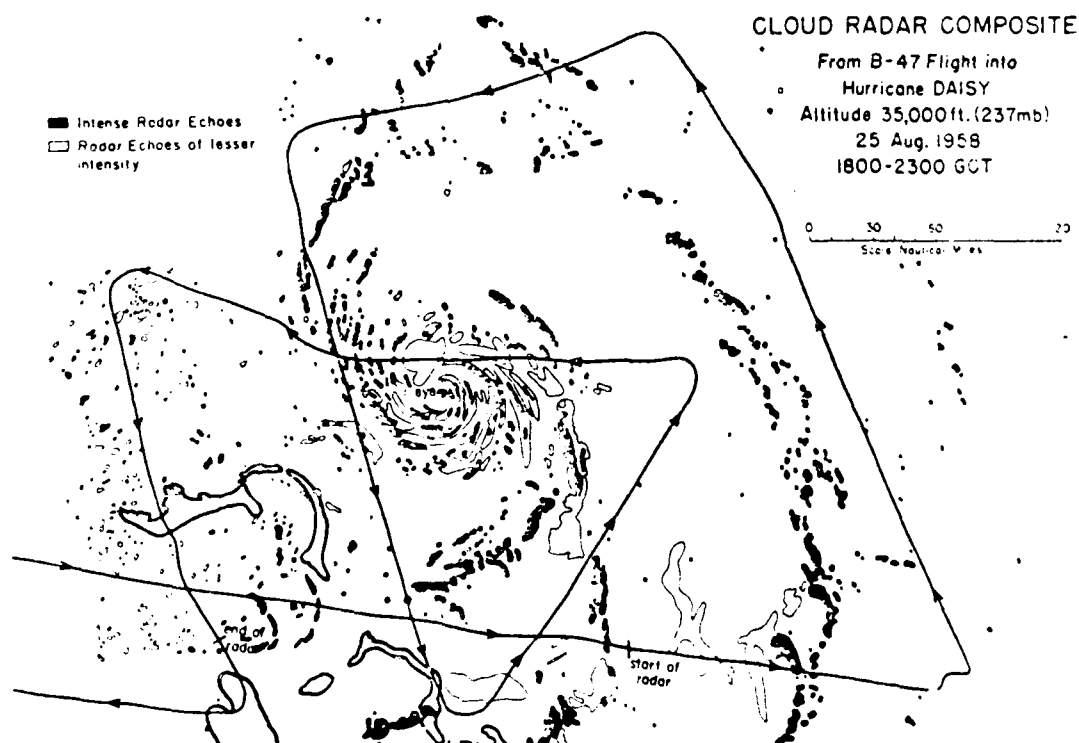
Fig. 23. Radar composite surrounding Daisy on 25 August 1958 when it was
located off the Florida coast and just reaching hurricane inten-
sity. Maximum sustained surface wind and minimum sea-level
pressure are about 70 knots and 990 mb respectively.
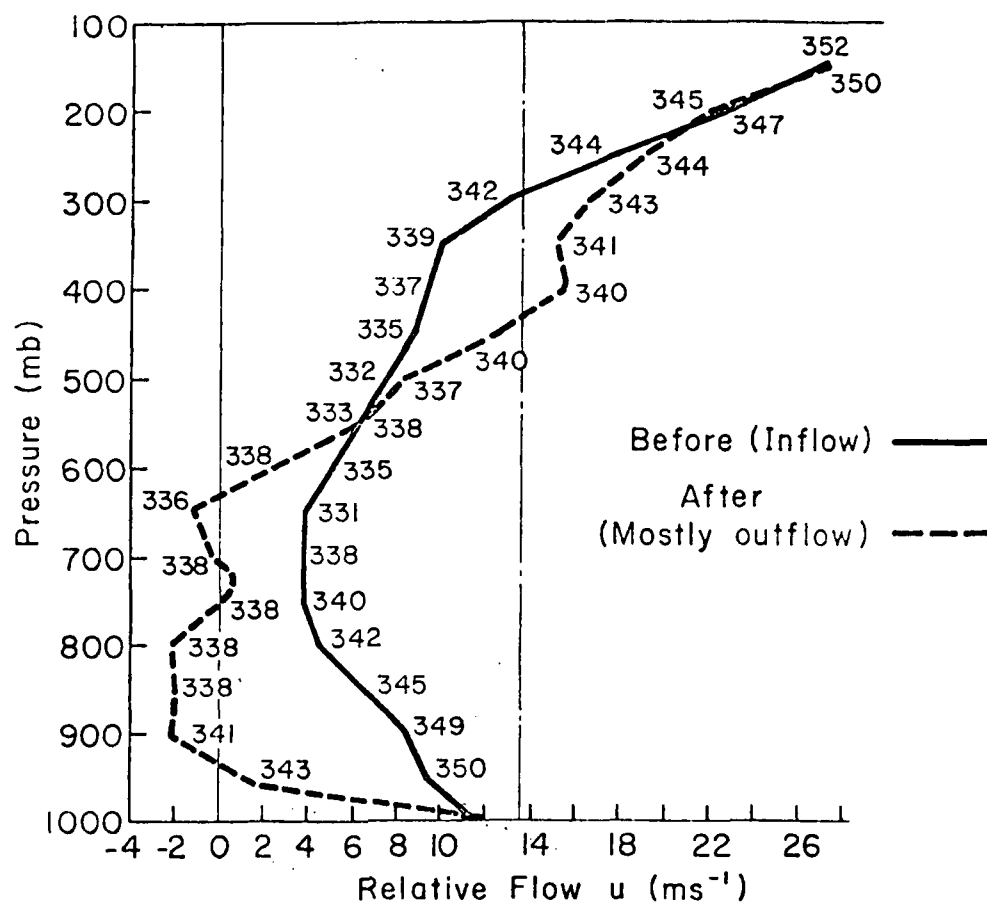
Fig. 24. Mean tropospheric profiles of zonal (U) and meridional (V)
wind components before (solid) and after (dashed) the passage
of traveling line type convective storms over the rawinsonde
site in Venezuela. This average includes 4 cases (from Betts
et al., 1976). θ_e values (also shown) indicate how often
squall line air has lower values.

while the typical middle latitude squall line tends to arrange itself

more perpendicular to the vertical shear vector (see Fig. 25). This

is likely a consequence of the quite different vertical shear profiles

in which these two types of squall lines exist - see Fig. 26. The

tropical cyclone squall line downdraft acts to increase the low level

wind in the direction in which the wind is already blowing, while

the opposite occurs with the downdraft from the middle latitude squall

line. Many other differences exist. One must be clear to differentiate
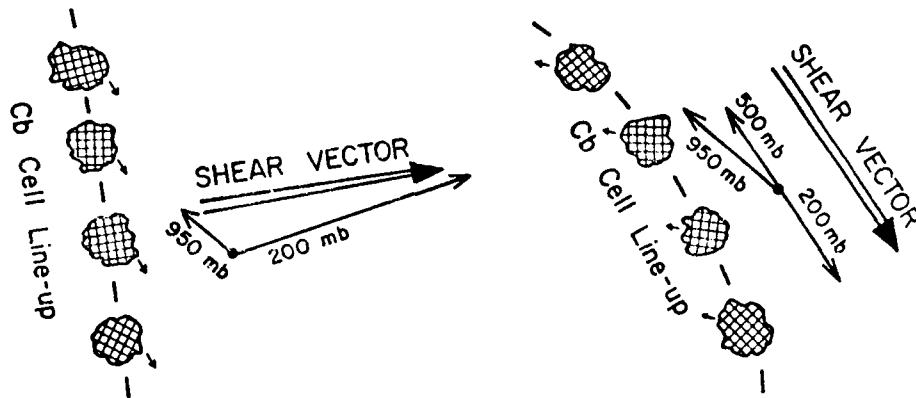
Fig. 25. Portrayal of how the usual US Great Plain squall line is oriented perpendicular to the 950 to 200 mb vertical wind shear vector (left diagram) while the usual tropical cyclone outer radii squall or convective line is typically oriented parallel to the low to upper level vertical wind shear vector.
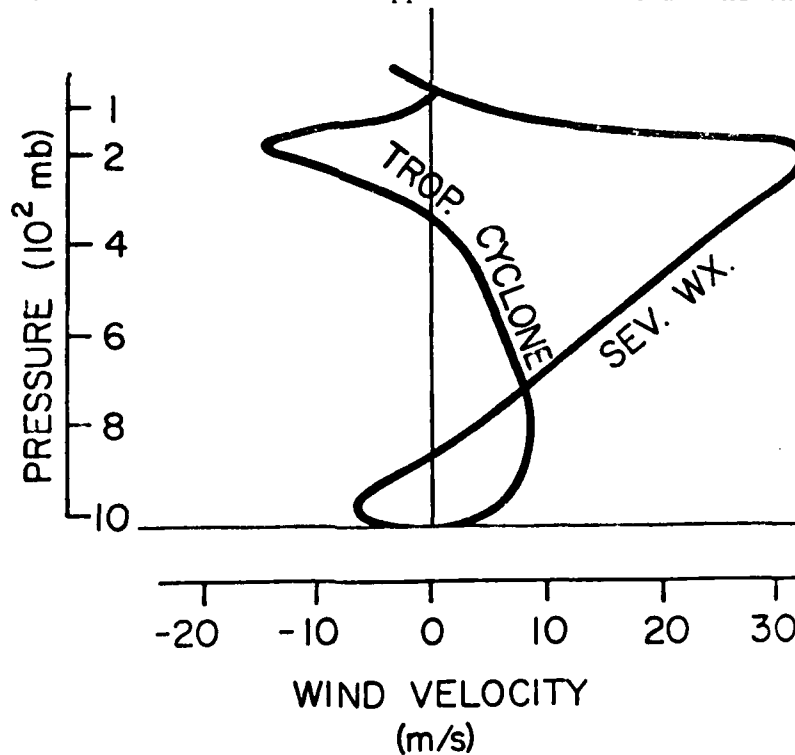
Fig. 26. Portrayal of the typical difference in the vertical profiles of wind velocity convection for the usual severe (SEV.) weather (WX.) event in the middle latitudes vs. the usual tropical cyclone outer radii squall convection. Not how different these two profiles are.

between these two distinct squall line classes. Nevertheless, both squall
line types act to increase the surface wind and dry the boundary layer.

Summary. Much observational information is available to support
the existence of greater amounts of line type convection around the
pre-hurricane disturbance than the non-developing disturbances. V.
Dvorak (private communication) has often stated that cyclone development
tip-off occurs with the beginning formation of curving outer cloud
lines. Observational evidence is also available attesting to the likely
influence of line convections on vertical rearrangement of horizontal
momentum in the sense of increasing lower and upper tropospheric
cyclonic momentum and decreasing middle level cyclonic momentum.

2.4 Discussion

To properly understand the physical processes which cause tropical
cyclone development one must also have a grasp of the physical processes
which normally inhibit such development. The pre-typhoon cloud cluster
is distinguished from the prominent non-developing cloud cluster primarily
by its surrounding 2 to 8° radius 900 to 200 mb vertical wind shear pat-
terns. These differences appear to be established by the large-scale
flow processes within the tropical atmosphere and are not (at least
initially) a result of the disturbance itself. Once a tropical cloud
cluster possesses a $0-3^o$ radius mean vertical motion at 300 mb of 100 mb/d
or greater, vertical motion is not a distinguishing feature of cyclone
development. Moisture, vertical stability, surface wind speed, and other
parameters also do not show significant distinguishing differences.

It is hypothesized that the role of the surrounding cloud cluster
900-200 mb tropospheric vertical wind shears is that of causing the

disturbance's surrounding cumulus convective elements to aline themselves
more in squall-type cloud lines. These cloud lines produce stronger
and drier downdrafts than would otherwise occur without such line orien-
tation. Such strong downdraft action produces an extra ventilation
of the tropical boundary layer and greater energy flux from the ocean.
This allows the tropical cloud clusters' energy depleting mean trans-
verse circulation to be sustained and/or increased. Without such extra
surface energy flux, the cluster's transverse circulation would export
more energy than it inputs and die. It is observed that the majority
of tropical cloud clusters which do not have such surrounding line con-
vection have lifetimes of a day or less.

The enhanced vertical mass recycling in the pre-typhoon's
surrounding 900 to 200 mb vertical wind shear fields also act to rearrange
horizontal momentum in the vertical and allow the disturbance's lower
troposphere to be warmed against the usual tendency of tropical convec-
tion to cool the lower troposphere. Lower tropospheric warming results
from an adjustment of the disturbance's mass field to convective enhanced
vertical wind shear. It is hypothesized that such lower tropospheric
warming would not occur without the special rearrangement of horizontal
momentum by the convective cloud lines which are themselves dependent
upon the special arrangement of the disturbance's surrounding tropospheric
vertical wind shear patterns. Thus, the physical link between the dis-
turbance's $2-8^{\circ}$ radius vertical wind shears and cyclone development
potential is one of extra cloud line generation and consequent enhance-
ment of surface energy flux and vertical momentum rearrangement.

3. DIURNAL VARIABILITY OF THE DEVELOPED TROPICAL CYCLONE

Notable diurnal differences in the divergence profiles of tropical

oceanic cloud clusters have been reported in a number of studies

(Ruprecht and Gray, 1976a, b; Gray and Jacobson, 1977; McBride and

Gray, 1978). Both Atlantic and Pacific cloud clusters have been observed

to have nearly twice as much upward vertical motion in the late morning

hours as in the early evening. This phenomenon has been attributed to

radiational forcing differences between the cloud cluster and the cloud

free environment which modulates the low level inflow and upper level

outflow (Gray and Jacobson, 1977; Fingerhut, 1980). We have also in-

vestigated the extent to which this diurnal radiational forcing mechan-

ism is operating in the developed tropical storm.

3.1 Rainfall

The hurricane and the typhoon have similar cloud patterns as the

tropical cloud cluster and are thus subject to similar radiational

forcing mechanisms. However, the tropical cyclone's more enhanced

dynamics and energetics make its diurnal response less detectable.

Frank (1977a) was able to find only a small diurnal variation in typhoon

precipitation by analyzing twenty-one years of hourly rainfall data

from nine island stations in the west Pacific. Figure 27 illustrates the

diurnal variations of total rainfall during heavy and light rain episodes

for these 9 Pacific islands. Heavy rain episodes were defined as those

having a rainfall rate $\geq$ 0.2 inches per hour. As was the case for the

cloud clusters a morning maximum from about 1000 to 1200 local time (LT)

was detected in the heavy rain events. A minimum is discernible at
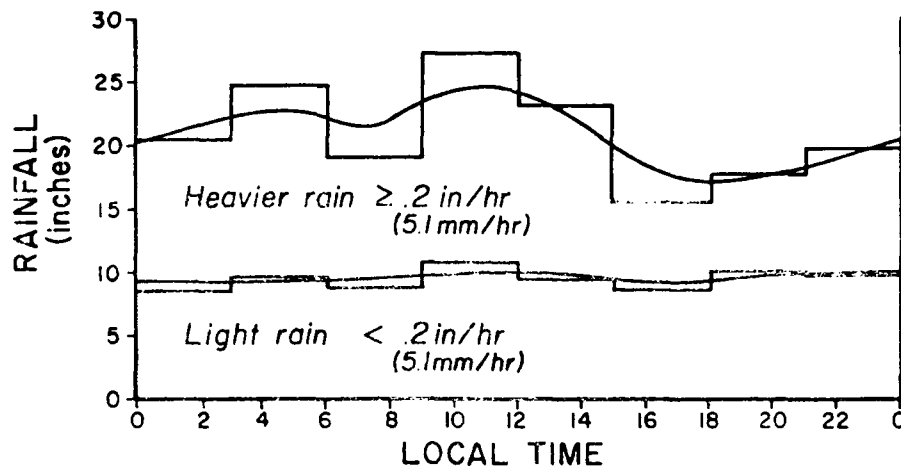
Fig. 27. Diurnal variations of total rainfall during heavier rain
episodes (> 0.2 in/hr) and during light rain episodes
(< 0.2 in/hr) for 9 Pacific islands (from Frank, 1977a).
Units: inches.

about 1800 LT. This morning maximum - evening minimum, although much

smaller in percentage difference, agrees well with the results reported

by Ruprecht and Gray (1974) and Gray and Jacobson (1977) where signi-

ficantly greater amounts of strong precipitation was found for Pacific

cloud clusters at 00Z ($\sim$ 10 LT) than at 12Z ($\sim$ 22 LT). The diurnal

variation of heavy rainfall variability is substantially smaller for the

very intense systems than for the weaker cloud cluster systems. It is

evident that the diurnal rainfall variability is due almost exclusively

to the modulation of the heavy rainfall events. No variation in the

light rain episodes can be observed.

3.2 Radial Winds and Vertical Motion

A similar rainfall data set was not available for the hurricane

data set. On the other hand, a diurnal variation in the radial wind

profile is slightly more evident of a diurnal cyclone for the hurricane than for the typhoon, although the differences are small. Figures 28 to 30 show the radial wind profiles at 00Z and 12Z for the hurricane data set. The 12Z ($\sim$ 07LT) radial mass flux at 2^O radius has a greater magnitude than the 00Z ($\sim$ 19LT) one. The average value of the radial wind over the inflow layer at 2^O radius is -1.7 m s^{-1} at 12Z ($\sim$ 07 LT) vs. -1.3 m s^{-1} at 00Z ($\sim$ 19 LT), corresponding to divergence values of -1.5 x 10^{-6}s^{-1} and -1.1 x 10^{-6}s^{-1} respectively. Convergence is about 30% greater at 12Z ($\sim$ 19 LT). For the outflow layer the average 12Z ($\sim$ 19 LT) wind is 2.1 m s^{-1} against 1.5 m s^{-1} at 00Z at 2^O radius. The 12Z divergence is about 40% greater than the 00Z ($\sim$ 19 LT) value.

At 4° radius, the 07 LT and 19 LT radial winds have approximately equal magnitude implying a very small diurnal range. The hurricane's cloud free region is located at approximately 6° radius. The 07 LT radial wind at 6° has somewhat greater magnitude at lower levels, the 19 LT profile shows convergence over a deeper layer.

These radial wind results are also borne out by the mean vertical motion calculations for the 0-2^O, 0-4°, and 0-6° radius areas which are presented in Figs. 31 to 33. The 12Z ($\sim$ 07 LT) maximum vertical motion inside 2^O is -630 mb d^{-1} vs. -480 mb d^{-1} for the 00Z ($\sim$ 19 LT) - a 30% difference. Inside 4 and 6° radius the maximum vertical motion for the two time periods is similar, although the values are invariably higher for the 12Z ($\sim$ 07 LT) soundings at all levels below $\sim$ 300 mb.

Satellite pictures frequently show an increased afternoon cirrus shield for these tropical storms by as much as 100% over early morning cloudiness (Browner, Woodley and Griffith, 1977). V. Dvorak (personal communication) has also reported similar large early morning to late
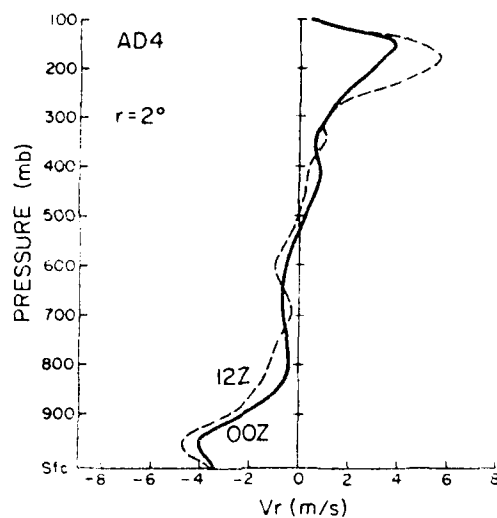
Fig. 28. 12Z (∿ 0700 LT) and 00Z (∿ 1900 LT) radial wind profiles for
the steady state hurricane (AD4) data set at 2° radius.
(from Núñez, 1981)

Fig. 29. Same as in Fig. 28 but
for the 4° radius.
(from Núñez, 1981)

Fig. 30. Same as in Fig. 28 but
for the 6° radius.
(from Núñez, 1981)
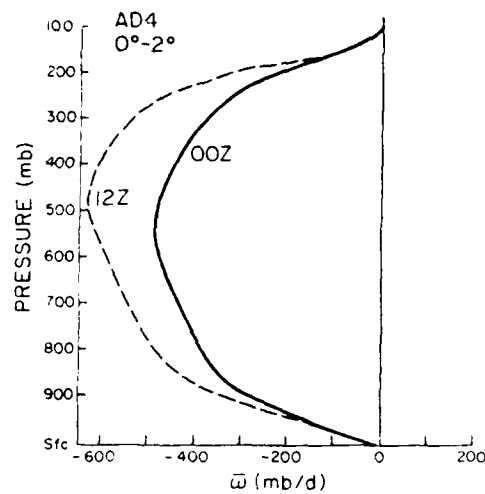
Fig. 31. 12Z (∿ 0700 LT) and 00Z (∿ 1900 LT) mean vertical motion from 0-2° radius for the mean steady state hurricane (AD4) data set. (from Núñez, 1981)
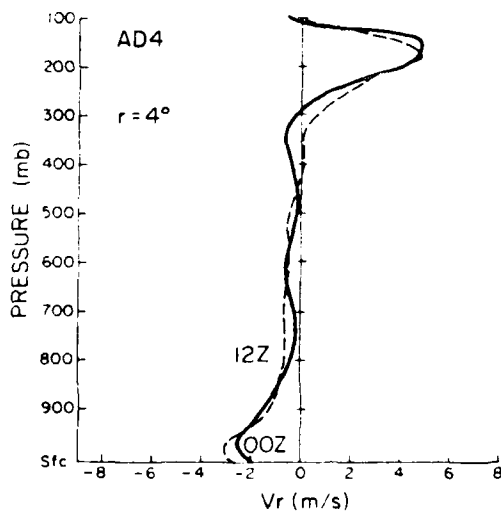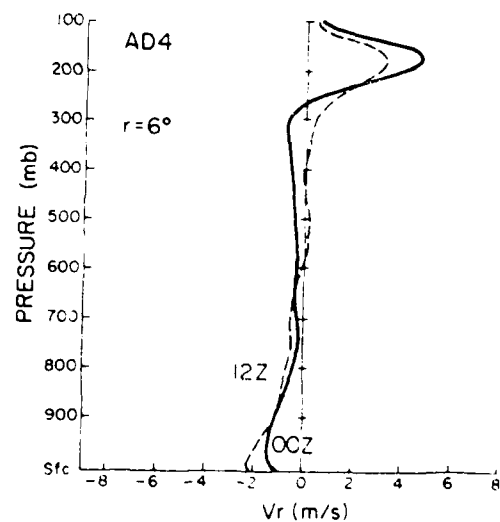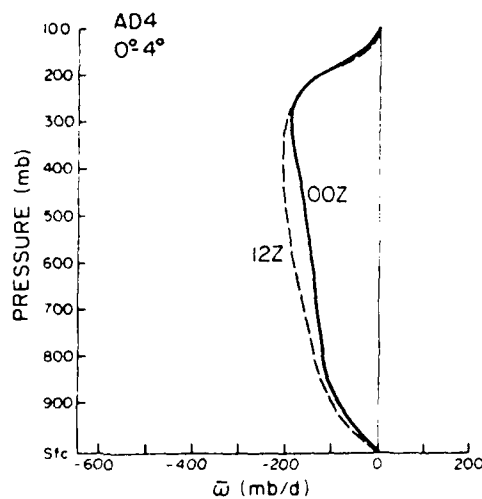

Fig. 32. Same as in Fig. 31 but for the 0-4° radius. (from Núñez, 1981)
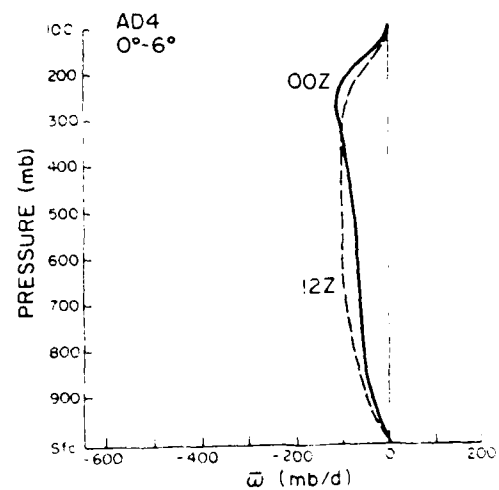
Fig. 33. Same as in Fig. 31 but for the 0-6° radius. (from Núñez, 1981)

afternoon diurnal cloud variations. These large diurnal cirrus cloudi-
ness variations are not viewed as a contradiction of these results which
show little diurnal vertical motion differences. These large changes
in cirrus shield cloudiness do not necessarily have to be attributed only
to the change in the mean circulation through the storm. Most likely,
a substantial amount of the extra cirrus in the afternoon is a result of
direct cloudiness generation by the absorption of solar radiation in the
upper storm levels and by a small undetectable upward vertical motion
response to wipe away such solar warming. Upper level vertical motion
would consequently be further enhanced and more cirrus would be produced.
Another part of the extra afternoon cirrus cloudiness could be the re-
sult of enhanced morning Cb activity near the eyewall. This cirrus,
however, would need 8 to 10 hours to propagate outwards towards the
cloud free region. This would be detected as increased cloudiness in
visible satellite pictures.

3.3 Tangential Winds

Can this small pulsation in the convergence and divergence fields
of the hurricane-typhoon be found in the tangential wind? Figure 34
shows the typhoon and hurricane's tangential wind profiles for the 2°, 4°
and 6° radius at 00Z and 12Z. It is clear that there is no significant
difference through all the troposphere between the tangential winds at
the two time periods. The diurnal variation in these intense storms had
gone previously undetected since it only manifests itself on the radial
wind component, a parameter which is noted for its unreliability on an
individual case basis. The tangential wind, which is substantially
easier to measure, remains (in the statistical average) practically
unaffected by the diurnal cycle in the convergence fields.
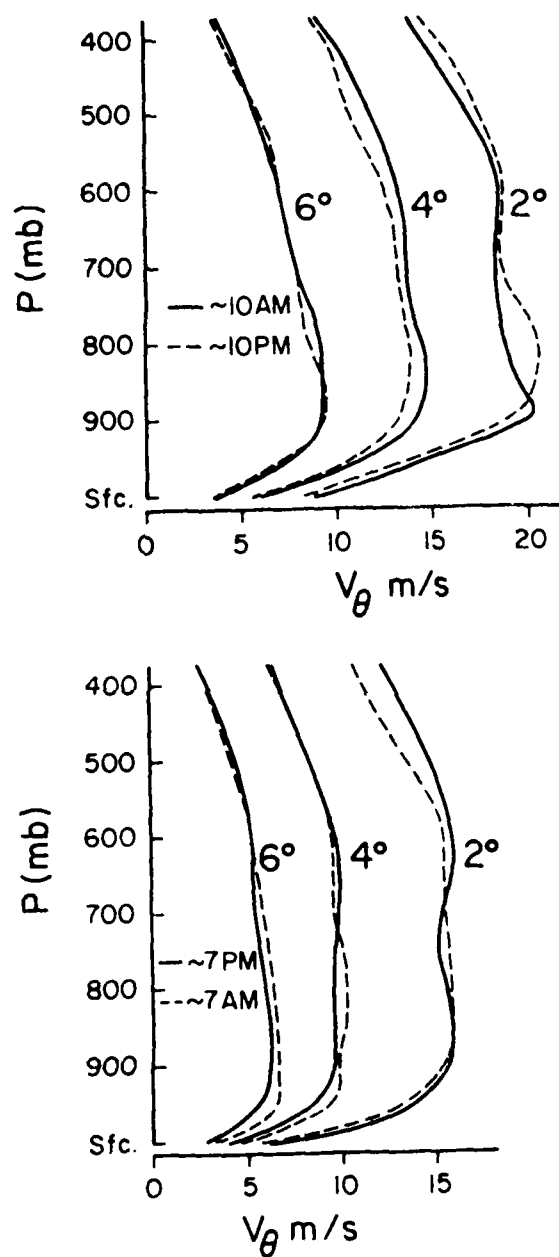
Fig.   34. Tangential wind profiles for the 2°, 4°, and 6° radius at 00Z
($\sim$ 10 AM) and 12Z ($\sim$ 10 PM) for the typhoon (top) and at 12Z
($\sim$ 7 AM) and 00Z ($\sim$7 PM) for the hurricane (bottom). (From
Núñez, 1981).

The lack of response by the tangential winds to changes in the convergence field could be explained in two different ways. A possible explanation may be that the adjustment time of the wind field to the mass field is well over 12 hours. This explanation assumes that the wind field adjusts to the mass field, a process which does not occur in the tropics. An alternate explanation exists which agrees better with the results of the present study and those of recent theoretical work by Silva Dias and Schubert (1979). No diurnal variability in the tangential wind fields should be expected because in the tropics the rotational part of the wind does **not** adjust to changes in the mass flow field. Quite the opposite takes place, it is the mass flow field which adjusts to changes in the rotational part of the wind field. An increased convergence and subsequently enhanced latent heat release within the disturbance will not suffice to appreciably increase the tangential winds if frictional acceleration and other processes act to oppose such tangential wind changes.

Summary. Hurricanes and typhoons possess a diurnal variability in convergence and heavy rainfall which is of the same phase, although much smaller in magnitude than the tropical cloud cluster. Day vs. night differences in radiational forcing between the cloud covered and cloud free areas seem to be the most likely explanation for this phenomenon. The tangential wind fields do not exhibit significant diurnal variability however.

The major hurricane-typhoon diurnal variations occur in total area of satellite observed cirrus cloudiness which can vary as much as 50-100% with a early morning minimum and an afternoon maximum.

4. TROPICAL CYCLONE INTENSITY CHANGE

By

Edwin Núñez and William M. Gray

Except for the obvious cases of tropical cyclones moving over land, cold water, or into the westerly wind belt, the general ability to forecast 24-hour cyclone intensity change is quite low. Yet, it is to be expected that a sizeable fraction of the future 24 hour intensity change occurring in the inner-core region of the tropical cyclone be related in some way to the $5-10^{o}$ radius surrounding storm parameters. But just what are such parameter relationships?

In order to study the surrounding condition differences between tropical storms undergoing intensity change we have stratified our composited tropical cyclone data sets into deepening and filling cases, and made comparisons between these cases. E. Núñez (1981) of our CSU group has recently completed a research report on this subject. The following sections summarize some of Núñez's findings.

The information to follow, of course, will not deal with the rapid up-and-down short term (1-6 hour) changes in cyclone intensity which are likely related to smaller scale inner storm and eye-convection variations not well associated with the large scale storm features. Short term interval synchronous satellite picture information likely provides the best clue to such small time-scale changes in cyclone intensity. This subject is being actively pursued by research groups of the US National Aeronautics and Space Administration (NASA) and the National Oceanic and Atmospheric Administration (NOAA) and results have yet to be fully synthesized.

4.1 Contrasting of Filling and Deepening Systems

Various classes of tropical storms and disturbances occurring in the northwest Pacific and west Atlantic have been studied. The Pacific data sets include rawinsondes for the years 1961-1970 and the Atlantic data sets include the 1961-1974 period.

Each of the data sets are identified by a code consisting of letters and numbers which describes some of its basic features. As in the previous chapters the first character in the code will be a letter - either A or P - indicating whether it is a composite of western Atlantic or western Pacific Ocean systems. The second character will denote if the composite disturbance develops into a hurricane or typhoon at some stage of its life cycle - D - or if it does not develop - N. A number is the third code character and it indicates the intensity of the set. These numbers correspond to the following stages of development:

    1 - Cloud cluster
    2 - Tropical depression
    3 - Tropical storm
    4 - Typhoon or Hurricane
    5 - Very intense Typhoon or Hurricane (central
            pressure ≤ 950 mb)

The code contains one last character - a letter - enclosed within parenthesis. This indicates whether the data set has a tendency towards deepening (D) or filling (F), i.e., if its central surface pressure decreases or its maximum winds increase or decrease within the next 24 hours. These data sets were created with the main intent of contrasting them against each other.

Table 2 contains a list of the intensity change data sets which will be discussed. We will compare surrounding cyclone parameter differences between these contrasting data sets.

TABLE 2

Northwest Pacific and west Atlantic data sets used to investigate tropical cyclone intensity change.

Intensifying Systems	Filling Systems
PD3(D) Deepening Pacific Tropical Cyclone	PN3(F) Filling Pacific Tropical Cyclone
PD4(D) Deepening Typhoon	PD4(F) Filling Pacific Typhoon
AD4(D) Deepening Hurricane	PD5 Supertyphoon (P < 950 mb) - begins to fill in the next 24 hours.

4.2 Comparison of Mixing Ratio

Mixing ratio anomalies (Δq) for deepening PD4(D) and filling PD4(F) typhoons and deepening PD3(D) and filling PN3(F) tropical cyclones are seen in Figs. 35 and 36. They were obtained by calculating the difference between the average mixing ratio inside 3° radius ($q_{0-3^{\circ}}$) and the average mixing ratio from 3 to 7° radius to the east and west of the storm. That is, $\Delta q = q_{0-3^{\circ}} - q_{EW,3-7^{\circ}}$. Maximum anomalies are observed for all sets between 700 and 750 mb. These figures indicate that there is only a small correlation between the tendency of the system to intensify or weaken and the available moisture at outer radii. Assuming the inner cyclone moisture is much the same, then these differences reflect about a one gm/kg increase in outer radius moisture for the intensifying as compared to the filling systems. Such outer radii moisture differences are likely related to the tendency for intensifying systems to have more outer radii deep convection, particularly on their poleward sides.

44
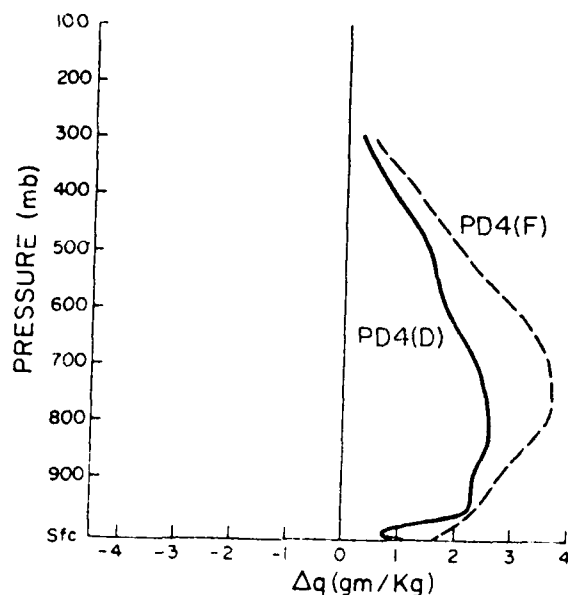
Fig. 35. Mixing ratio anomaly (Δq) profile for the deepening typhoon PD4(D) and filling typhoon PD4(F) data sets. The moisture anomaly was calculated by obtaining the average mixing ratio inside 3° radius (q_{0-3°}) and subtracting from it the average mixing ratio from 3° to 7° radius to the east and west of the storm ($q_{EW,3-7^o}$), i.e., $\Delta q = q_{0-3^o} - q_{EW,3-7^o}$. (from Núñez, 1981)
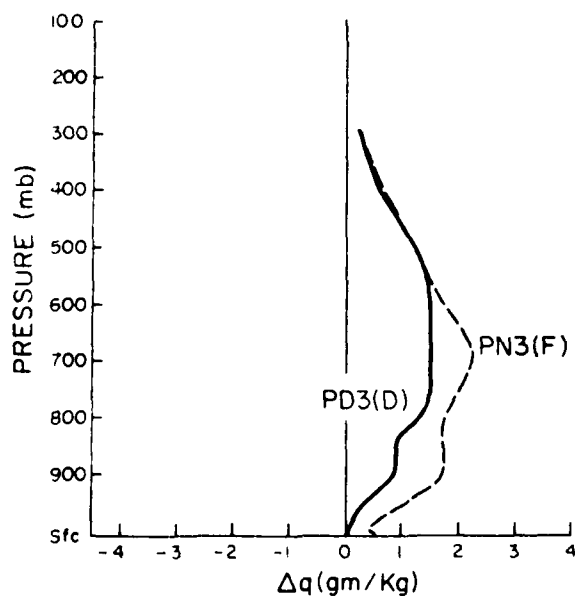
Fig. 36. Same as Fig. 35 but for the Pacific deepening tropical cyclone PD3(D) and the Pacific filling tropical cyclone PN3(F) data sets. (from Núñez, 1981)

4.3 Horizontal Temperature Gradients

In order to obtain knowledge of the relationships of cyclone inten-
sity change to the tropical cyclone's upper level warm center, plan views
of the temperature field at 300 mb have been constructed. Figures 37
to 40 show plan views of the temperature deviation from -29°C at 300 mb
for the deepening and filling typhoon and the deepening and weakening Pacific
tropical cyclone. The temperature deviation from -32°C for the deepening
hurricane appears in Fig. 41 and the deviation from -31°C for the super-
typhoon (typhoons central pressure < 950 mb) is presented in Fig. 42.
It is assumed that the future intensity of the super-typhoon is one of
filling because the pressure is already about as low as it will be.
The temperature field on the northern side of these composites shows
significant differences between disturbances which are gaining strength
and those which are losing it.

Table 3 gives the temperature gradient from 2 to 14° radius on the
northern side of the data sets under consideration. The northwestern
side of the storm is represented by octant 2 and the north and north-
eastern sides by octants 1 and 8, respectively. Since the PD5 data set
is biased toward the filling tendency due to its already developed
extreme strength, we have included it among the filling data sets. It
can be appreciated from Table 3 that the largest contrast between the
filling and deepening sets appears on the northwestern side of the
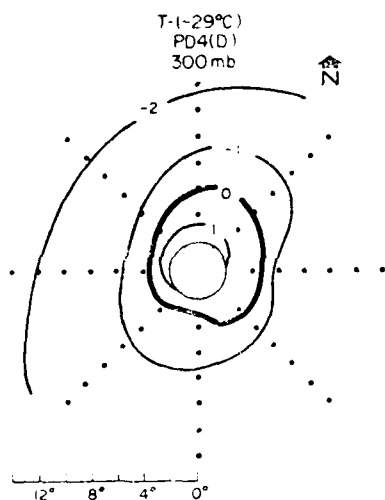
Fig. 37. Plan view of the temper-
ature deviation from
$-29°C$ at the 300 mb level
for the Pacific deepening
typhoon PD4(D) data set.
Units: $°C$. (from Núñez.
1981).
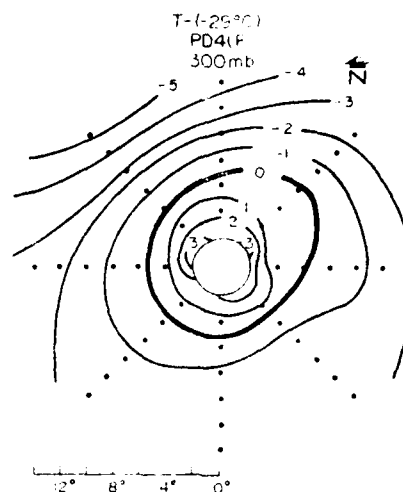
Fig. 38. Same as Fig. 37 but for
the Pacific filling
typhoon PD4(F) data set.
(from Núñez, 1981)
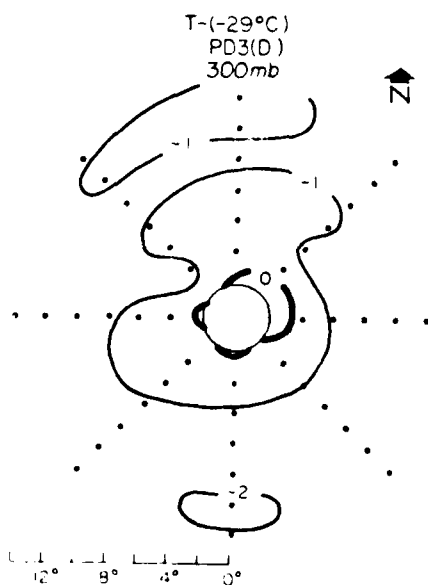
Fig. 39. Same as Fig. 37 but for
the Pacific deepening
tropical cyclone PD3(D)
data set.
(from Núñez, 1981)
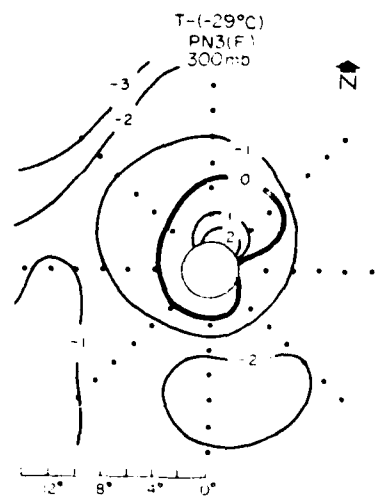
Fig. 40. Same as Fig. 37 but for
the Pacific filling
tropical cyclone PN3(F)
data set.
(from Núñez, 1981)
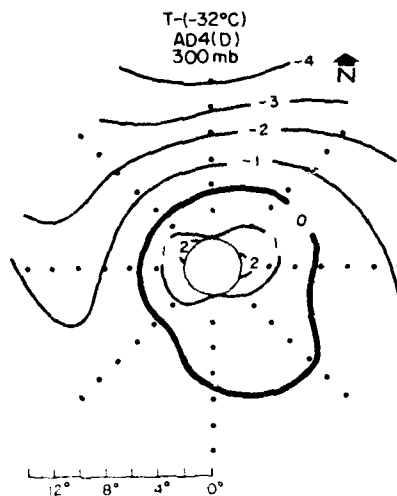
Fig. 41. Plan view of the temperature deviation from $-32^{\circ}C$ at the 300 mb level in NAT coordinates for the Atlantic deepening hurricane AD4(D) data set. Units: $^{\circ}C$. (from Núñez, 1981)
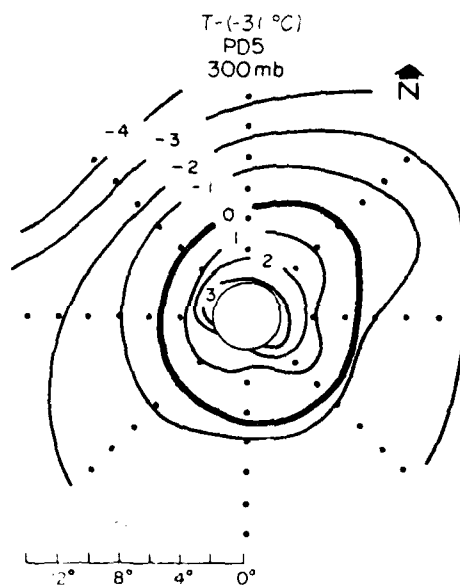
Fig. 42. Plan view of the temperature deviation from $-31^{\circ}C$ at the 300 mb level in NAT coordinates for the Pacific supertyphoon PD5 data set. Units: $^{\circ}C$. (from Núñez, 1981)

TABLE 3

300 mb temperature gradient from 2 to 14° radius on the northern side
of the following data sets: deepening typhoon PD4(D), filling typhoon
PD4(F), deepening tropical cyclone PD3(D), filling tropical cyclone
PN3(F), deepening hurricane AD4(D) and supertyphoon PD5. Octants 2, 1
and 8 represent the NW, N and NE side of the storm. Data set PD5 was
included among the filling sets due to its bias toward weakening storms
(see text for explanation). (from Núñez, 1981)

$$\Delta T = T_{14}o - T_{2}o \ (^O K)$$

Deepening Data Sets	NW(Octant 2)	N(Octant 1)	NE(Octant 8)	Average (Octants 2, 1 and 8)
PD4(D)	-1.4	-3.4	-3.4	-2.7
PD3(D)	-1.0	-1.1	-2.1	-1.4
AD4(D)	-4.5	-5.1	-3.3	-4.3
Average	-2.3	-3.2	-2.9	-2.8
Filling Data Sets				
PD4(F)	-8.6	-7.1	-5.9	-7.2
PN3(F)	-3.6	-4.0	-3.9	-3.8
PD5	-7.1	-6.4	-4.8	-6.1
Average	-6.4	-5.8	-4.9	-5.7
Ave. Deep./ Ave. Fill.	36%	55%	59%	49%
Ave. PD4(D)/ Ave. PD4(F)	16%	48%	58%	38%
Ave. PD3(D)/ Ave. PN3(F)	28%	28%	54%	37%

storm. On the average the deepening disturbances have but 36% of the temperature gradient exhibited by the filling ones. The northern and northeastern octants display 55% and 59% respectively. When octants 8, 1 and 2 are averaged together we see that the northern quadrant of the deepening storms has only half of the temperature gradient (49%) of the filling storms. We can also compare individual data sets against each other. The deepening typhoon exhibits 16%, 48% and 58% of the filling typhoon's temperature gradient on the NW, N and NE octants, respectively. Their average is 38%. Similarly, if we compare the deepening tropical cyclone PD3(D) against the filling tropical cyclone PN3(F) we obtain 28%, 28% and 54% for the NW, N and NE octants. The average is 37%.

Differences in the latitudinal positions of these data sets cannot account for the temperature differences on the northern side. For example, the PD4(D) set is located at about latitude 19°N and the PD4(F) set at about 23°N. Only 4 degrees of latitude separate them. A difference of just 3° latitude exists between sets PD3(D) and PN3(F), their respective positions being 17°N and 20°N. Large gradients can only be explained by the penetration on the northwestern side of a trough or strong westerly winds and their concomitant cold air. Consequently, the presence of a strong baroclinic region near the storm is conducive to weakening. For the deepening systems these temperature gradients are significantly smaller.

4.4 Heights and Height Gradients

Further evidence for the presence of stronger westerly winds to the northwest of the filling systems can be detected by examining the

height fields. Figures 43 to 48 depict the height fields at the 300 mb
level around the PD4(D), PD4(F), PD3(D), PN3(F), AD4(D) and PD5 data
sets. A comparison of the deepening typhoon (Fig. 43) and the filling
typhoon (Fig. 44) shows for the deepening case the existence of tight
height gradients on its northwestern side beyond 10° radius; with the
filling case the packed height gradients penetrate almost to the storm
center. In the case of the deepening and filling tropical cyclone (Fig.
45 and 46) the strong height gradient is only present in the filling
set. The AD4(D) data set likely exhibits stronger height gradients
due to the presence of the North American continent and its associated
enhanced baroclinicity. Table 4 summarizes the differences in height
between the deepening and filling sets from 2° to 14° radius. Height
gradients are either positive or very small on the northeastern octant;
they were not utilized in the computation of the averages and in the com-
parisons.

Substantial differences in the height gradients between the deep-
ening and filling data sets can be discerned, especially on the north-
western octant. In that octant, the deepening sets possess merely 42%
of the filling sets' height gradient. When the north and northwest
octants are averaged together the deepening sets show only 54% of the
filling's height gradient. When individual sets are compared we see
that the deepening typhoons have to the north and northwest just 60% of
the height gradient observed for the filling typhoons. The difference
is even more noticeable for the tropical cyclones. Only 20% of the
height difference between 2° and 14° shown by the filling cyclones is
found for the deepening cyclones. Height gradient discrepancies of
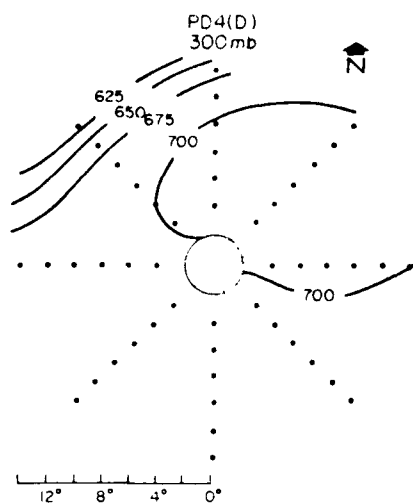
Fig. 43. Plan view of the height
field at the 300 mb level
for the Pacific deepening
typhoon PD4(D) data set.
First digit was omitted;
actual height obtained by
adding 9000 m.
(from Núñez, 1981)
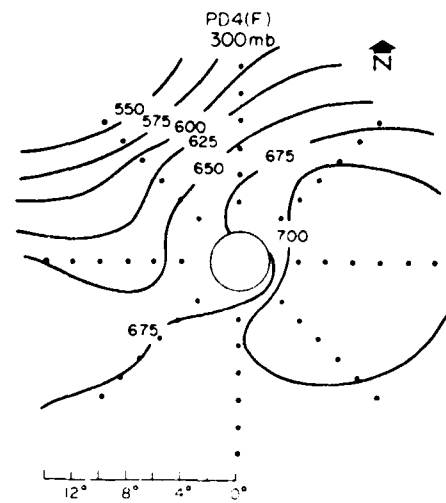
Fig. 44. Same as Fig. 43 but for
the Pacific filling
typhoon PD4(F) data set.
(from Núñez, 1981)
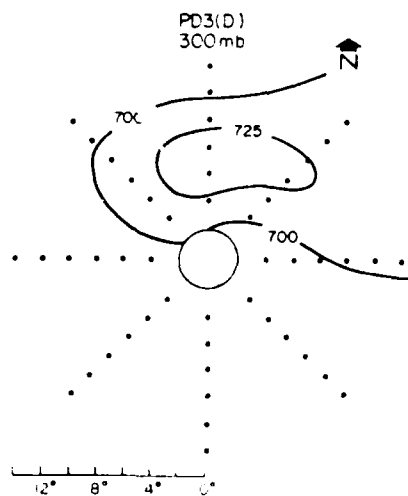
Fig. 45. Same as Fig. 43 but for
the Pacific deepening
tropical cyclone PD3(D)
data set. (from Núñez, 1981)
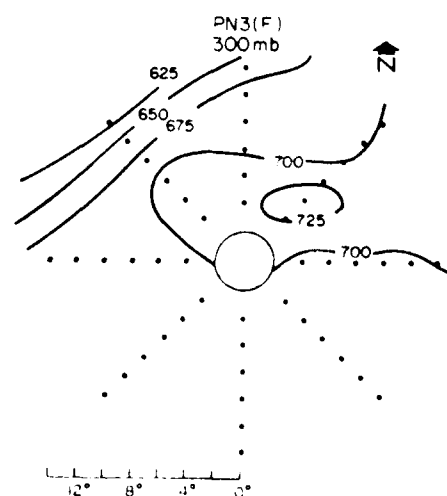
Fig. 46. Same as Fig. 43 but for
the Pacific filling
tropical cyclone PN3(F)
data set. (from Núñez, 1981)
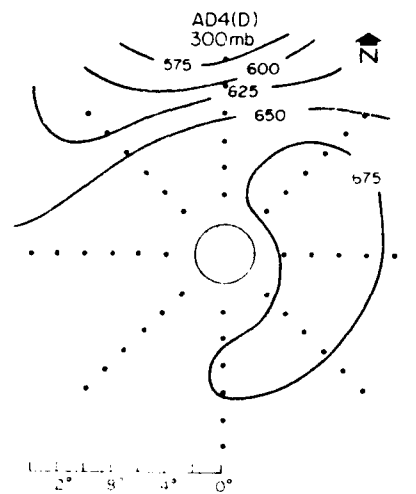
Fig. 47. As in Fig. 43 but for the Atlantic deepening hurricane
AD4(D) data set. (from Núñez, 1981)
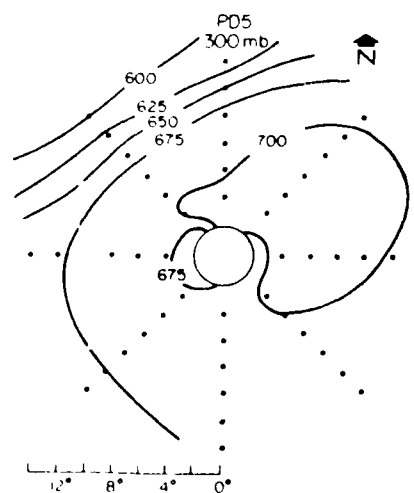
Fig. 48. Same as Fig. 43 but for the Pacific supertyphoon PD5 data
set. (from Núñez, 1981)

TABLE 4

300 mb height gradient from 2 to $14°$ radius on the northern side of the following data sets: deepening typhoon PD4(D), filling typhoon PD4(F), deepening tropical cyclone PD3(D), filling tropical cyclone PN3(F), deepening hurricane AD4(D) and supertyphoon PD5. Octants 2, 1 and 8 represent the NW, N and NE side of the storm. Data set PD5 was included among the filling sets due to its bias toward weakening storms (see text for explanation). (from Núñez, 1981)

Deepening Data Sets	$Z_{14}° - Z_2°$ (m) NW (Octnat 2)	N (Octant 1)	NE (Octant 8)	Average (Octants 2, 1)*
PD4(D)	−72	−51	− 1	−62
PD3(D)	−18	−11	+31	−14
AD4(D)	−22	−92	−21	−57
Average	−37	−51	+ 3	−44
Filling Data Sets				
PD4(F)	−123	−83	−14	−103
PN3(F)	−79	−63	− 3	−71
PD5	−59	−84	+ 6	−72
Average	−87	−77	−11	−82
Ave. Deep./ Ave. Fill.	42%	66%	**	54%
Ave. PD4(D)/ Ave. PD4(F)	58%	61%	**	60%
Ave. PD3(D)/ Ave. PN3(F)	23%	17%	**	20%

*Only octants 1 and 2 used in this computation. The tendency of the height gradient to be positive or very small in Octant 8 rendered the averages less meaningful if it were used.

**Ratio not meaningful in this octant due to one of the values being positive.

this magnitude cannot be accounted for by the small latitude position
difference of the data sets.

4.5 Mean Tropospheric Temperatures to the Poleward Side

Do these differences manifest themselves through the whole tropo-
sphere or are they compensated for at the lower levels? Table 5 gives
the difference between the mean tropospheric temperature at 14° and at
2° for the deepening typhoon PD4(D), filling typhoon PD4(F), deepening
tropical cyclone PD3(D), filling tropical cyclone PN3(F), deepening
hurricane AD4(D), and supertyphoon PD5. The mean temperature at each
radius was calculated between the 150 and 900 mb levels using the
equation:

$$\bar{T} \; (^\circ K) = \frac{- \delta z}{R \; \delta \ln p}$$

where δz represents the height difference between the 150 and 900 mb
levels, R is the gas constant for dry air, and $\delta \ln p$ is the difference
between the natural logarithms of the pressures at the 150 mb and 900 mb
levels. The results agree very well with previous information indicating
that on the northwest octant the enhanced horizontal temperature gradient
exists throughout the troposphere.

This analysis indicates that intensity decrease in mature tropical
systems takes place through enhancement of deep layer baroclinic layers
to the poleward side of the system.

4.5 Intensity Change Related to Wind Field Differences

Tangential winds to the poleward side of the cyclone systems is
also a major distinguishing feature of intensity change. Radial and
vertical winds show very little distinguishing power. Corresponding to

TABLE 5

Differences between the mean tropospheric temperatures (900 mb to 150 mb) at 14° and 2° radius for the deepening typhoon PD4(D), filling typhoon PD4(F), deepening tropical cyclone PD3(D), filling tropical cyclone PN3(F), deepening hurricane AD4(D) and supertyphoon PD5 data sets. The mean temperature at each radius was calculated from: $\overline{T}(^{\circ}K) = -\delta z / R \delta \ln p$. (from Núñez, 1981)

$$\Delta \overline{T} = \overline{T}_{14^{\circ}} - \overline{T}_{2^{\circ}} \quad (^{\circ}K)$$

Deepening Data Sets	NW (Octant 2)	N (Octant 1)	NE (Octant 8)	Average (Octants 2, 1, and 8)
PD4(D)	-2.1	-3.0	-2.5	-2.5
PD3(D)	0	-0.6	-2.0	-0.9
AD4(D)	-2.7	-3.1	-2.2	-2.7
Average	-1.6	-2.2	-2.2	-2.0
Filling Data Sets				
PD4(F)	-5.8	-6.1	-3.8	-5.2
PN3(F)	-2.3	-4.0	-2.9	-3.0
PD5	-5.3	-5.8	-3.3	-4.8
Average	-4.4	-5.3	-3.3	-4.4
Ave. Deep./ Ave. Fill.	36%	42%	67%	45%
Ave. PD4(D)/ Ave. PD4(F)	36%	49%	66%	48%
Ave. PD3(D)/ Ave. PN3(F)	0%	15%	69%	30%

the tendency of filling systems to have significantly stronger baroclinic regions to their poleward sides is the tendency of filling cyclone systems to have significantly stronger horizontal gradients in tangential wind. Figures 49-54 indicate that the horizontal gradient of tangential wind at 300 mb to the poleward side of filling systems is nearly twice as large as with the deepening systems. However, the distinguishing power of poleward differences of tangential wind gradient are less than those of 950-200 mb mean tropospheric temperature or of the 300 mb temperature gradient.
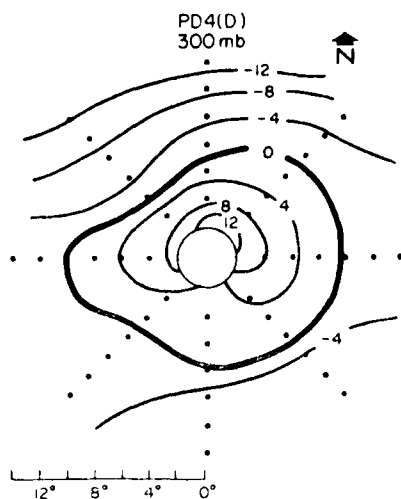
Fig. 49. Plan view of the tangential wind (V_θ) at the 300 mb level for the Pacific deepening typhoon PD4(D) data set. Units: $m\ s^{-1}$. (from Núñez, 1981)
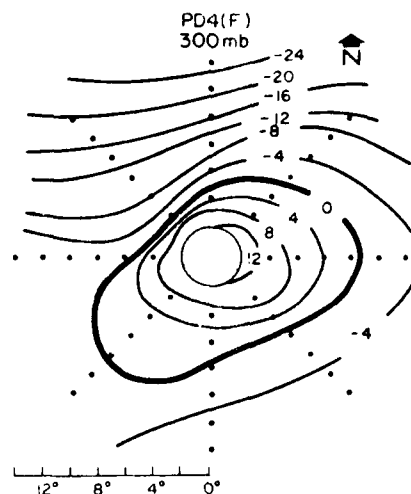
Fig. 50. Same as Fig. 49 but for the Pacific filling typhoon PD4(F) data set. (from Núñez, 1981)
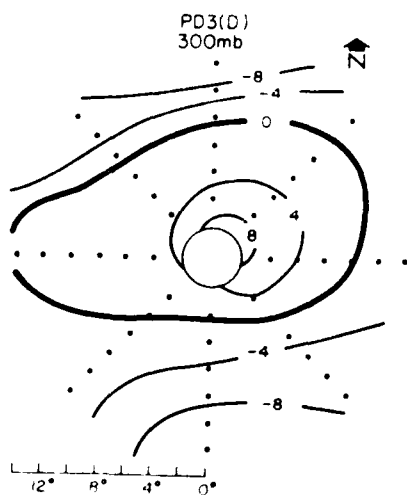
Fig. 51. Same as Fig. 49 but for the Pacific deepening tropical cyclone PD3(D) data set. (from Núñez, 1981)
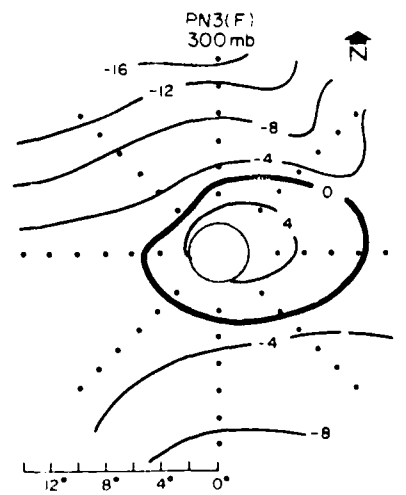
Fig. 52. Same as Fig. 49 but for the Pacific filling tropical cyclone PN3(F) data set. (from Núñez, 1981)
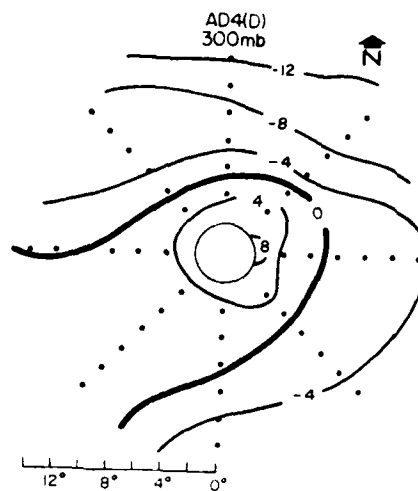
Fig. 53. Same as Fig. 49 but for the Atlantic deepening hurricane
AD4(D) data set.   (from Núñez, 1981)
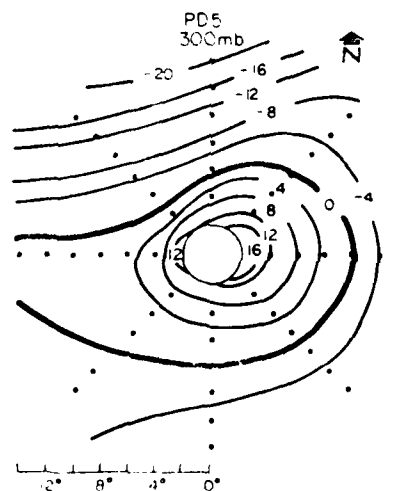
Fig. 54. Same as Fig. 49 but for the supertyphoon PD5 data set.
(from Núñez, 1981)

A summary of the northern side 3 octant differences in temperature, height, and wind gradients between deepening and filling sets is given in Table 6.

It is evident that at least for the storms which are in the process of weakening there exists a strong interaction with the circulation of the higher latitudes. The penetration of upper level westerlies comes much closer to these storm systems.

Summary. Moisture, radial winds, and vertical motion are not well correlated with the system's tendency toward deepening or filling. A comparison of the deepening and filling data set wind and temperature fields indicates that deepening systems have smaller temperature gradients to their poleward sides than do filling systems. In contrast, filling systems would have much stronger horizontal temperature gradients to their poleward side.

4.6 Cyclone Intensity Change Related to Wind-Pressure and Thermal-Wind Balances

The gradient wind equation has been evaluated for deepening and filling/steady systems. Deepening data sets have been found to possess supergradient winds at the 900 mb level, while filling/steady sets have less supergradient or subgradient winds. In the upper troposphere (200 mb) both groups have subgradient winds, although deepening sets have less subgradient winds. Radial frictional acceleration by cumulus clouds and mass recycling likely accounts for a substantial part of any existing imbalance. The tropical disturbance responds to these imbalances created by the stronger winds by adjusting its mass or pressure gradient fields. As long as the winds remain more supergradient than normal at low levels and less subgradient than normal at upper levels, the more the system

TABLE **6**

Summary of the differences on the northern side between deepening and filling data sets. Deepening sets: PD4(D), PD3(D), AD4(D). Filling sets: PD4(F), PN3(F), PD5. Given are the horizontal temperature gradient at 300 mb from 2^O to 14° radius, the horizontal gradient from 2^O to 14° of the mean 900-150 mb temperatures; horizontal height gradient at 300 mb from 2^O to 14° radius, and the horizontal gradient of the tangential wind from 2^O to 14° radius at 300 mb. (from Núñez, 1981)

	NW (Octant 2)	N (Octant 1)	NE (Octant 8)	Average (Octants 2, 1 and 8)
$(T_{14}o-T_2o)$ 300 mb (^OK)				
Ave. Deepening	-2.3	-3.2	-2.9	-2.8
Ave. Filling	-6.4	-5.8	-4.9	-5.7
Ave. Deep./ Ave. Fill.	36%	55%	59%	49%
$(\overline{T}_{14}o-\overline{T}_2o)$ 900-150 mb (^OK)				
Ave. Deepening	-1.6	-2.2	-2.2	-2.0
Ave. Filling	-4.4	-5.3	-3.3	-4.4
Ave. Deep./ Ave. Fill.	36%	42%	67%	45%
$(Z_{14}o-Z_2o)$ 300 mb (m)				
Ave. Deepening	-37	-51	+ 3	-44
Ave. Filling	-87	-77	-11	-82
Ave. Deep./ Ave. Fill.	42%	66%	*	54%
$(V_{\theta_{14}o}-V_{\theta_2o})$ 300 mb (m s^{-1})				
Ave. Deepening	-16.6	-24.1	-16.2	-18.9
Ave. Filling	-25.7	-31.3	-22.4	-26.5
Ave. Deep./ Ave. Fill.	65%	77%	72%	71%

* Ratio not meaningful in this octant due to one of the values being positive.

will intensify. Weakening occurs when the winds are less supergradient than normal at low levels and more subgradient than normal at upper levels. The pressure field adjusts to these weaker wind fields by reducing the inner storm's warm core and consequently its intensity.

This intensity change mechanism is in general agreement with the results of Silva Dias and Schubert (1979) and the modeling work of Fingerhut (1980) which indicates that the pressure field adjusts to the wind field and not the other way around.

4.7 Gradient Wind Balance

The key to the problem of deepening/filling thus appears to lie in the balance between the wind and the thermodynamic fields. In order to investigate this balance an evaluation of the gradient wind equation for eighteen different tropical cyclone data sets in different stages of intensity change was made. The gradient wind equation in cylindrical coordinates can be expressed in the following manner:

$$(fV_\theta + \frac{V_\theta^2}{r}) = \frac{g\partial z}{\partial r}\Big|_p \tag{6}$$
$$\quad\text{(a)}\quad\text{(b)}\qquad\text{(c)}$$

where f = Coriolis parameter

V_θ = tangential wind, positive counterclockwise

r = radius

g = gravitational acceleration

z = height of a pressure surface

p = subscript which denotes a constant pressure surface.

Term (a) in Eq. 6 represents the acceleration due to the Coriolis force, term (b) the centrifugal acceleration and term (c) the acceleration due to the height gradient. Since the height field can be directly related to the pressure field, term (c) also describes the acceleration due to the pressure gradient. The left-hand side of Eq. 6 gives the acceleration due to the wind field which should be balanced by that due to the height (or pressure) field as presented by the right hand side term. Any imbalance occurring between these three forces will tend to produce an acceleration in the radial direction.

The three terms in Eq. 6 were evaluated at each octant and radial belt for every data set. Two levels were used: 200 mb and 900 mb. They are representative of the upper and lower troposphere. The 900 mb level was selected so as to minimize the effects of surface friction. An average of the eight octants was obtained for each radial belt and then area weighted. A mean value representing the 3° to 11° area was produced. The data sets were divided into two categories: (a) deepening (b) filling or steady-state. These two categories were averaged and contrasted against each other. We observe that at 900 mb, in general, the average for the deepening systems indicates that the wind acceleration is greater than the pressure gradient acceleration, i.e., deepening systems have supergradient winds in the lower troposphere. On the contrary, systems which are either filling or in a steady state have subgradient winds. The difference between the two sets at 900 mb is 21%. In the upper troposphere (200 mb), both systems have subgradient winds. However, deepening systems possess less subgradient winds than do filling or steady state systems. The difference between the two sets of systems at 200 mb is 14%. Table 7 presents a summary of these results.

TABLE 7

Ratio of the average wind to pressure gradient accelerations for the deepening and filling or steady state data sets area weighted from 3° to 11° radius. Average of the eight octants. (from Núñez, 1981)

Level	Deepening	Filling/Steady	Difference
900 mb	1.12	0.91	21%
200 mb	0.75	0.61	14%

Of the three terms appearing on Eq. 6 the most difficult to evaluate will be the pressure gradient acceleration. Heights are difficult to measure accurately at upper levels and their gradients are subject to noise. During the early stages of development, when the height gradients are small, there is some difficulty in obtaining reliable values for the pressure gradient acceleration term at upper levels. If this noise is random, however, composited heights should be reliable. Systematic errors should be in both sets of weather systems and, consequently, the differences between them should be meaningful. Deepening sets have more supergradient winds, filling/steady state sets have more subgradient winds at the lower levels; in the upper levels deepening sets show less subgradient winds.

Our previous analysis of the deepening and filling data sets indicated the presence of differences on the northern side of the disturbances. The wind and pressure gradient accelerations for the deepening and filling or steady data sets have been evaluated in octants 8, 1 and 2. These are representative of the northern side of the system. The average of all the filling or steady disturbances at the 900 mb level indicates that the systems are essentially in balance, the ratio of

wind to pressure accelerations is 1.05. For the deepening systems, however, the ratio is 1.53 - a difference of 48%. The deepening systems are definitely supergradient at their poleward side. At the 200 mb level there is basically no difference. For the filling or steady state systems the winds are somewhat less subgradient than for the deepening but the difference is only 6% which is within the noise level. Even without performing any smoothing on the data deepening systems clearly show the existence of supergradient winds at the 900 mb level, while filling or steady systems indicate subgradient or near balance winds. A summary of the results is presented in Table 8.

The analysis of the composite data indicates that both for systems which are in the process of deepening and those which are filling or steady, an imbalance between the wind and thermodynamic field exists. Winds are stronger than what balance conditions call for in the lower troposphere for the deepening data sets, and weaker for the filling or steady ones. At the upper levels even though both sets indicate subgradient winds, the deepening systems have less subgradient winds than the filling or steady ones. Between deepening and filling or steady sets, the ratio of wind to pressure gradient accelerations are very distinct.

TABLE 8

Ratio of the average wind to pressure gradient accelerations on the northern side of the deepening and filling or steady state data sets area weighted from 3 to 11° radius. Average evaluated from octants 8, 1 and 2. (from Núñez, 1981)

Level	Deepening	Filling	Difference
900 mb	1.53	1.05	48%
200 mb	0.57	0.63	-6%

Furthermore, these results are in general agreement with the findings

of Silva Dias and Schubert (1979) and Fingerhut (1980) which indicate

that intensification results mainly when the momentum fields are altered.

A stronger tangential wind field will cause the temperature field and

the radial circulation field to adjust. As long as the imbalance is

maintained the disturbance continues to intensify. On the other hand,

if the winds are subgradient, the adjustment process will weaken the

disturbance.

4.8 Thermal Wind Imbalance

In the previous section we explained how a determination of the

gradient wind balance requires the evaluation of the height gradient

at individual levels, which is difficult to determine accurately in

tropical disturbances. The establishment of the balance between the

wind and pressure fields is crucial to our understanding of the rea-

sons which lead tropical disturbances to intensify or weaken. Another

way of determining wind-pressure imbalances is by the use of the thermal

wind equation which expresses the difference between two vertical

levels of the horizontal momentum equation. In essence, this is an in-

tegration of the equation of motion through a layer and as such is a

more stable quantity.

The thermal wind equation can be expressed as:

$$(f + 2 \frac{V_\theta}{r}) \frac{\partial V_\theta}{\partial p} - (- \frac{R}{p} \frac{\partial T}{\partial r}\Big|_p) = - \frac{\partial F_r}{\partial p} + \frac{\partial}{\partial p} (\frac{dV_r}{dt}) \qquad (7)$$

$$\phantom{(f + 2 \frac{V_\theta}{r})} W \qquad\quad S - \qquad B \qquad\qquad = \qquad Res$$

where   W = rotational parameter

           S = vertical wind shear

           B = baroclinicity (evaluated on a constant pressure surface)

     Res = thermal wind residual

A knowledge of the tangential wind at two levels and the mean
temperature gradient between these levels is required to evaluate the
left hand side of this equation. These two fields are easier to
evaluate than height gradients at individual levels because they contain
less noise.

By evaluating (WS-B) we can determine the thermal wind residual
(Res). It is found that substantial imbalances exist between the wind
shear and baroclinicity and that systematic differences exist between
the developing and weakening systems.

Profiles of WS-B, area weighted from 3 to 11° radius, are shown
in Figs. 55 and 56 for the 8 octant or radial average and for the 3-
octant average to the north (octants 8, 1, 2). All the deepening sets
were averaged together and compared with all the filling/steady sets.
The smoothed temperature and wind fields were utilized. Both the
average for the eight octants and the average to the north indicate a
large difference in the upper levels between the deepening and the
filling/steady data sets. The upper-level contrast is more marked on
the northern side. WS-B is much more negative for the filling than for
the deepening. In fact, in Fig. 56 we see that the values are slight-
ly negative for the deepening sets while they are strongly negative for
the filling/steady ones. Consequently, the tropospheric winds on the
average are more supergradient or less subgradient for disturbances
which have a deepening tendency.

These figures indicate that for both the deepening and the filling/
steady systems WS-B is positive in the 900-500 mb layer and negative
from about the 500-200 mb layer. WS is less negative than B in the
200-150 mb layer. This tendency is most evident for the northern side
of the deepening sets.

$3° - 11°$
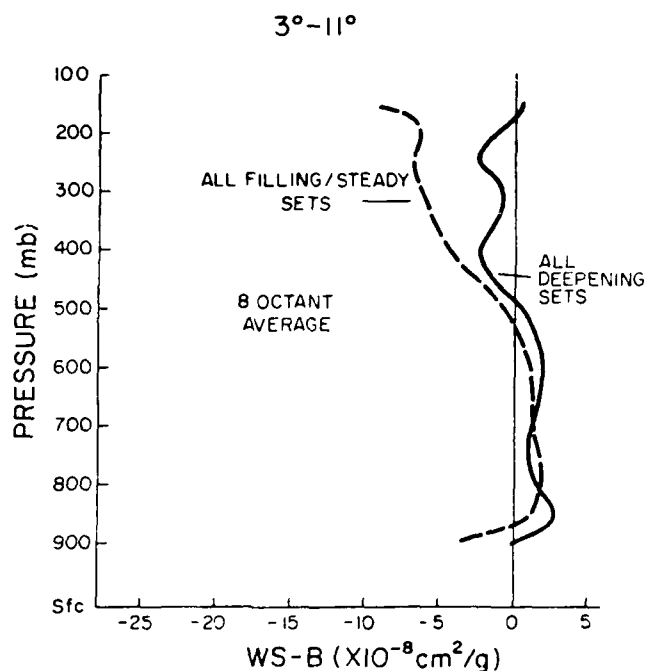
Fig. 55. Vertical profile of the mean WS-B, area weighted from $3°$ to $11°$ radius, for all the deepening and all the filling/steady data sets. Calculated for the 8 octant average around the sets. (from Núñez, 1981)

$3° - 11°$
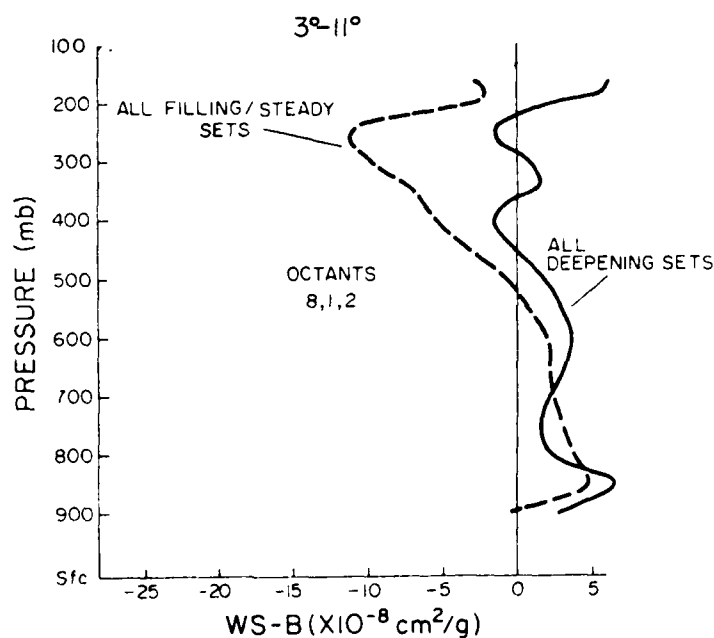
Fig. 56. Vertical profile of the mean WS-B, area weighted from $3°$ to $11°$ radius, for all the deepening and all the filling/steady data sets. Calculated on the northern side (octants 8, 1, 2) of the sets. (from Núñez, 1981)
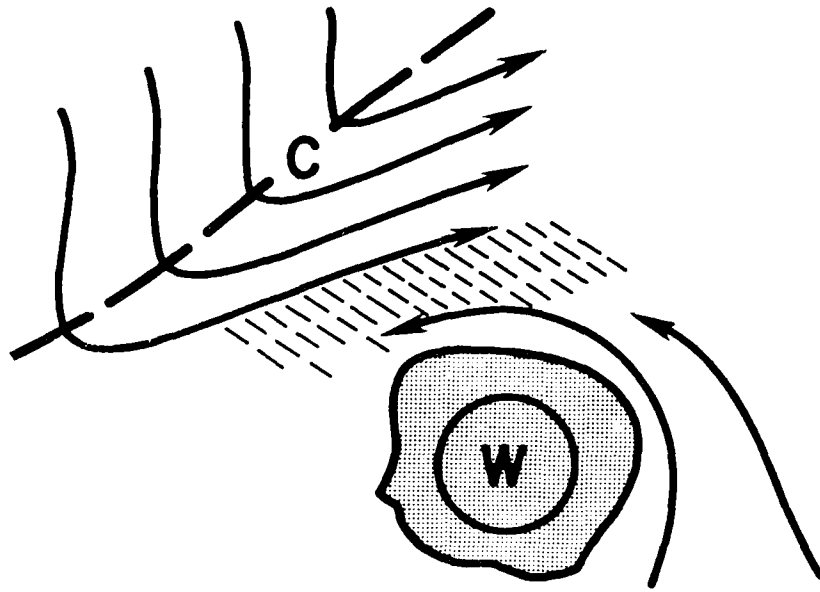
Fig. 57. Schematic representation of how an upper level baroclinic
trough to the northwest of a cyclone leads to its weakening.
The trough produces an enhanced baroclinic field to the north-
west. Simultaneously, a weakening of the storm's cyclonic
flow due to momentum mixing in the hashed area would be ob-
served. Such an influence would bring about a thermal wind
imbalance such that WS < B. The unbalanced flow mechanism
requires that the baroclinicity be reduced and the storm
would weaken.

A definite predictive ability exists by examining the balance
between WS and B, especially on the northern side of the disturbance.
For instance, whenever the WS-B imbalance is negative it means that B
is larger than WS. Winds and vertical wind shears are weaker than
baroclinicity. The disturbance will adjust by acting to reduce the
baroclinicity and pressure gradient as shown in Fig. 57. This acts to
weaken the storm system. When WS > B, the opposite tendency change
occurs.

It appears that changes in the large-scale circulation alter the
tangential wind field around developing disturbances such that develop-
ing disturbances have stronger lower level cyclonic and upper level
anticyclonic vorticity. An imbalance is created such that the wind

shear field (WS) is larger than the baroclinicity (B). Winds for

these deepening systems will be supergradient or less subgradient than

those which characterize filling/steady disturbances. The system will

seek to adjust by augmenting the baroclinicity in order to match the

enhanced WS field.

4.9 Summary of Similarities and Differences Between Developing and
     Filling Tropical Cyclones

A comparison of the basic thermodynamic and wind fields of two

groups of deepening vs. filling storms indicates only a selective number

of meteorological parameters offer a good distinguishing power. They

are:

1) deep layer baroclinicity on the northwest and north of the
    cyclone and its associated height and temperature gradients,

2) supergradient winds in the lower troposphere, and

3) thermal wind imbalance such that wind and wind shear is larger
    than corresponding horizontal temperature gradient.

Poor distinguishing parameters are:

1) humidity

2) absolute temperature

3) vertical stability

4) vertical motion

5) total cloudiness

In addition to the influence of poleward baroclinic conditions on

tropical cyclone weakening, there are also cases (although less frequent)

of tropical cyclone weakening at low latitudes without apparent baro-

clinic influence. Such cyclone filling cases can often be associated

with a weakening of the cyclone's surrounding low level circulation

(Wachtmann, 1968). Such a weakening can result from the cyclone's motion

into a less favorable environment or a large-scale in-situ alteration of this environment.

4.10 Prognosis

As these thermal wind imbalances and baroclinic conditions occur through a deep layer and over a broad scale and are especially pronounced on the poleward sides of the cyclone, it may be possible to make routine analysis of such conditions at national meteorological centers having large-scale analysis capability. Such analysis would be much enhanced when or if satellite sounding readout capability becomes available.

5. STATISTICAL ANALYSIS OF VALIDITY OF RAWINSONDE COMPOSITING METHODOLOGY

By

W. M. Gray, E. Buzzell, P. Mielke and K. Berry

To properly interpret the rawinsonde data composite information that has been discussed, it is important to make statistical analysis of the typical scatter of individual rawinsonde parameters about their mean values. Such analysis allows the statistical significance of the information that has been presented to be better understood.

Statistics of individual soundings show that the typical zonal (u), meridional (v), tangential (V_θ), and radial wind components (V_R) have standard deviations from individual radial leg averages (1-3° radius radial belt, 3-5°, 5-7°, etc.) of about 5-7 m/s at lower and middle tropospheric levels and about 10-12 m/s at upper tropospheric levels as listed in Table 9. Standard deviations of soundings within individual octants of a particular 2° radial belt are about 5 m/s at lower and middle levels and about 7 m/s at upper tropospheric levels.

These wind deviations from belt and octant average values are representative of all rawinsonde data sets. Deviations are 25-50° larger on the poleward than equatorial side. Data set differences are believed real to the extent that sounding numbers allow the largely random and unrepresentative soundings to cancel themselves out in the data set average.

All radial belt and octant individual sounding wind deviations (and most other parameters) approximate a normal distribution. Typical individual sounding deviations of radial wind (V_R), pressure height, and temperature at 900 mb for 888 soundings occurring in the 9-11° radial belt surrounding 14 years of hurricane soundings are shown in Figs. 58, 59 and 60. This data approximates a normal distribution. A typical distribution of 101 tangential winds (V_θ) reports about an individual octant
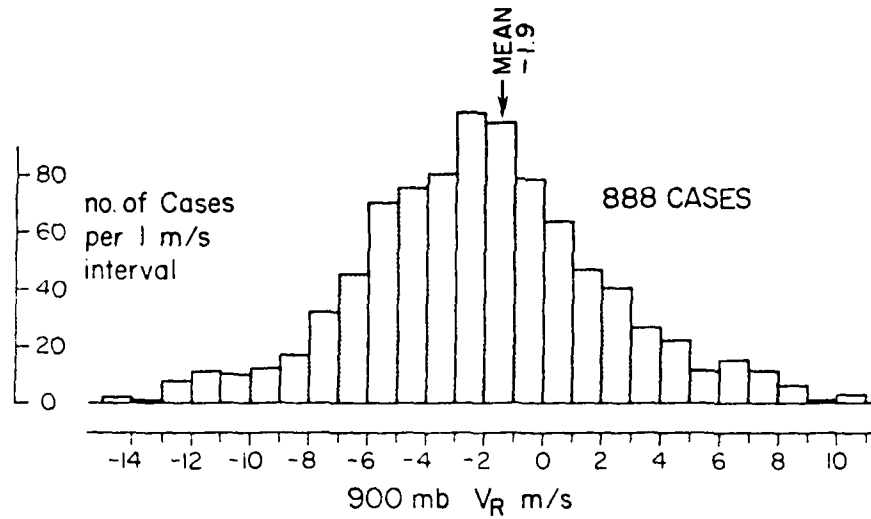
Fig. 58. Distribution of 900 mb individual radial wind values about the mean for the 888 soundings contained in the 9-11° radial belt of west Atlantic hurricanes south of 30° during the period 1961-1974.
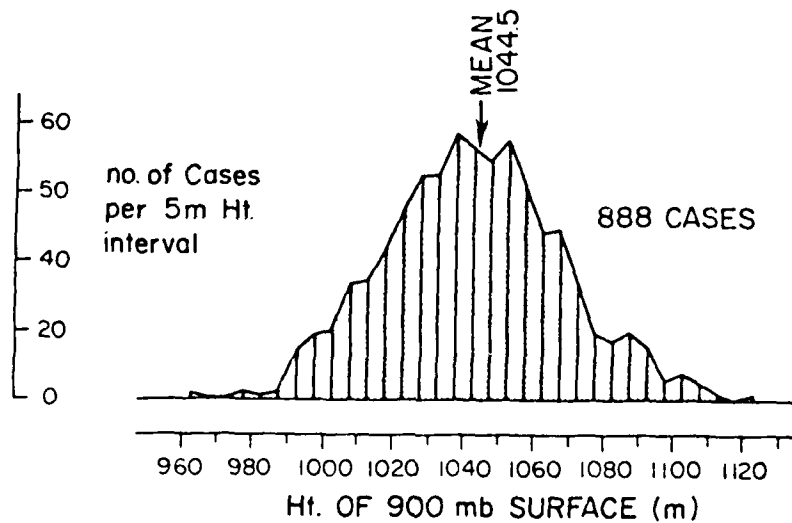
Fig. 59. Same as Fig. 58 except for 900 + individual pressure-height.
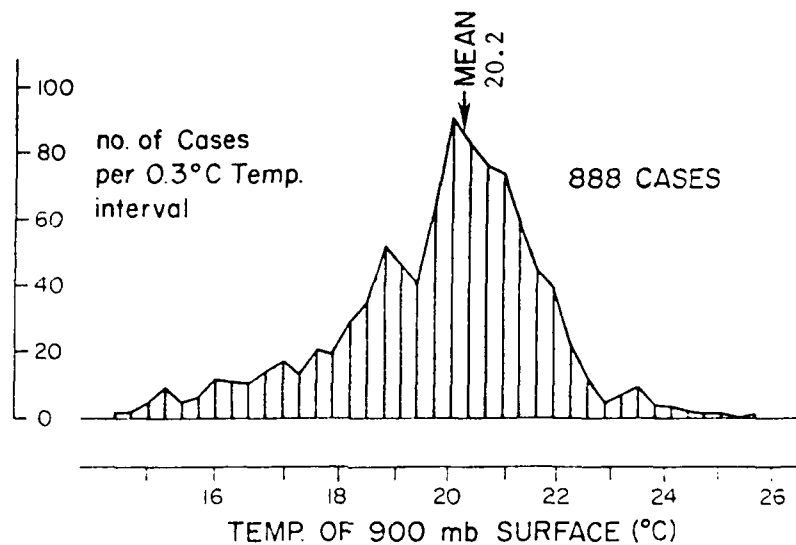
Fig. 60. Same as Fig. 58 except for 900 mb individual temperature values.
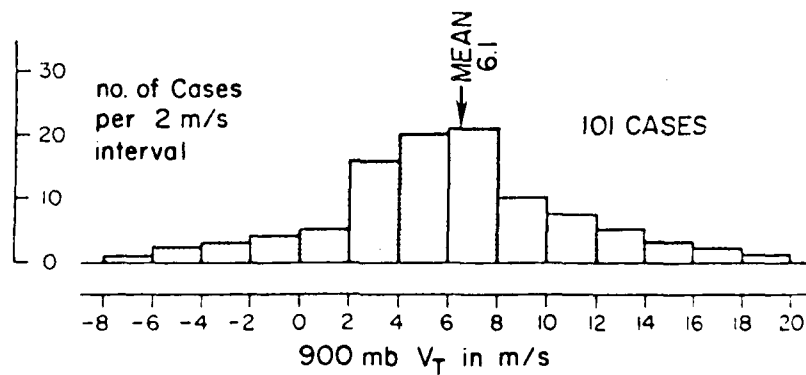
Fig. 61. Distribution of 900 mb individual tangential wind values about the mean of 101 soundings contained in Octant 1 of the 9-11° radial belt of 1961-1974 hurricanes south of 30°.

TABLE 9

Approximate standard deviations of various wind components from wind averages at individual levels (in m/s) for all our tropical cyclone data sets.

	900 mb	500 mb	200 mb
Zonal wind (u)	~5	~6	~10
Meridional wind (v)	~5	~5	~10
Tangential wind (V_θ)	~7	~7	~10
Radial wind (V_R)	~7	~7	~10

average are shown in Fig. 61.

Table 10 lists the typical magnitude of individual wind component standard deviations from octant averages at 900 mb, 500 mb and 200 mb levels for our various data sets of the western Atlantic and western Pacific. Tables 11 and 12 give the typical standard deviations of pressure height and temperatures at 900 mb, 500 mb and 200 mb for our tropical data sets. Table 13 gives the usual standard deviation of specific humidity (q) and relative humidity at 900 mb, 700 mb and 500 mb for nighttime soundings. Parameter deviations to the poleward side are typically larger by 25-50% than parameter deviations on the equatorward side.

TABLE 10

Approximate standard deviations of various wind components from individual octant wind averages at specific levels in m/s for all of our data sets.

	900 mb	500 mb	200 mb
Zonal wind (u)	~5	~5	~8
Meridional wind (v)	~5	~5	~8
Tangential wind (V_T)	~5	~5	~8
Radial wind (V_R)	~5	~5	~8

TABLE 11

Approximate standard deviations of pressure level heights (in meters) from radial belt and octant averages for all our tropical cyclone data sets.

	900 mb	500 mb	200 mb
Standard deviation from belt averages	∿30	∿30	∿55
Standard deviation from individual octant averages	∿25	∿25	∿50

TABLE 12

Approximate standard deviations of temperature (in $^{\circ}$C) from radial belt and octant averages for all of our tropical cyclone data sets.

	900 mb	500 mb	200 mb
Standard deviation from belt average	∿1.0	∿1.2	∿1.4
Standard deviation from individual octant average	∿0.7	∿0.9	∿1.2

TABLE 13

Approximate standard deviations of specific humidity (gm/kg) relative humidity for radial belt and octant averages for all of our tropical cyclone data sets. Only nighttime soundings have been used.

	900 mb	700 mb	500 mb
Standard deviation from belt average	∿2.0/12	∿1.3/14	∿0.7/ 17
Standard deviation from individual octant average	∿1.4/8	∿0.9/10	∿0.6/15

The more research and the more stratifications we make with these rawinsonde data sets the more confident we become as to the authenticity of the composite averages. We have now made over three hundred rawinsonde composite runs on various tropical weather systems and tropical cyclones over the last 12 years. Repeatability of results from independent

data sets consistently occurs in parameters which are required or expected to be similar. For instance, the integrated tropospheric mass divergence of data sets very closely balances itself to zero when the data sample is sufficiently large. Nonrepresentative data and sounding errors average themselves out in the large data sample and are believed to be random. Levels of inflow and outflow are quite consistent. Momentum, energy and water budgets can be consistently and reasonably made. The reader should review a number of our project reports over the last decade for more information on the basic consistency of the composited rawinsonde data sets.

As an example of some of the expected data composite consistencies one could compare independent data sets which are expected to yield similar results. For instance, 14 years of hurricane composited "even-day" vs. "odd-day" parameters should indicate very similar values. Figures 62 to 67 show that cross sections of tangential and radial wind components and temperature are almost identical. Similarly, a comparison of the "even-day" vs. "odd-day" plan view 200 mb outflow patterns of radial and tangential wind are almost identical as can be seen in Figs. 68 to 71. Plan views of other parameters at other levels (not shown) shown like similarity.

It is observed that the strong winds of the hurricane-typhoon do not experience much of a diurnal variation in wind speed. 00Z vs. 12Z composited data sets of tangential winds are very similar (see Chapter 3). Figures 72 and 73 show cross-section analysis of tangential wind for independent data sets of 00Z and 12Z for 14 years of west Atlantic hurricanes and for 10 years of west Pacific typhoons. 00Z and 12Z values, as expected, are almost identical.

76
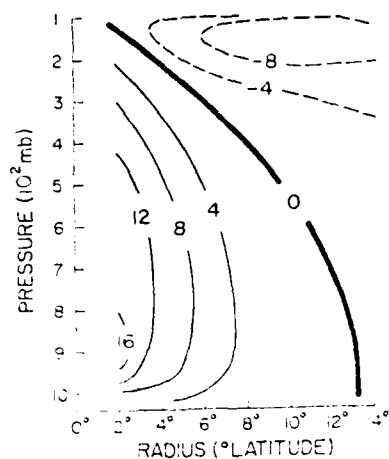
Fig. 62. Cross-section of rawinsonde composite of all 1961-1974 hurricane (<30°N) tangential winds (in m/s) on even days.
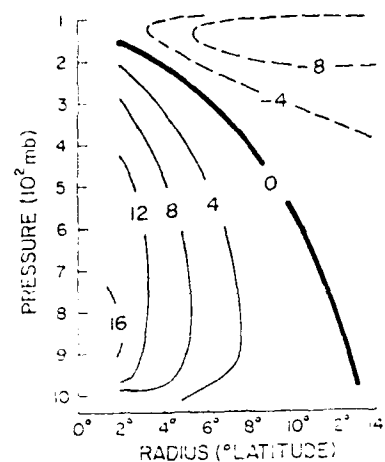
Fig. 63. Same as Fig.62 but for odd days.
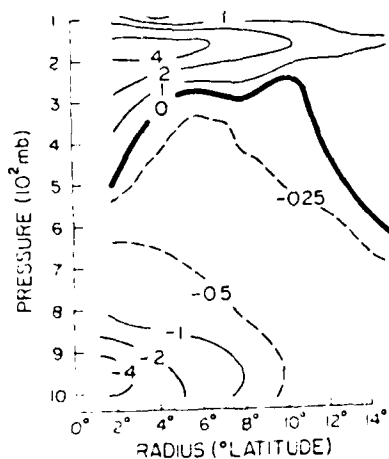
Fig. 64. Cross-section of rawinsonde composite of all 1961-1974 hurricane (<30°N) radial winds (in m/s) on even days.
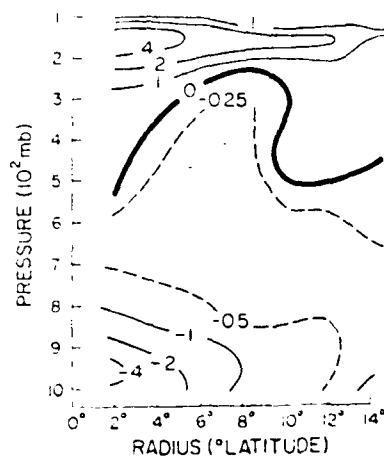
Fig. 65. Same as Fig.64 but for odd days.
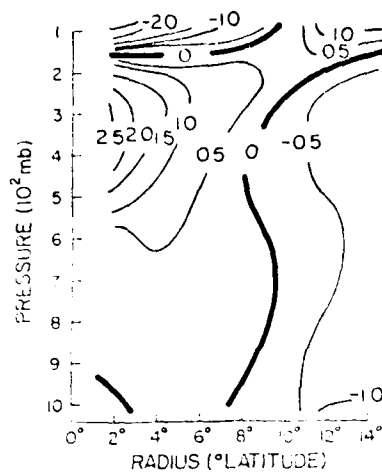
Fig. 66. Cross-section of rawinsonde composite of 1961-1974 hurricane (<30°N LAT.) of temperature deviation (in °C) on _even_ days.
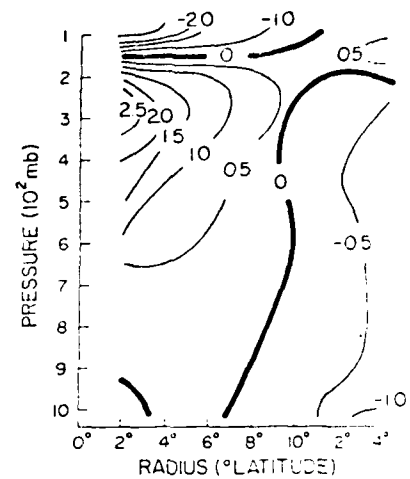
Fig. 67. Same as Fig. 66 but for _odd_ days.

Such similarity of even-day vs. odd-day hurricane results and of 00Z vs. 12Z typhoon and hurricane results from independent data sets should (in the authors' view) lend confidence to the rawinsonde compositing philosophy which has been espoused by our research group for the last decade.
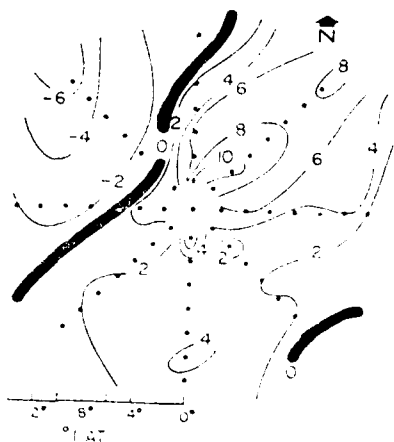
Fig. 68. Plan view of rawinsonde composite of 1961-1974 hurricane (<30° LAT.) 150 mb level radial wind (in m/s) on even days.

Fig. 69. Same as Fig. 68 but for odd days.
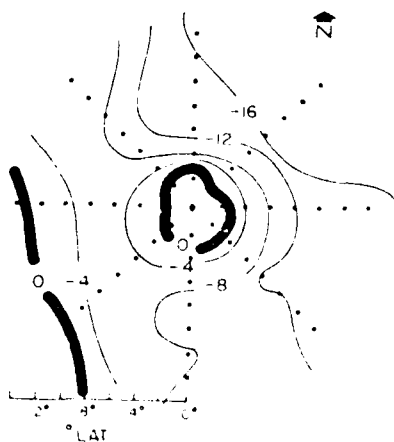
Fig. 70. Plan view of rawinsonde composite of 1961-1974 hurricane (<30°LAT.) 150 mb level tangential wind (in m/s) on even days.
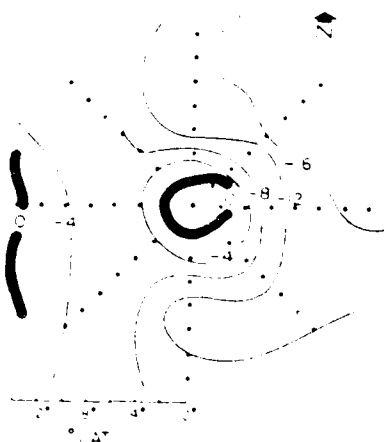
Fig. 71. Same as Fig. 70 but for odd days.
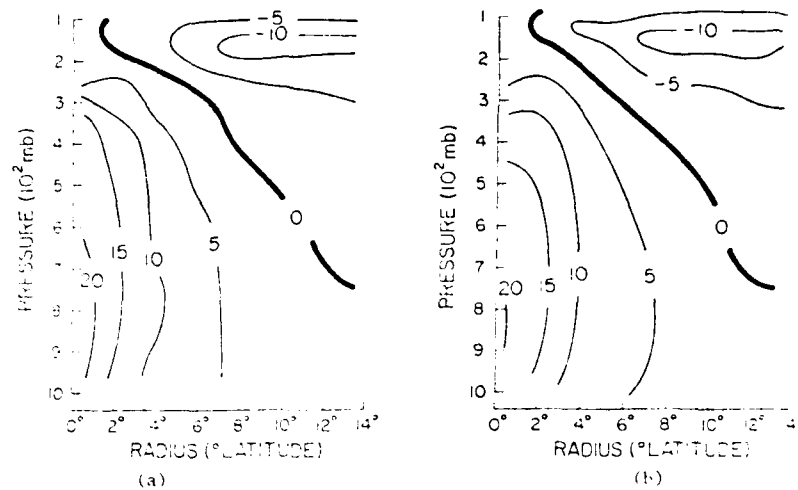
Fig. 72. Composite tangential wind field at 12Z (∿07 LT) - diagram (a)
and at 00Z (∿19 LT) diagram (b) for all west Atlantic hurri-
canes (< 30°LAT.) during the period of 1961-1974.
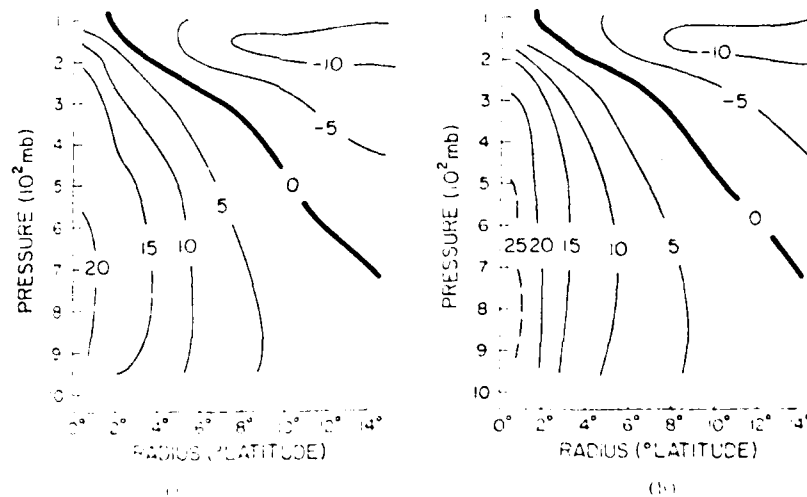
Fig. 73. Same as Fig. 72 but for west Pacific typhoons at 00Z (∿10 LT)-
diagram (a) and 12Z (22 LT) - diagram (b).

5.1 Statistical Procedures (by P. Mielke)

In meteorological composite studies which are concerned with inter-
pretation of large quantities of data a number of measured responses
are obtained from each object in question (an observational unit). An
immediate example of a number of measured responses for a given object
is rawinsonde data (here the object is a specified location and time
increment). To avoid making the unjustified (but convenient) assumption
that the joint distribution of these various dependent response mea-
surements (transformed or otherwise) is multivariate normal, one
naturally seeks alternative multivariate inference procedures which
beneficially replace MANOVA, Hotelling's T^2, and other related techniques
based on the multivariate normal distribution (cf. Morrison, 1967).
For this purpose, a large number of multivariate nonparametric and
permutation procedures have been developed (cf. Puri and Sen, 1971).
An additional class of conceptually simple permutation procedures des-
ignated multi-response permutation procedures (MRPP) appears to be a
very useful tool for detecting the multivariate differences anticipated
with the present type of study. Though complete details of MRPP are
described elsewhere (Mielke et al., 1976; Mielke, 1979b), the following
brief description of MRPP is given.

Let $\Omega = (\omega_1, \ldots, \omega_N)$ be a finite population of N objects, let
$x_I' = (x_{1I}, \ldots, x_{rI})$ denote r commensurate response measurements (or
residuals adjusted by predictors) for object ω_I (I = 1, ..., N), and let
$\ldots$ be an exhaustive partitioning of Ω into g+1 disjoint sub-
sets. Also let $\Delta_{I,J}$ be a monotone increasing function of
between ω_I and ω_J which is zero when the normed dis-
tance form of $\Delta_{I,J}$ in this discussion is confined to:

$$\Lambda_{I,J} = [\sum_{k=1}^{r} (x_{kI} - x_{kJ})^2]^{v/2}$$

where $v > 0$. The recommended version of MRPP (Mielke, 1979b; O'Reilly and Mielke, 1980) is based on the statistic given by

$$\delta = \sum_{i=1}^{g} (n_i/K)\xi_i$$

where $\xi_i = \binom{n_i}{2}^{-1} \sum_{I<J} \Lambda_{I,J} I_{S_i}(\omega_I) I_{S_i}(\omega_J)$ is the average distance for all pairs of objects in subgroup S_i ($i = 1,\dots, g$), $\sum_{I<J}$ is the sum over all I and J such that $1 \leq I \leq J \leq N$, $I_{S_i}(\omega_I)$ is 1 if ω_I belongs to subgroup S_i and 0 otherwise for $I = 1,\dots, N$, $n_i \geq 2$ is the number of (classified) objects in subgroup S_i ($i = 1,\dots, g$), $K = \sum_{i=1}^{g} n_i$, and $n_{g+1} = N-K$ is the number of remaining (unclassified) objects in subgroup S_{g+1}. The underlying permutation distribution of δ implies that each of the possible $M = N!/(\prod_{i=1}^{g+1} n_i!)$ allocation combinations of the N objects to the $g+1$ subgroups will occur with equal chance. With the underlying permutation distribution of δ assumed, let μ_δ, σ^2_δ and γ_δ respectively denote the mean, variance and skewness of δ. If δ_i denotes the ith value among M possible values of δ, then

$$\mu_\delta = M^{-1} \sum_{i=1}^{M} \delta_i, \quad \sigma^2_\delta = M^{-1} \sum_{i=1}^{M} \delta_i^2 - \mu_\delta^2 \quad \text{and}$$

$$\gamma_\delta = (M^{-1} \sum_{i=1}^{M} \delta_i^3 - 3\mu_\delta \sigma^2_\delta - \mu_\delta^3)/\sigma_\delta^3.$$

Efficient computation techniques for obtaining μ_δ, σ^2_δ and γ_δ for a realized set of data are described by Mielke (1979b) and Mielke et al.

(1976). A simple intuitive interpretation of MRPP results is that
small values of δ infer a concentration of response measurements within
the g subgroups.

Because the calculation of the M possible values of δ is not com-
putationally feasible even for relatively small values of N, an approx-
imation of the underlying permutation distribution of δ is indispensable.
The standardized test statistic given by

$$T = (\delta - \mu_\delta)/\sigma_\delta$$

is approximately distributed as the Pearson type III distribution with
parameter $\gamma = \gamma_\delta$. In particular, this distribution compensates for the
fact that the underlying permutation distribution of δ is often very
skewed in the negative direction (cf. Mielke, 1979b; O'Reilly and Mielke,
1980). If K = N (as the case would be with most comparisons), then
even the asymptotic value of γ_δ is usually less than $-(g-1)^{-1}$. As pre-
viously mentioned, specific details for computing γ_δ are given by Mielke
(1979b) and Mielke et al. (1976).

Being a permutation based technique, MRPP routinely avoids specific
problems associated with narrowly specified null hypothesis features
(i.e., level of significance being specified by a fabricated null dis-
tribution) which are assumed in parametric inference techniques. In
addition, the efficient discrimination characteristics of MRPP are
consistent with the fact that special cases of MRPP coincide with well
known parametric and nonparametric techniques which provide optimum
efficiency under prescribed conditions. For example, if $v = 2$, $r = 1$,
$g \geq 2$ and S_{g+1} is empty, then the univariate version of MRPP is equi-
valent to the permutation versions of the classical two-sample t and

one-way ANOVA class of tests. Also if $v = 2$, $r = 1$, $g \geq 2$, S_{g+1} is

empty and the univariate response measurements are replaced by ranks,

then the resulting univariate nonparametric version of MRPP is equivalent

to the two-sample Wilcoxon (Mann-Whitney) and Kruskal-Wallis class of

tests. Instead, if $v = 1$, $r = 1$, $g \geq 2$, S_{g+1} is empty and the univariate

response measurements are replaced by ranks, then the resulting univariate

nonparametric version of MRPP (Mielke, 1979a) is substantially superior

to the case with $v = 2$ under some general situations. Specifically the

nonparametric version of MRPP with $v = 1$ is superior to $v = 2$ for

detecting location shifts associated with either a double exponential

distribution or a U-shaped distribution (even when logistic and normal

distributions are considered, the case with $v = 2$ shows only a minor

improvement over the case with $v = 1$). A point worth mentioning is

that none of the known types of nonparametric tests coincide with the

present univariate nonparametric versions of MRPP indexed by $v \cdot 0$

(with the obvious exception of $v = 2$).

MRPP is a general purpose inference technique and consequently

possesses a broad spectrum of potential applications. Though special

univariate cases of MRPP are equivalent to the permutation versions of

commonly employed statistical techniques (e.g., Mann-Whitney, Kruskal-

Wallis, two-sample t, and one-way ANOVA tests), the extent of possible

univariate and multivariate versions of MRPP is enormous (i.e., the

choice of $\Delta_{I,J}$ is essentially unlimited).

5.2 Examples of Initial Statistical Analysis with MRPP Technique

We have tested the MRPP statistical scheme on composited rawinsonde data from individual storm octants for our 14 year west Atlantic data set. Two pairs of data sets have been initially chosen and statistically tested. One pair of data sets is expected to be similar and the other pair of data sets are expected to be different. The paired data sets expected to be similar are those which compare "even" (E) with "odd" (OD) hurricane days. The paired sets expected to be different are those which compare weak tropical disturbances which later develop into tropical cyclones (data set D) with tropical disturbances which do not show such development (data set N).

Figure 74 shows plan views of the probabilities that the zonal u (top) and meridional v (bottom) components of the wind in various octants are similar at 900, 500 and 200 mb. Data are for the radial belt of $5-7^o$ radius. Approximately 15 to 60 rawinsonde reports were in each octant and level sample. Figure 75 shows similar information on Temperature (T) and pressure-height (Ht) between these data sets.

Table 14 shows the probability in each octant of the $5-7^o$ radius belt that tangential (V_θ) and radial (V_r) component of the wind, temperature (T), and pressure-height (Ht) are the same. The four octant combined belt probabilities that these two paired data sets are similar is also given.

These r sults show us that for most parameters and levels the $5-7^o$ radius average data of the even vs. odd day hurricane data samples are very similar. By contrast, the same $5-7^o$ radius data information applied to the developing vs. non-developing tropical disturbances shows very distinct differences in tangential wind (V_θ) and height in

HURRICANE
EVEN VS ODD DAYS

DEVELOPING VS NON-DEVELOPING

.61
.38

1.00
.82

1.00
.47

.65
.29

900 mb

.00016
.16

.82
.00004

.07
.19

.11
.72

U WIND COMPONENT

V WIND COMPONENT

.33
.09

.55
.22

.27
.80

.33
.28

500 mb

.02
.01

.91
.003

.64
.06

.03
.77

.30
.60

1.00
.37

.38
.23

.76
.31

200 mb

.46
.17

.76
.18

1.00
.03

.36
.31
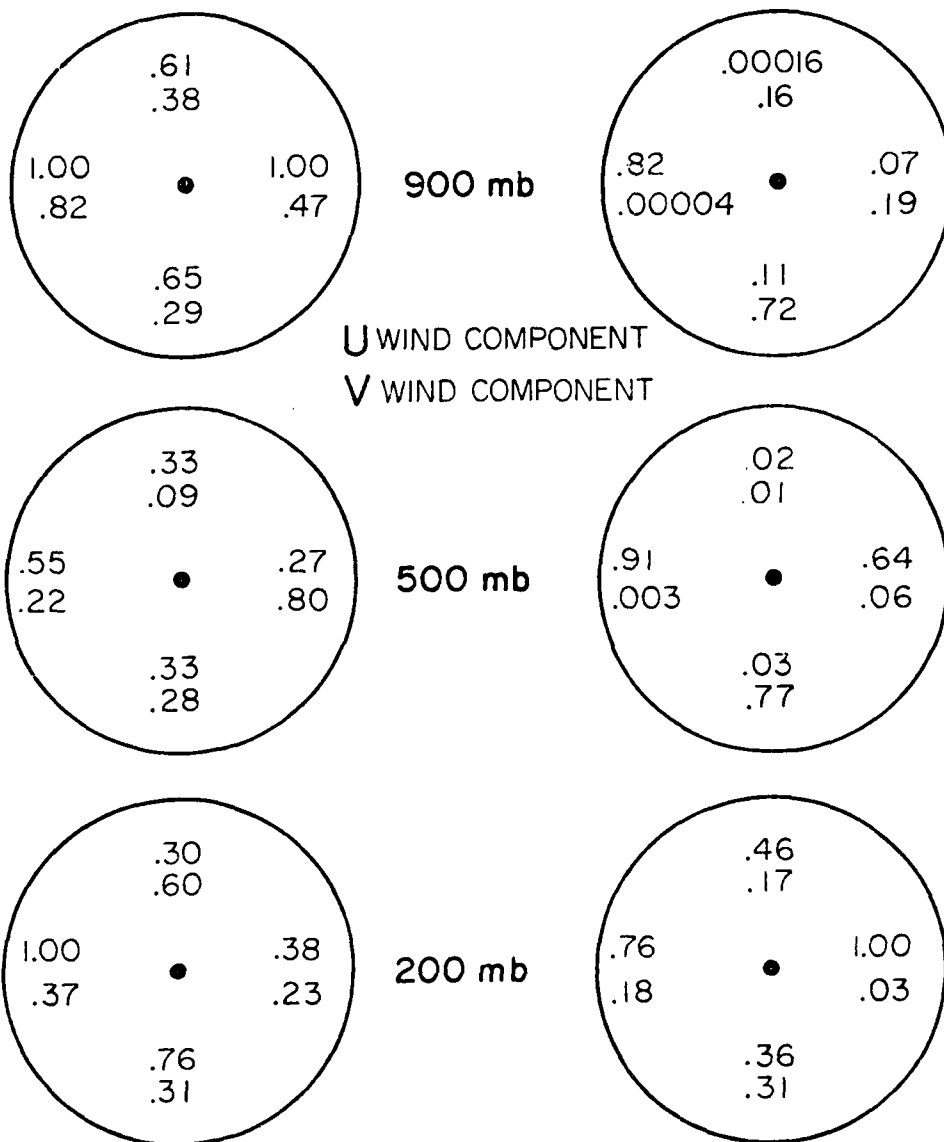
Fig. 74.   MRPP determined probability that zonal (u) - top - and
meridional (v) - bottom - wind components are the same for
the hurricane "even" vs. "odd" day comparison (left set of
circles) and for the developing vs. non-developing tropical
disturbances at the three levels of 900 mb, 500 mb and 200 mb.
Top figures are for Octant 1, left figures are for Octant 3,
bottom figures are for Octant 5, and right figures are for
Octant 7.

Fig. 75. Same as Fig. 74 but for the parameters of temperature and height.

TABLE 14

MRPP probability for developing vs. non-developing disturbance (left figure) and even vs. odd day (in parenthesis) being different for various parameters, levels, and octants. Four octant combined probabilities are also shown as are North, West and 900 mb, 500 mb combined probability for tangential wind (V_θ) and pressure-height (Ht).

Tangential Wind (V_θ)

	900 mb		500 mb		200 mb	
N. Octant	.00016	(.61)	.02	(.33)	.46	(.30)
W. Octant	.00004	(.82)	.003	(.22)	.18	(.37)
S. Octant	.11	(.18)	.03	(.33)	.36	(.76)
E. Octant	.19	(1.00)	.06	(.27)	.03	(.38)
Combined 4 Octant Probability	.000032	(.78)	.000099	(.26)	.081	(.919)

Radial Wind (V_r)

	900 mb		500 mb		200 mb	
N. Octant	.16	(.38)	.01	(.09)	.17	(.60)
W. Octant	.81	(1.00)	.91	(.55)	.76	(1.00)
S. Octant	.72	(.29)	.77	(.28)	.31	(.31)
E. Octant	.07	(1.00)	.64	(.27)	1.00	(.38)
Combined 4 Octant Probability	.26	(.82)	.21	(.19)	.95	(.72)

Temperature (T)

	900 mb		500 mb		200 mb	
N. Octant	.32	(.38)	.06	(.52)	.02	(.71)
W. Octant	.39	(.40)	.09	(.43)	.81	(.38)
S. Octant	.09	(.18)	.65	(.50)	.66	(.41)
E. Octant	.17	(.26)	.02	(.86)	.32	(.74)
Combined 4 Octant Probability	.13	(.27)	.014	(.80)	.18	(.75)

Height (Ht)

	900 mb		500 mb		200 mb	
N. Octant	.002	(.26)	.002	(.20)	.06	(.77)
W. Octant	.05	(.42)	.01	(.08)	.03	(.22)
S. Octant	.77	(.69)	.65	(.75)	.41	(.25)
E. Octant	1.00	(.79)	.58	(1.00)	.57	(.87)
Combined 4 Octant Probability	.015	(.69)	.0026	(.36)	.049	(.58)

Combined N and W Octants for 900 mb and 500 mb

Developing vs. Non-developing Disturbances
For V_θ .0000000017
For Ht. .0000041

the North and West quadrants at 900 mb and 500 mb. Probabilities that
the tangential wind components are similar are .00016 (N. Octant - 900 mb),
.00004 (W. Octant - 900 mb), .02 (N. Octant - 500 mb) and .003 (W. Octant -
500 mb). The probabilities that the pressure-heights at these octants
and levels are similar is also quite low - .002, .05, .002 and .01. By
contrast, probability of differences in these octant's radial wind and
temperatures are very much higher - .16, .81, .01, .91 (radial winds)
and .32, .39, .06, .09 (temperatures).

When the four separate octant $5-7^O$ radius statistics are combined,
the statistical probability that the $5-7^O$ radial belt V_θ winds are the
same for the developing and non-developing disturbances is .000032 (at
900 mb) and .000099 (at 500 mb). Comparable values for the "odd" vs.
"even" day analysis is .78 and .26.

By combining the tangential wind (V_θ) and heights (ht) in the North
and West octants at 900 mb and 500 mb, the probability that the $5-7^O$
radius V_θ and Ht are similar is < .0000000017 (for V_θ) and .0000041
(for Ht). Comparable parameter probabilities for the "even" vs. "odd"
day sample are .58 and .12. We can thus be quite confident that V_θ and
Ht are primary distinguishing components of the developing and non-
developing disturbances. Although these results well agree with our
previous information on the mean parameter differences, they, for the
first time, offer us quantitative statistical verification.

Summary. We can thus in an objective and quantitative way determine
what are the parameters which best distinguish between data sets. These
statistical results give much physical insight into the real physical
processes which are occurring and appear to offer much promise if
applied to a variety of other data sets at other radial intervals,
octants, levels, etc. We thus have a greater confidence and understanding
of our composited (or averaged) rawinsonde information.

6.   TROPICAL CYCLONE LOOPING/STALLING MOTION AS RELATED TO SURROUNDING
      LARGE-SCALE CIRCULATION PATTERNS - By Jianmin Xu and W. M. Gray

6.1 Background

Major forecasting problems occur when tropical cyclones
undergo looping/stalling motion. It is important to recognize the
distinct synoptic situations which occur with such stalling and looping
situations so that better forecasts can be made.

This chapter investigates the typical 500 mb and surface surrounding
synoptic scale flow patterns associated with looping motion storms in
the northwest Pacific and west Atlantic. Looping motion is stratified by
clockwise (C) and counterclockwise (CC) looping, and by diameter and
period of looping. It is shown that the type of looping motion which
occurs is dependent upon the storm's latitudinal position relative to
the subtropical ridge(SR), strength and longitude of upper level troughs
and ridges to the poleward side, motion of such troughs and ridges, and
(in cases of double vortex looping) by the proximity of a neighboring
cyclone, etc. This information shows what a profound influence the
surrounding synoptic scale wind patterns have on tropical cyclone motion.
Looping can even be correlated to trough position in the opposite side
of the globe. Significant looping differences are found between Atlantic
and Pacific cyclones. The surrounding cyclone flow patterns which are
characteristic of different types of looping motion has yet to be well
specified and compared with each other.

6.2 Data Sources

All tropical cyclone tracks in the West Atlantic and West Pacific

TABLE 15

Western Pacific Looping Cyclones

Year	Cyclone Intensity[1]	Cyclone Name	Date/Time of Start of Looping	Date/Time of End of Looping	Period of Looping Days	Location of Looping Lat.	Long.	Diameter of Loop °Lat.	Looping Direction[2]	Type of Looping[3]
1957	S	Irma	10. 8.12	10.10.00	1.0	14.5	117.5	1	CC	S
1958	T	Marie	10.26.12	10.28.12	1.0	17.0	155.0	1	CC	D
1958	S	Pamela	11.30.12	12. 2.12	1.5	18.0	138.5	1	C	S
1960	T	Polly	7.22.00	7.25.00		23.5	127.0	0.5	CC	S
1960	T	Bess	8.22.12	8.23.12	2.0	35.5	154.0	2.5	C	N
1960	T	Della	8.21.12	8.25.12	2.5	22	137.0	1	CC	N
1961	S	Grace	7.21.00	7.23.00	1.5	22.5	127.5	1	CC	S
1961	T	Helen	7.30.00	7.31.12	1.0	28.0	129.5	0.5	CC	D
1961	T	Lorna	8.21.12	8.22.12	0.8	16.5	127.5	0.5	CC	X
1961	T	Clara	10.27.00	10.28.12	1.0	19.0	169.0	1	C	N
1962	T	Georgia	4.16.12	4.17.12	1.0	9.5	140.0	1	CC	S
1962	T	Kate	7.20.00	7.21.12	1.0	19.5	119.0	0.5	CC	S
1962	T	Sarah	8.16.00	8.18.12	2.5	23.5	125.0	1	CC	D
1962	T	Gilda	10.21.00	10.24.00	0.5	15.5	132.5	0.5	CC	X
1963	S	Lora	10.10.12	10.13.12	2.5	13.5	143.5	2	CC	S
1964	S	Tess	5.14.12	5.17.12	3.0	12.0	130.5	2	∞	S
1964	T	Kathy	8.17.00	8.21.12	5.0	26.0	129.0	5	CC	D
1964	T	Kate	11.13.00	11.15.00	3.0	9.5	112.5	2	CC	S
1964	S	Opal	12.14.12	12.15.12	0.8	15.0	120.5	1	CC	X
1965	T	Ivy	7.28.00	7.31.12	5.0	13.5	128.5	5	CC	D
1965	T	Jean	7.31.12	8. 1.00	0.5	17.5	130.5	0.5	CC	X
1965	S	Elaine	11. 9.12	11.11.00	0.8	17.0	112.5	1	CC	X
1966	S	Winnie	8.20.12	8.22.00	1.0	28.0	130.0	1	CC	D
1966	T	Alice	8.26.12	8.28.12	2.5	28.0	145.0	2	C	N
1966	T	Elsie	9.11.12	9.13.12	2.0	18.5	118.0	1	C	D
1966	S	June	9.24.12	9.26.00	1.0	19.0	137.5	0.5	CC	S
1966	T	Kathy	10. 9.00	10.12.12	3.0	19.5	151.0	1	C	N

TABLE 15 (cont'd)

Year	Cyclone Intensity[1]	Cyclone Name	Date/Time of Start Looping	Date/Time of End of Looping	Period of Looping Days	Location of Looping Lat.	Long.	Diameter of Loop °Lat.	Looping Direction[2]	Type of Looping[3]
1967	T	Violet	4. 9.00	4.10.12	0.5	21.0	118.0	0.5	C	X
1967	S	Louise	8.16.12	8.18.12	2.0	19.0	142.0	1	∞	D
1967	T	Wanda	9.19.12	9.21.12	2.5	23.0	142.5	1	∞	D
1967	S	Amy	9.28.12	10. 1.12	3.5	20.5	158.5	2	C	N
1968	T	Jean	4.13.12	4.15.00	0.8	21.0	145.0	0.5	CC	X
1968	D	Mary	7.28.00	7.30.12	2.5	33.0	132.0	3	CC	X
1968	S	Nadine	7.21.12	7.23.00	1.5	18.0	126.5	1	CC	D
1968	S	Nadine	7.26.00	7.28.00	2.0	21.5	117.0	2	CC	D
1968	S	Polly	8. 6.00	8. 7.12	1.5	24.5	156.0	0.5	C	N
1968	S	Polly	8.14.00	8.15.12	1.5	27.5	124.0	1	CC	N
1968	S	Trix	8.23.12	8.27.00	3.0	24.0	129.5	2	CC	S
1968	T	Wendy	8.29.00	8.30.00	0.5	16.0	146.0	0.5	CC	X
1968	T	Wendy	9. 4.00	9. 5.00	0.5	21.0	123.5	1	CC	X
1968	T	Agnes	9. 4.00	9. 7.12	2.5	20.0	137.0	1	CC	S
1968	T	Bess	9. 1.12	9. 2.12	0.5	19.5	114.0	0.5	CC	X
1968	T	Gloria	10.22.00	10.23.00	0.8	26.0	133.0	0.5	CC	X
1968	D	Mamie	11.14.00	11.16.00	0.5	13.0	130.5	0.5	C	X
1969	T	Phillis	1.20.12	1.22.00	0.5	14.0	149.5	0.5	C	X
1969	T	Grace	9.30.00	10. 2.00	5.5	25.0	162.0	5	∞	N
1969	S	Lorna	11.26.00	11.27.00	1.0	14.0	131.5	0.5	C	S
1970	S	Nancy	2.20.00	2.21.00	0.5	8.5	147.5	0.5	CC	X
1970	T	Anita	8.17.12	8.18.12	0.5	21.0	139.0	0.5	CC	X
1970	S	Ellen	9. 5.12	9. 6.00	0.5	25.0	125.0	2	CC	X
1970	T	Hope	9.23.00	9.24.00	0.3	20.0	149.0	0.5	C	X
1970	S	Marge	11. 3.00	11. 6.00	1.5	15.0	115.5	0.5	CC	S
1971	S	Sarah	1. 9.12	1.10.12	0.5	11.0	136.5	0.5	CC	C
1971	D	Thelma	3.18.00	3.19.00	0.8	10.5	129.5	1	∞	X
1971	T	Elaine	10. 5.12	10. 7.12	0.3	16.5	115.5	0.5	CC	X
1971	T	Faye	10.10.12	10.12.12	3.0	14.5	120.5	3	CC	S

TABLE 15 (cont'd)

Year	Cyclone Intensity[1]	Cyclone Name	Date/Time of Start Looping	Date/Time of End of Looping	Period of Looping Days	Location of Looping Lat.	Long.	Diameter of Loop °Lat.	Looping Direction[2]	Type of Looping[3]
1971	T	Irma	11. 8.00	11. 9.12	0.3	8.0	141.5	0.5	CC	X
1972	D	Nina	6. 1.00	6. 2.00	1.5	9.0	143.5	1	CC	X
1972	T	Rita	7.11.12	7.13.00	1.0	18.0	132.5	0.5	CC	D
1972	T	Rita	7.21.00	7.25.00	4.0	27.0	126.5	3	CC	D
1972	T	Susan	7. 9.12	7.14.00	1.5	22.0	117.0	0.5		S
1972	S	Grace	9.12.00	9.16.12	5.0	20.0	127.0	3	CC	D
1972	T	Ida	9.16.00	9.19.12	4.0	21.0	156.5	3	C	N
1972	S	Helen	9.17.12	9.19.12	1.5	42.5	139.0	2	CC	N
1972	S	Nancy	10.21.12	10.23.00	2.5	20.5	143.0	2	CC	N
1972	S	Violet	12.13.12	12.14.12	0.8	9.5	170.5	0.5	C	X
1973	T	Ellen	7.20.12	7.28.00	7.0	32.0	128.0	5	∞	N
1973	S	Iris	8.10.12	8.14.00	2.0	23.5	131.0	0.5		D
1973	S	Nora	10. 2.12	10. 4.12	0.5	11.0	133.5	0.5	CC	X
1974	S	Mary	8.19.12	8.25.00	8.0	28.0	126.0	9	CC	N
1974	D	Polly	8.26.00	8.26.12	0.5	15.5	146.5	0.5	CC	X
1975	S	Lola	1.26.00	1.28.00	1.0	16.0	112.5	1	C	S
1975	D	Flossie	10.20.00	10.21.12	0.5	15.5	116.5	0.5	C	X
1975	S	Grace	10.24.00	10.30.00	6.0	8.0	129.0	2		S
1975	S	June	11.16.00	11.18.00	1.0	6.5	142.5	0.5	C	X
1976	S	Marie	4. 3.00	4. 7.00	1.5	8.5	140.5	0.5	CC	S
1976	S	Olga	5.19.00	5.20.00	1.0	15.5	124.5	0.5	CC	S
1976	T	Pamela	5.14.12	5.18.00	3.5	7.5	152.0	3	CC	X
1977	S	Diana	9.16.12	9.21.00	1.0	17.0	116.0	1	CC	S
1977	S	Ivy	10.21.00	10.23.00	1.0	17.5	146.0	1	CC	S
1977	D	Jean	11. 2.00	11. 3.00	1.5	27.0	146.5	1	CC	X
1977	T	Mary	12.24.00	12.25.00	0.5	13.0	169.5	0.5	C	X

TABLE 15 (cont'd)

[1]T = Typhoon
S = Tropical Storm
D = Depression

[2]C = Clockwise
CC = Counterclockwise
∞ = Irregular looping

[3]N = North of Subtropical Ridge
S = South of Subtropical Ridge
D = Double Vortex Looping
X = Looping less than one day and intensity weaker than tropical storm

TABLE 16

Western Atlantic Looping Cyclones

Year	Cyclone Intensity[1]	Cyclone Name	Date/Time of Start Looping	Date/Time of End of Looping	Period of Looping Days	Location of Looping Lat.	Location of Looping Long.	Diameter of Loop °Lat.	Looping Direction[2]	Type of Looping[3]
1957	S	Frieda	9.20.12	9.24.12	4.5	30.5	69.0	6.5	C	N
1959	H	Gracie	9.24.12	9.27.00	0.5	28.0	73.0	0.5	C	X
1960	D		6.24.12	6.26.00	1.0	28.5	98.5	1	CC	X
1960	D	Florence	9.22.00	9.22.12	1.0	22.5	83.5	1	CC	X
1961	S	Esther	9.21.12	9.25.12	4.5	38.5	68.0	6	C	N
1961	D	Jenny	11. 4.12	11. 7.12	1.5	27.0	45.0	3	CC	X
1962	S	Celia	9.17.00	9.20.12	2.5	30.0	53.0	3	C	N
1963	H	Flora	10. 5.00	10. 9.00	3.0	21.0	77.5	2	C	N
1963	H	Ginny	10.20.00	10.28.00	8.5	31.0	77.0	5	∞	N
1964	D	Isbell	10.11.12	10.12.12	1.5	19.0	86.0	0.5	CC	X
1965	H	Betsy	9. 4.12	9. 6.00	1.5	28.5	75.5	0.5	C	N
1965	H	Carol	9.23.12	9.28.12	3.5	33.5	41.5	1	C	N
1966	H	Inez	10. 3.12	10. 4.12	0.5	25.5	78.5	0.5	CC	X
1966	S	Lois	11. 4.12	11. 7.12	3.5	25.5	53.0	4.5	CC	N
1967	H	Doria	9.11.12	9.17.00	8.0	36.5	72.5	7.0	CC	N
1968	D	Abby	6. 8.12	6.11.12	3.5	34.0	80.5	3.5	C	
1969	H	Inga	9.29.12	10.15.00	14.5	29.5	57.0	10.0	C	N
1969	S	Kara	10.12.00	10.15.00	4.5	33.0	73.0	2.5	∞	D
1969	H	Laurie	10.20.00	10.25.12	5.0	25.0	89.0	5	∞	N
1971	H	Ginger	9.14.12	9.21.12	9.5	37.5	53.5	6.5	C	N
1971	S	Laura	11.16.00	11.19.12	2.0	21.0	83.5	1.5	C	N
1972	H	Betty	8.29.12	9. 1.00	2.5	41.0	34.0	2.5	CC	N
1972	H	Dawn	9. 7.12	9.11.00	3.5	35.0	72.0	4.0	CC	N
1973	S	Delia	9. 5.00	9. 6.00	1.0	28.5	95.5	1.0	CC	N
1974	H	Gertrude	9.30.00	10. 1.00	0.5	11.0	56.5	0.5	CC	S
1976	S	Belle	8. 6.12	8. 8.12	0.5	26.0	73.0	0.5	CC	
1977	S	Clara	9. 9.00	9.11.00	2.0	33.5	63.0	1.5	C	N

TABLE 16 (cont'd)

[1]H = Hurricane
 S = Tropical Storm
 D = Depression

[2]C = Clockwise
CC = Counterclockwise
∞ = Irregular looping

[3]N = North of Subtropical Ridge
 S = South of Subtropical Ridge
 D = Double Vortex
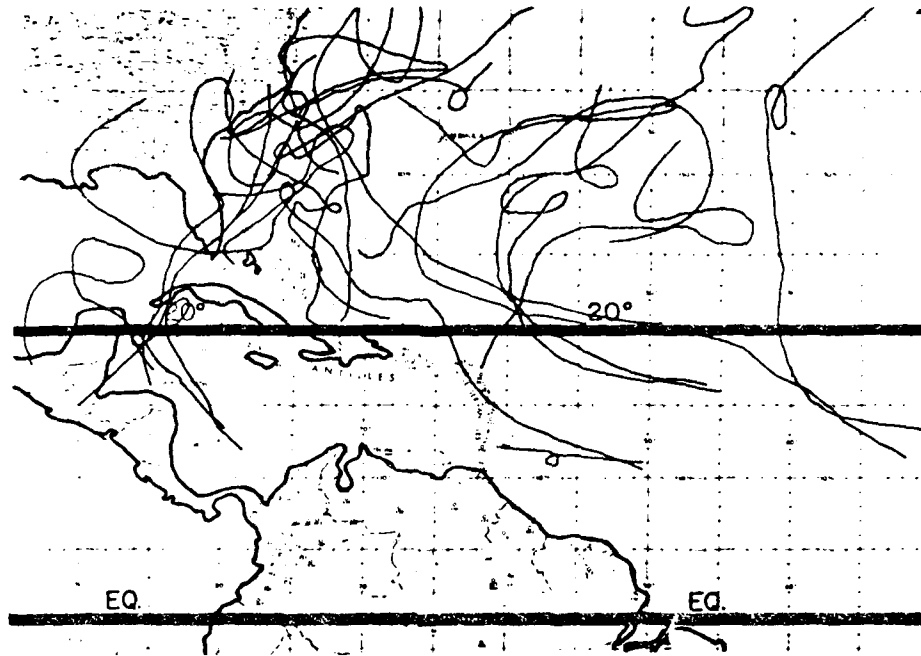 X = Looping less than one day and intensity weaker than tropical storm

Fig. 76. Typical example of tropical cyclones looping tracks in the northwest Atlantic.
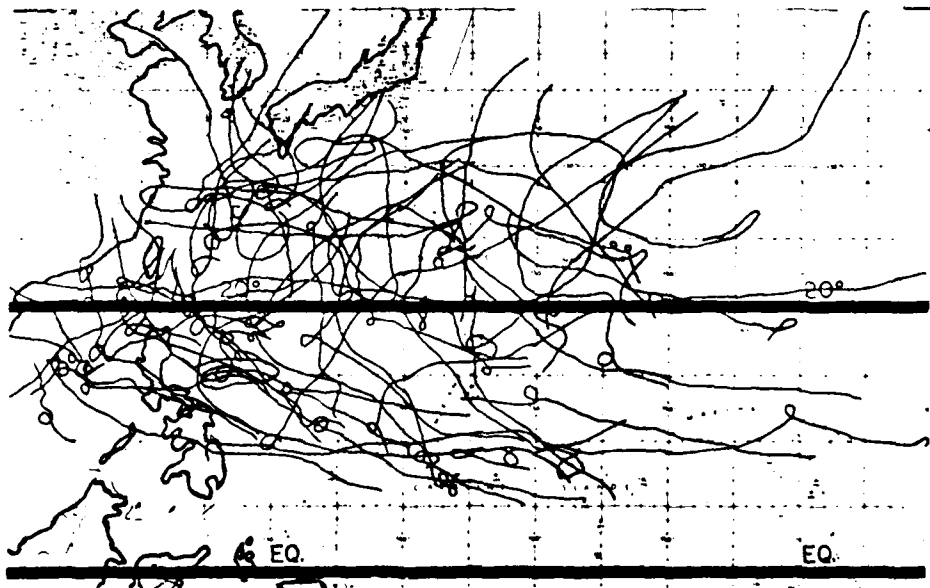

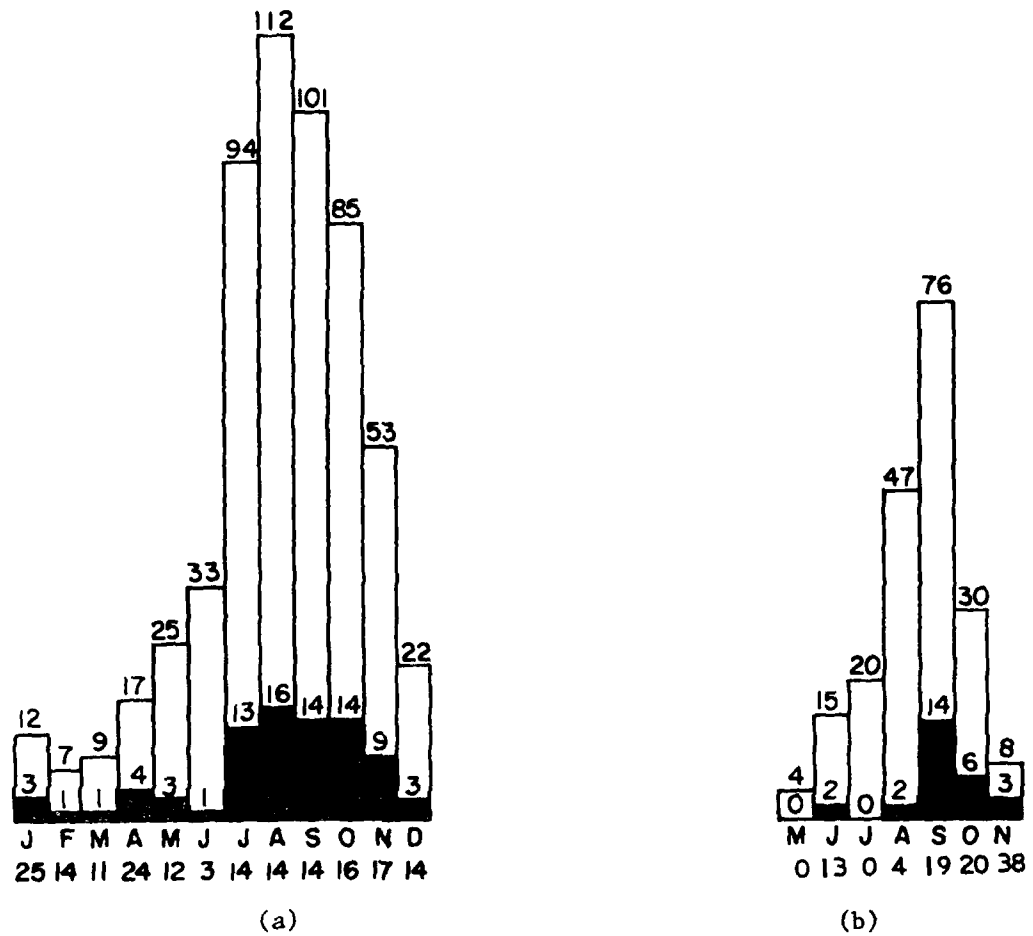Fig. 77. Typical example of tropical cyclone looping tracks in the northwest Pacific.

Fig. 78. Total tropical cyclone occurrence (blank) and looping cyclone
events (shaded) by month during 1957-1977 for the western
Pacific (a) and the western Atlantic (b). The numbers shown
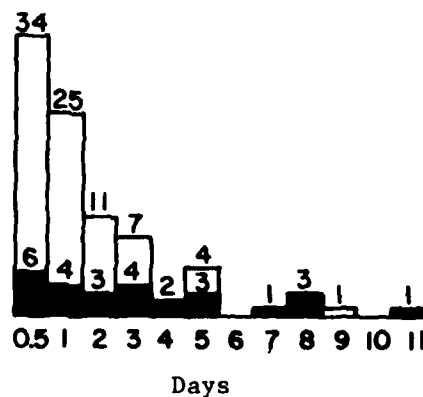at the bottom is the ratio of looping event numbers to total
storm number in percent.

Fig. 79. Distribution of looping period in days for the western Pacific
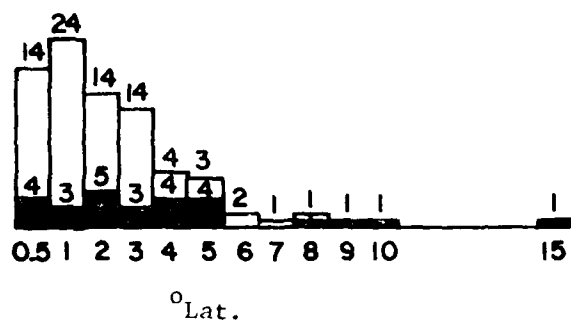(no shading) and western Atlantic (shaded).

Fig. 80. Distribution of looping diameter in °latitude for the west Pacific (no shading) and for the western Atlantic (shaded).
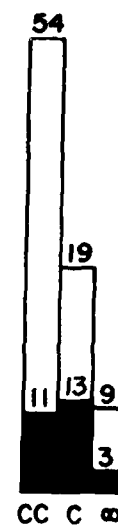
Fig. 81. Direction of looping, clockwise (C), counter-clockwise (CC), and both ways (∞). Unshaded numbers for west Pacific, shaded numbers for west Atlantic.
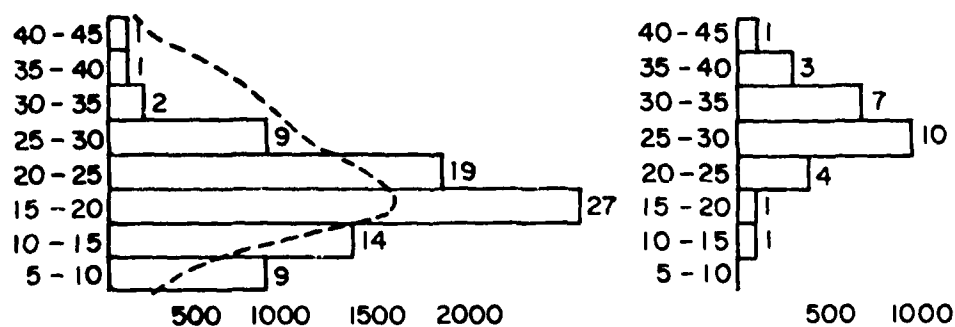

Fig. 82. The latitudinal distribution of tropical cyclone looping storms in the Pacific (left) and in the Atlantic (right). The dashed line of the left diagram shows the latitude distribution of the total tropical storm occurrences during the 21 period of 1949-1969 as indicated by the numbers at the bottom.

during the 21 year period of 1957-1977 were examined for looping motion.
Only named storms are used. In addition, it was required that west
Pacific cyclones underwent a complete circular looping while west
Atlantic cyclones had a circular motion of at least 3/4 of a loop.
Figures 76 and 77 show typical looping motion in the Pacific and Atlantic.

Tables 15 and 16 present information on all the looping cyclones
studied. The start and end time of looping was defined as the time at
which the cyclone lost or gained stable direction and velocity. Looping
time was defined as the period during which the cyclone was in a circular
track. Looping diameters constitute the mean values of the long and
short axes of the track circles. The looping locations were the centers
of the track circles.

6.3 Looping Climatology

There were 82 cyclone loops in the West Pacific and 27 loops in the
West Atlantic during the 21 year period of 1957-1977, or about 4 per
year in the Pacific and 1 per year in the Atlantic. This results in
about one tropical cyclone in seven experiencing a looping motion.
Fig. 78 shows the monthly distribution of looping cyclones to total
tropical cyclones in each ocean basin.

Fig. 79 shows the distribution of looping period in days. Looping
can take anywhere from 1/2 to about 10 days. In the Pacific, the mean
looping period is about 2 days. More than 85% of West Pacific looping
cyclones have looping periods less than 3 days. In the Atlantic, the
mean and 85 percentile looping periods are larger - being 3.7 and 5.0 days
respectively. Figure 80 shows the distribution of the looping diameter.
In the Pacific, the mean looping diameter is only about 1.4° latitude.

More than 85% of the West Pacific looping storms have looping diameter of less than 2^O latitudes. Loops are larger in the Atlantic. Here the mean and 85 percentile loops are of 3.3^O and 7.0^O latitude respectively. Thus, loops are larger in size and take longer in the Atlantic than in the Pacific.

Figure 81 shows the direction of looping. In the Pacific counter-clockwise (CC) loops are more frequent than clockwise (C) ones by a ratio of 2 to 1, while in the Atlantic, clockwise and counterclockwise loops have a similar frequency.

Figure 82 shows the latitudinal distribution of looping storms. Tropical cyclones loop at lower latitudes in the Pacific than in the Atlantic. The mean latitude of looping cyclones in the Pacific is 19° while it is 29° in the Atlantic. Only 5% of the loops in the Pacific occurred to the north of $30^O N$, while in the Atlantic 40 percent did. On the other hand, as many as 60% of the loops in the Pacific occured to the south of $20^O N$, while in the Atlantic only about 7% did. Figure 83 shows the geographic distributions of looping cyclones in both oceans. Looping occurs at significantly higher latitude in the Atlantic and clockwise loops are more prevalent to the east and north. These storm basin and regional looping differences are closely related to the large scale environmental flow fields in which the looping cyclones are embedded in.

6.4 Broadscale Circulation Patterns in Which Looping Occurs

It is well known that the surrounding cyclone "steering" flow patterns are the dominant factor affecting the movement of tropical cyclones. Although this concept is used all the time, it has not yet
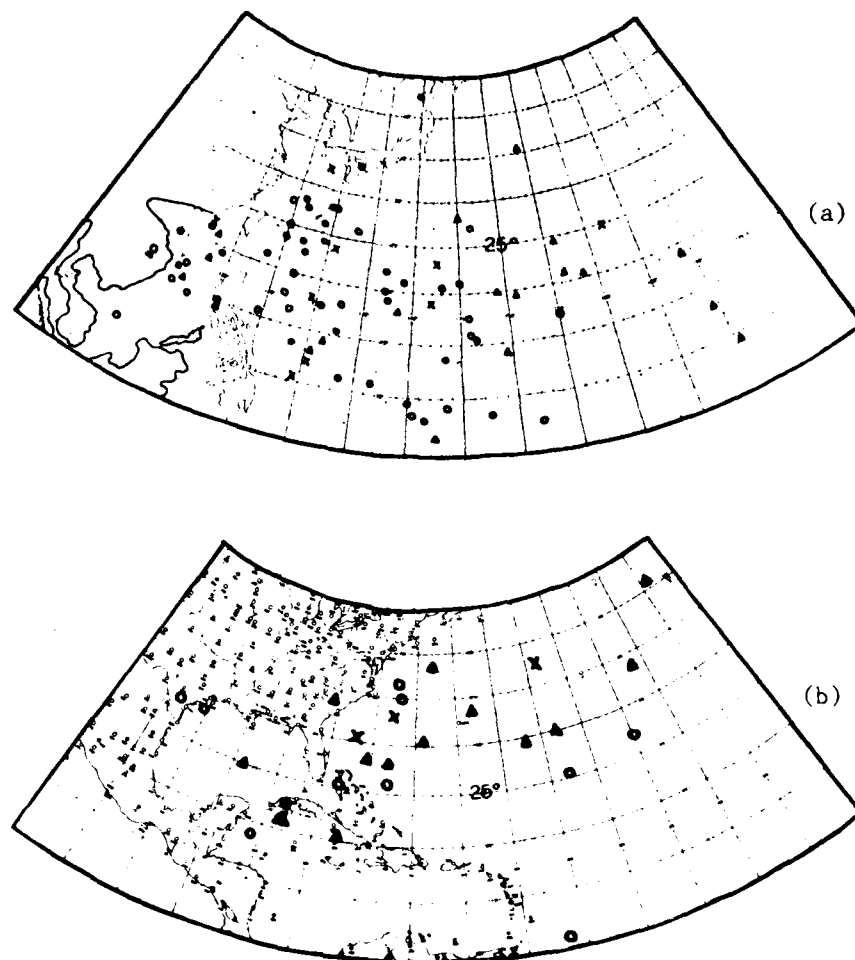
Fig. 83. Geographic distributions of looping cyclones in the Pacific
(a) and Atlantic (b). Triangles (Λ) *denote clockwise looping,*
open circles(o) counterclockwise (CC) looping and x's looping
in both directions.

been well established for looping storm cases. It would be helpful
to the cyclone forecaster if these looping patterns could be better
specified.

Daily series synoptic weather maps (Northern Hemisphere) during
1957-1970 published by U.S. NOAA Environmental Data Service, daily
weather maps (North West Pacific) during 1962-1977 published by Japan
Meteorological Agency, and daily weather map microfilms of Miami National
Hurricane Center North West Atlantic) during 1971-1977 were used to

study the broad scale circulation features in which looping cyclones
were embedded. 69 looping events in both oceans which had looping
length more than one day and which had tropical storm strength at least
once during the loop have been studied. In addition, 69 rapidly moving
cyclones in the Atlantic during 1957-1969 which maintained velocity
greater than 10 m/s for more than 36 hours were gathered and contrasted
with 38 slow moving cyclones which had velocity slower than 2.5 m/s for
more than 36 hours.

In order to illustrate the principal character of the broadscale
flow surrounding looping and other types of cyclone motion typical 500 mb
and surface flow maps have been constructed for the different looping
cases so that surrounding flow comparisons and contrasts can be made.
Storms were stratified by their position north, south or at the sub-
tropical ridge.

Figures 84-86 show the typical westerly moving flow patterns for
fast, slow, and looping storms which are located to the south of the
subtropical ridge. Comparing these flow patterns, we observe that when
the storm is looping or moving very slowly there is a 500 mb long wave
trough at similar longitude to its poleward side. Normally when the
storm is located to the south of a strong subtropical ridge the westerly
velocity of the storm is rapid. But when there is a large amplitude
westerly trough at the cyclone latitude the storm moves only slowly west-
ward or will loop as the trough to the north passes across its position.

Comparing Fig. 86 to Figs. 87 and 88 we can see the difference
between recurving storms and looping storms. For the recurving storms
the 500 mb trough has penetrated into the latitude
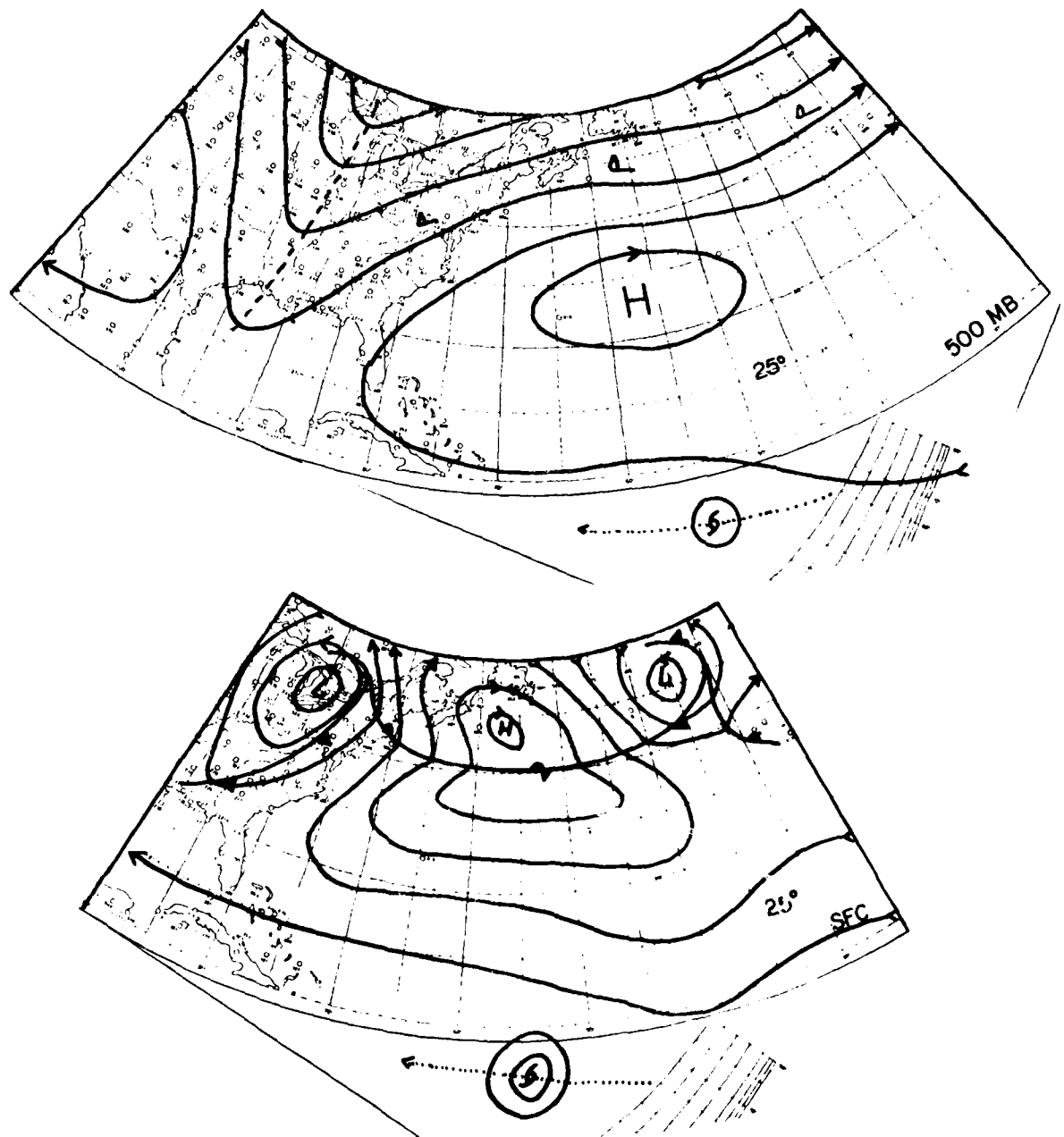ridge and the trough is located to the west of the

Fig. 84. Schematic of fast moving storms to the south of the subtropical
ridge (SR) at 500 mb (top) and at the surface (bottom). The
wind barb(△—)denotes the nearest 20 m/s isotach to the storm
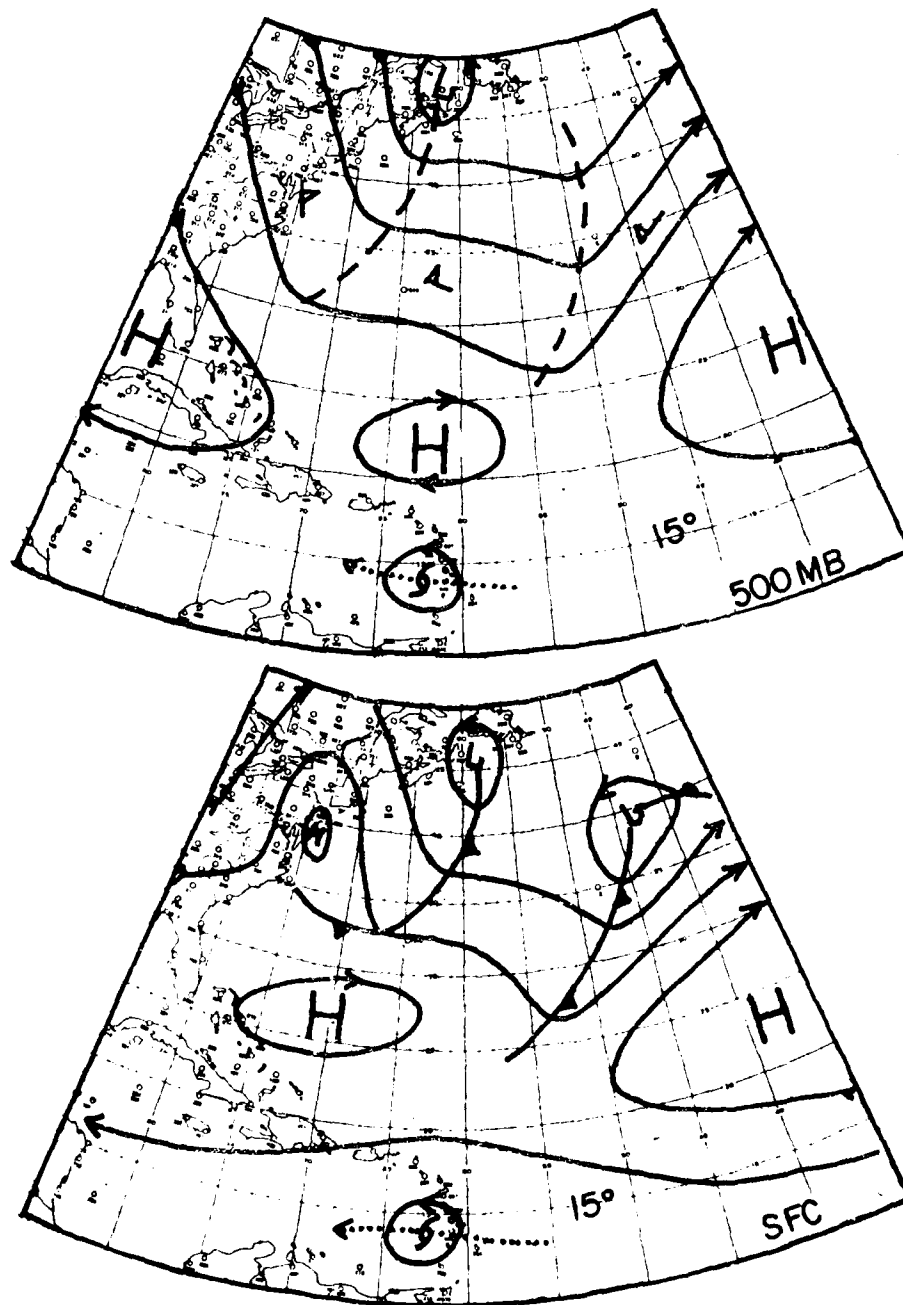center at 500 mb.

Fig. 85. Schematic of slow moving storms to the south of the subtropical ridge at 500 mb and the surface. The wind barb(△—)denotes the nearest 20 m/s isotach to the storm center at 500 mb.
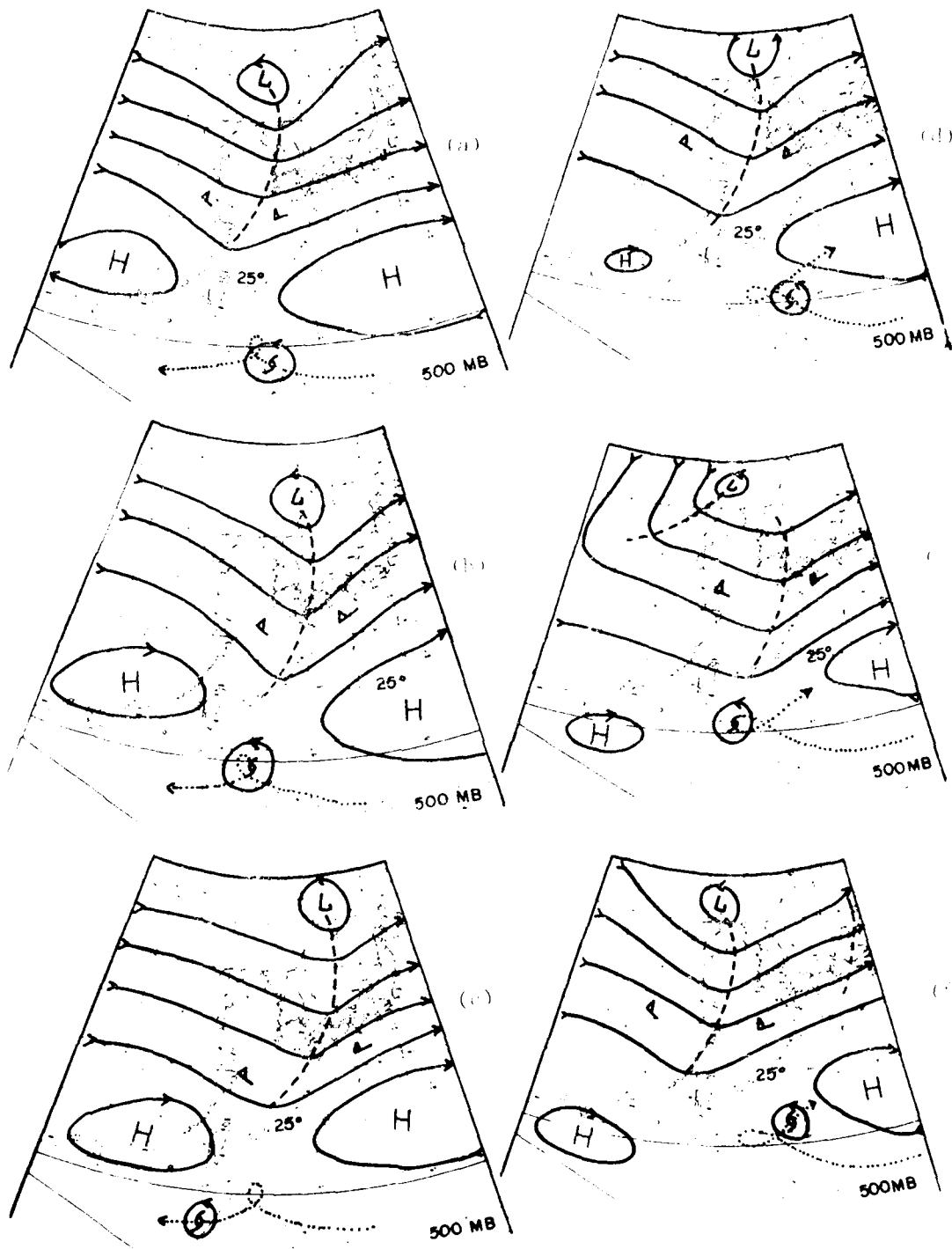
Fig. 86. Typical 500 mb flow patterns for looping storms to the south
of the subtropical ridge (SR). Diagrams a, b, and c are for
clockwise (C) looping while diagrams d, e, and f are for
counterclockwise looping. Wind barb(△—)denotes the nearest
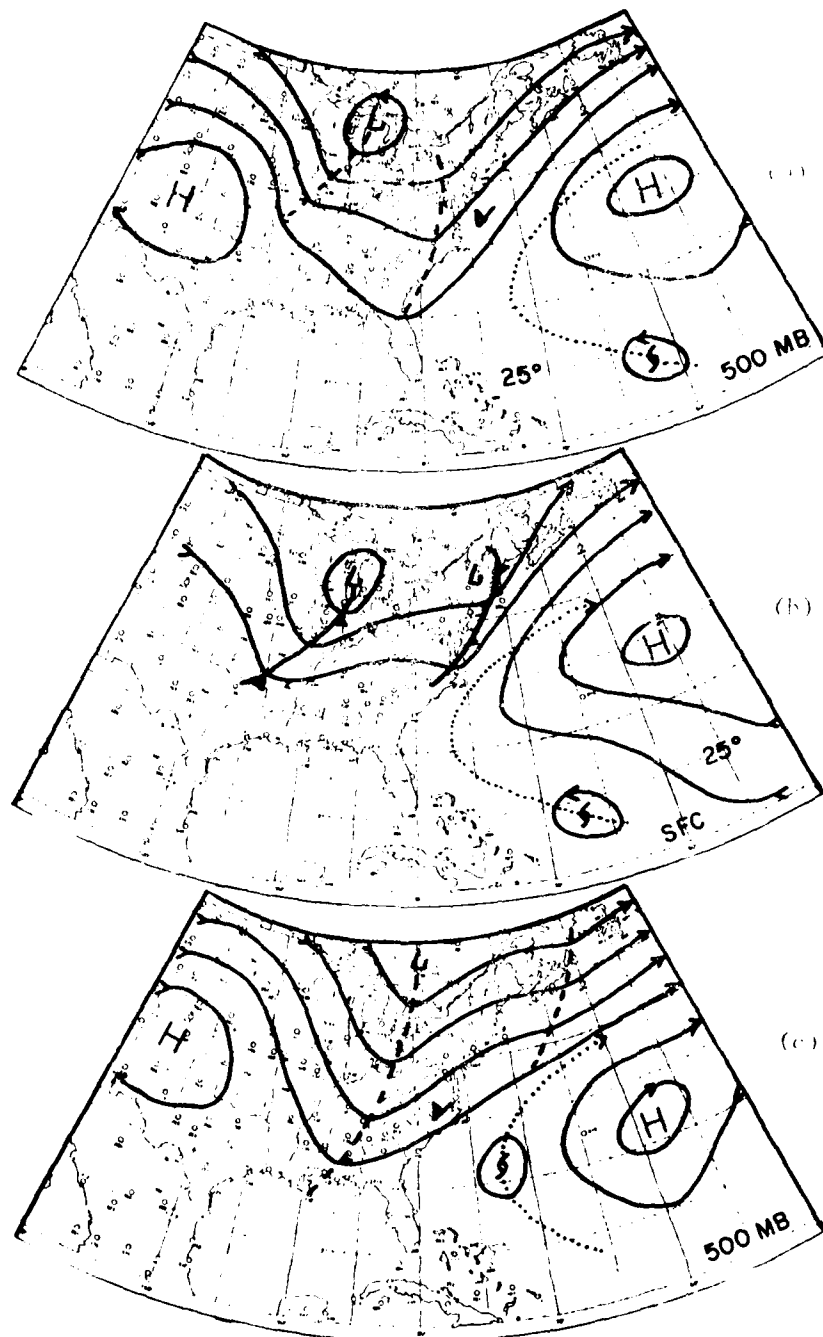20 m/s isotach to the storm center at 500 mb.

Fig. 87. Typical 500 mb and surface weather maps for a fast moving cyclone crossing the subtropical ridge towards the north. Wind barb(△—) denotes the nearest 20 m/s isotach to the storm center at 500 mb.
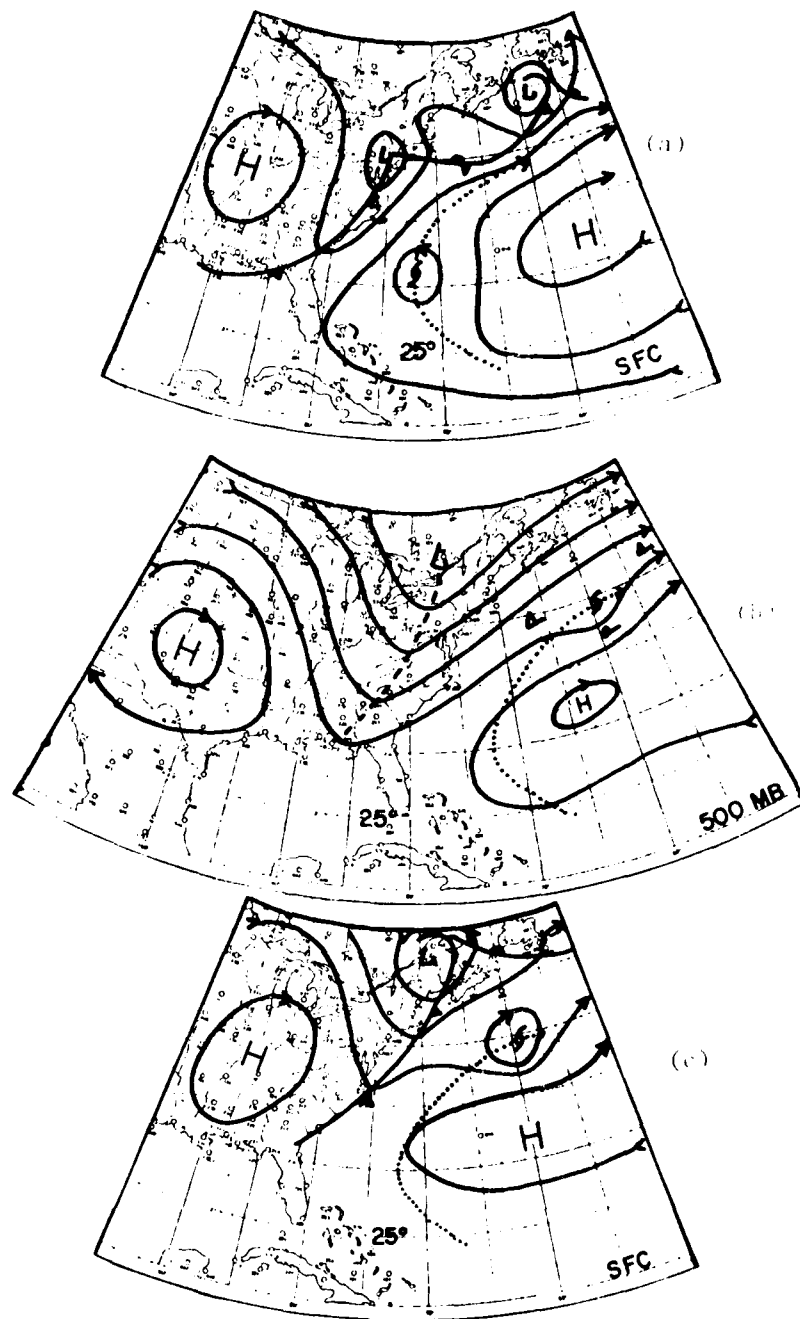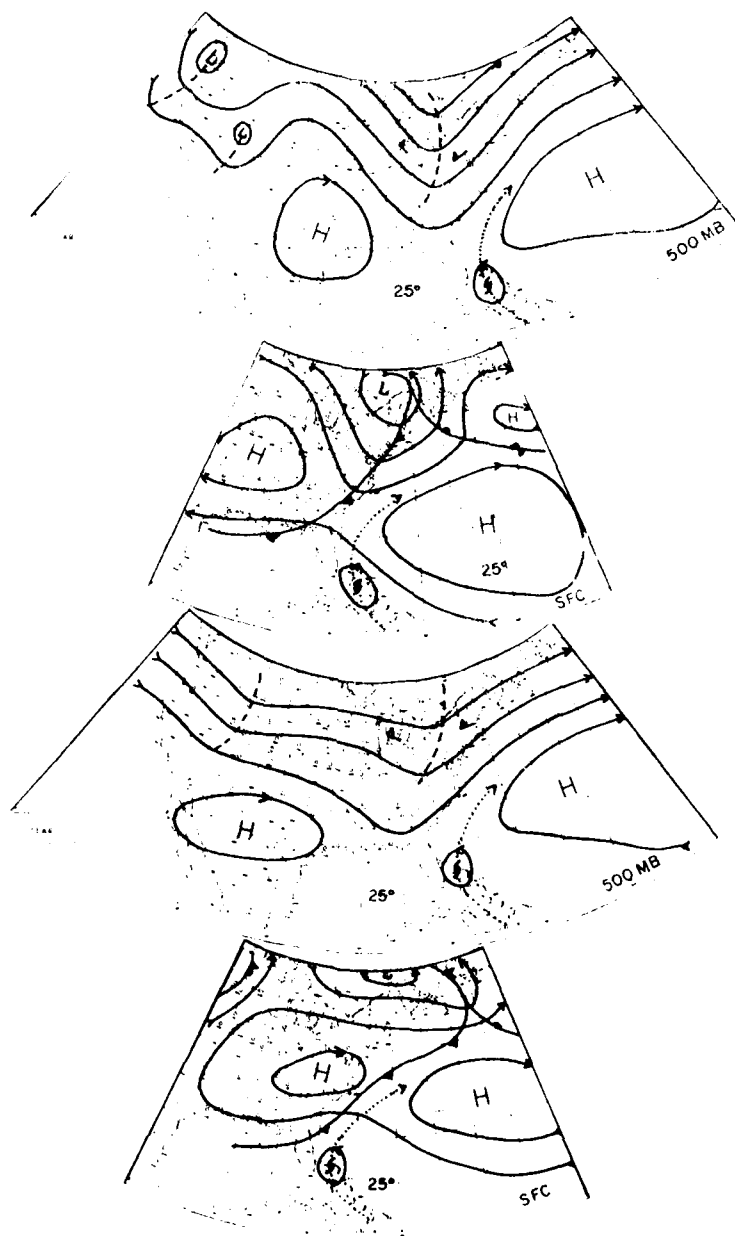
Fig. 87. Continued.

Fig. 88. Typical 500 mb and surface weather maps for a slow moving
cyclone crossing the subtropical ridge (SR). Wind barb (△—)
denotes the nearest 20 m/s isotach to the storm center at
500 mb.

looping storms, the 500 mb trough is still to the north of the sub-
tropical ridge and the trough is at about same latitude as the storm.
The right side of Fig. 86 also shows the looping processes when a short
wave trough passes by the storm to the north. The storm is forced toward
the south by the north wind behind the trough. If the westerly trough is
deepening near the end of the looping motion (similar to Fig. 88) the
storm recurves. Otherwise, it will move toward the west again.

Figures 87-89 show the situation when the storm is at the latitudes
of the subtropical ridge. In all three situations there is a westerly
long wave trough to the west of the storm. Although all of these storms
move toward the north, their velocities are very different.

In Fig. 87 the westerly long wave trough is very deep and penetrates
south of subtropical ridge. When the storm approaches the western side
of the subtropical ridge it finds itself embedded in strong southerly
steering flow and moves very rapidly to the north. By contrast, Fig.
88 shows the typical case of a westerly long wave trough which does not
penetrate so far equatorwards. The westerly jet stream keeps further
to the north. The storm follows a stable northward path but it moves
very slowly.

Figure 89 shows the usual situation of cyclonic looping associated
with double vortex storms. Although there is also a westerly trough
to the west of the storm another storm is located about 15° to the east.
The two storms have a tendency to loop about with each other in a
manner discussed by Fujiwhara (1913); Haurwitz (1951); Hoover (1961);
and Brand (1970). As a result, the east storm recurves very quickly.
The cyclone to the west usually follows a counterclockwise looping track.

Figures 90-92 show the typical synoptic conditions when cyclones
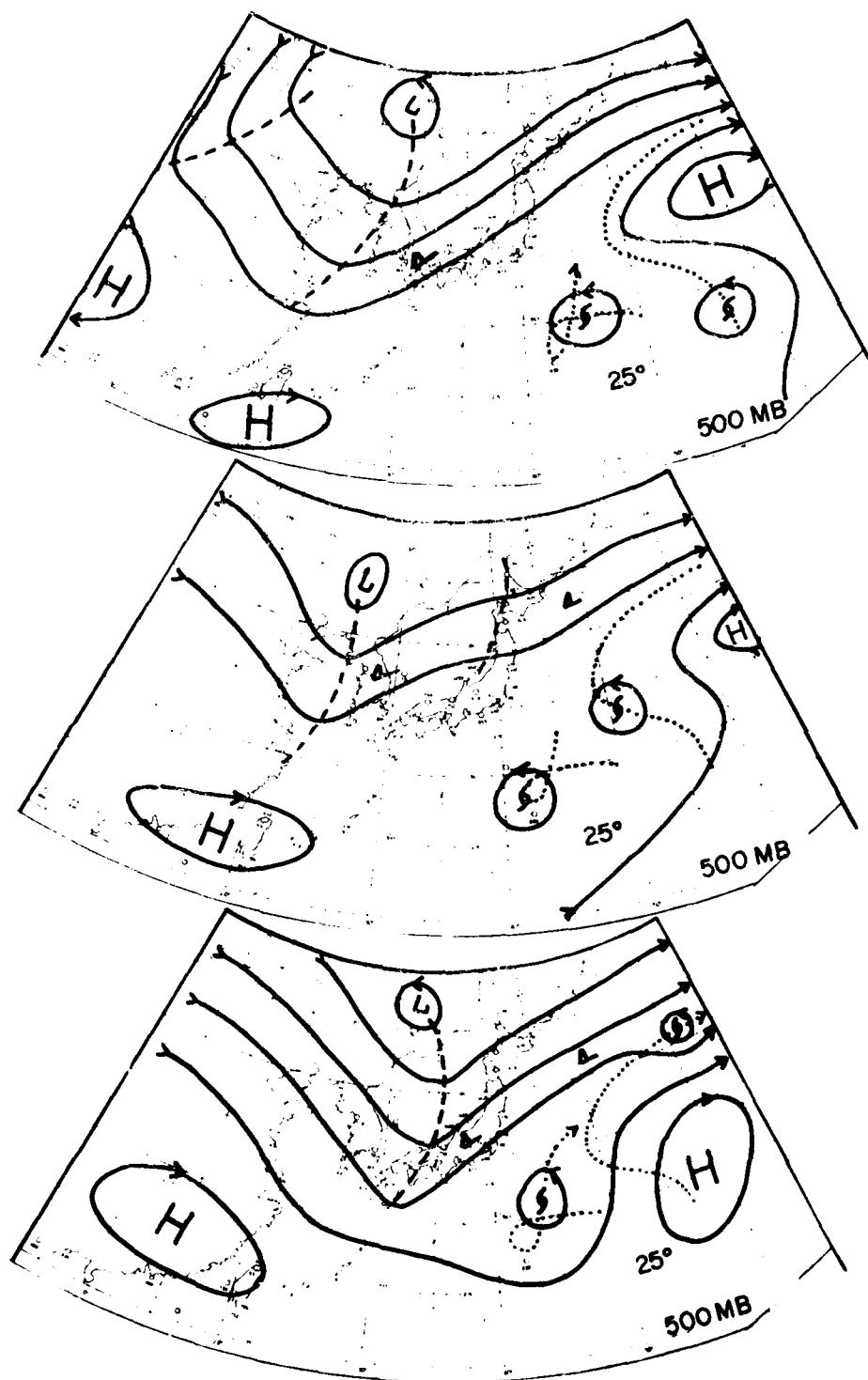are located to the north of the subtropical ridge and are strongly

Fig. 89. Typical 500 mb flow patterns of tropical cyclone looping caused by double vortex cyclones. Wind barb(△—) denotes the nearest 20 m/s isotach to the storm center at 500 mb.

111

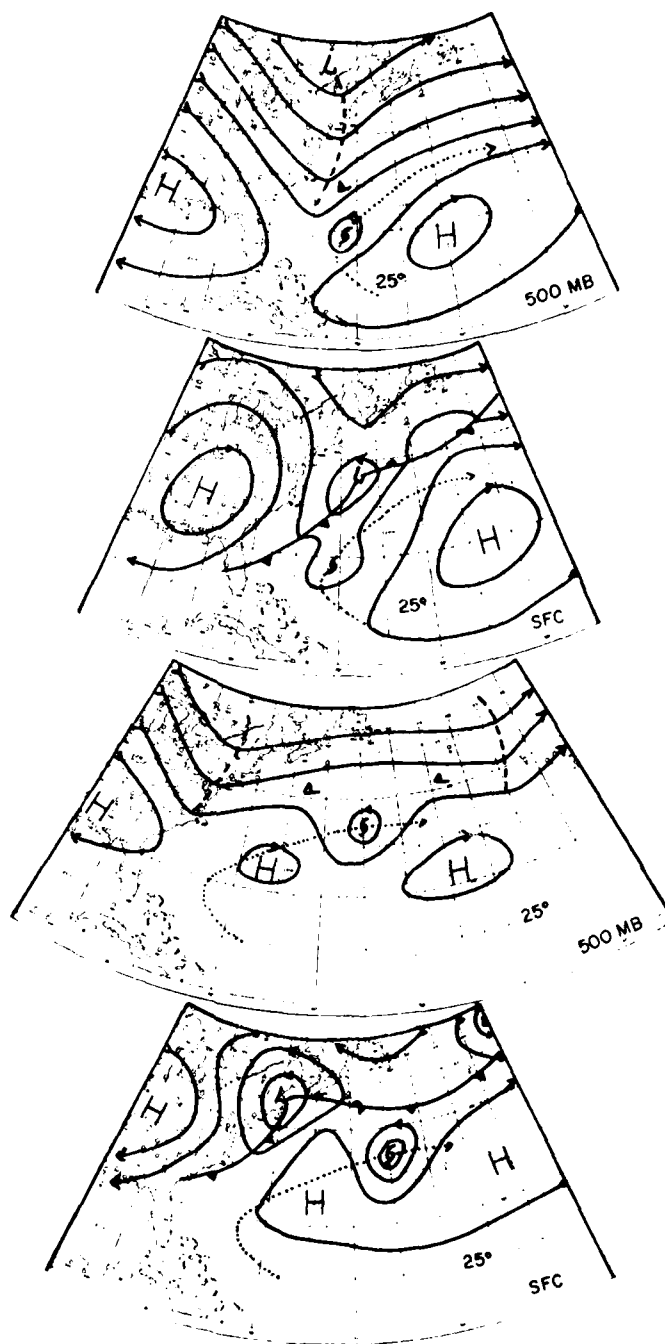Fig. 90. Typical 500 mb and surface flow patterns of fast moving cyclones
to the north of the subtropical ridge (SR) Wind barb(⌐)denotes
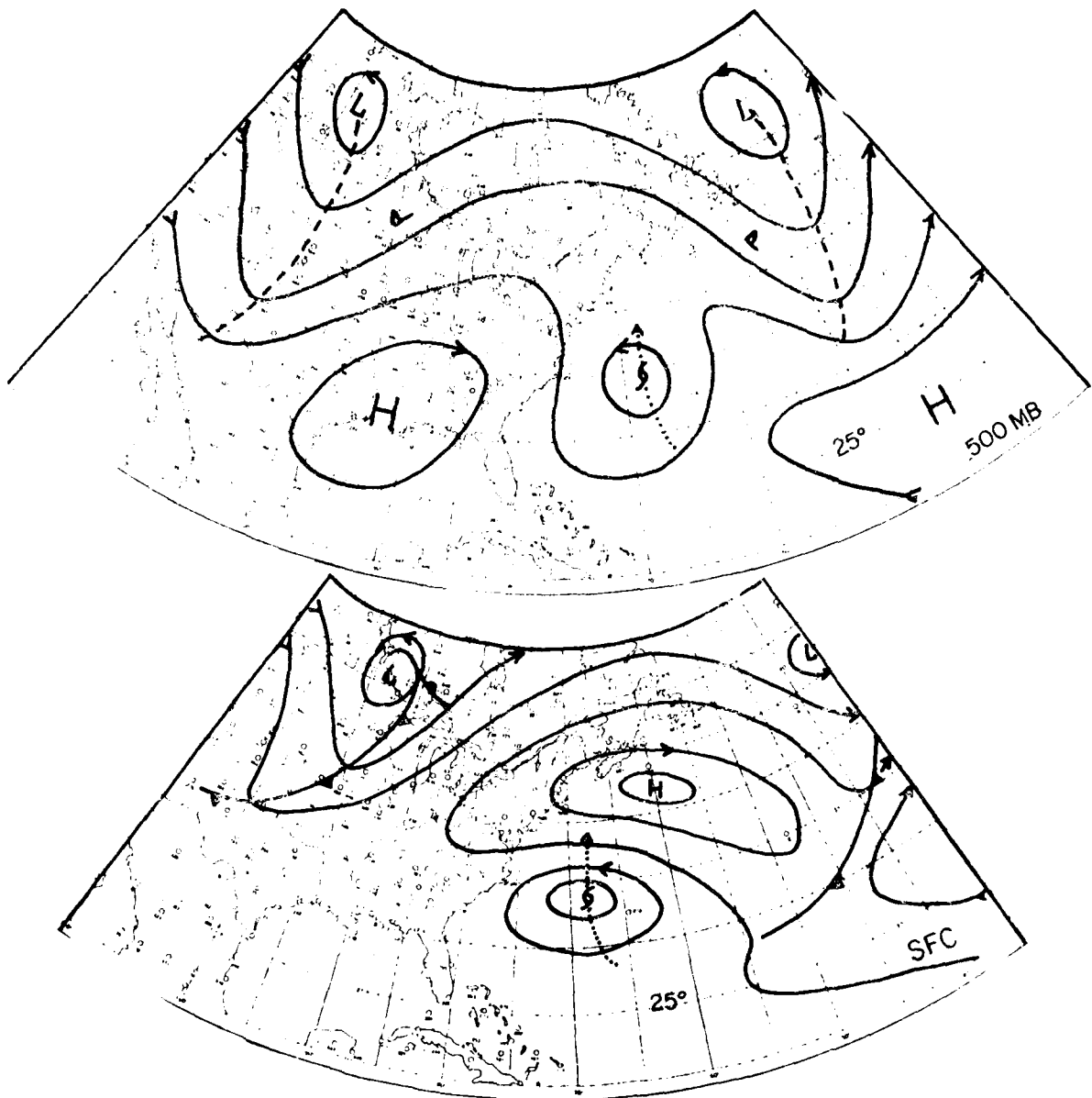the nearest 20 m/s isotach to the storm center at 500 mb.

Fig. 91. Typical 500 mb and surface flow patterns for slow moving
tropical cyclones to the north of the subtropical ridge.
The wind barb(△—) denotes the nearest 20 m/s isotach to
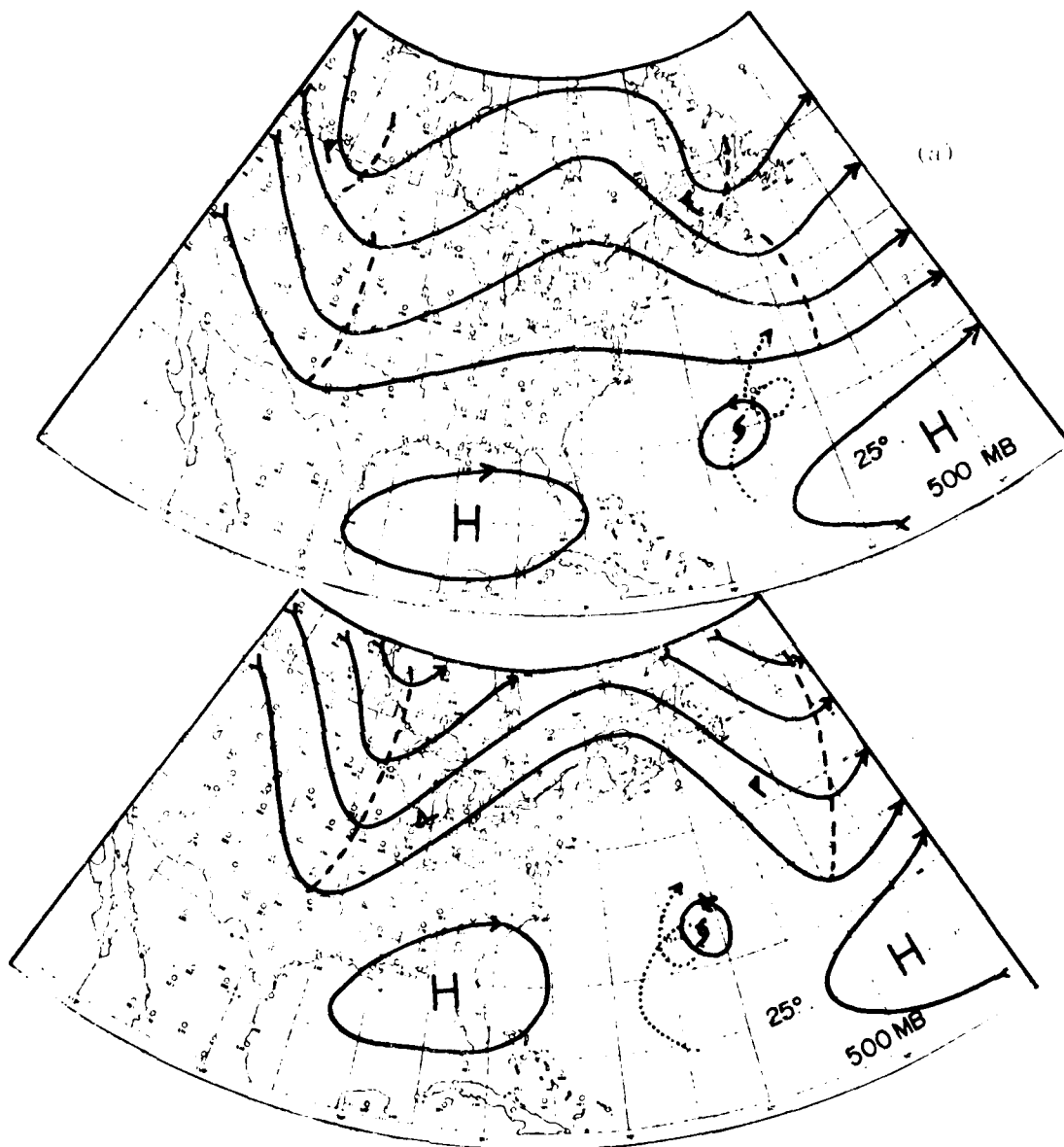the storm center at 500 mb.

Fig. 92. Typical 500 mb flow patterns for tropical cyclone looping motion to north of the subtropical ridge.
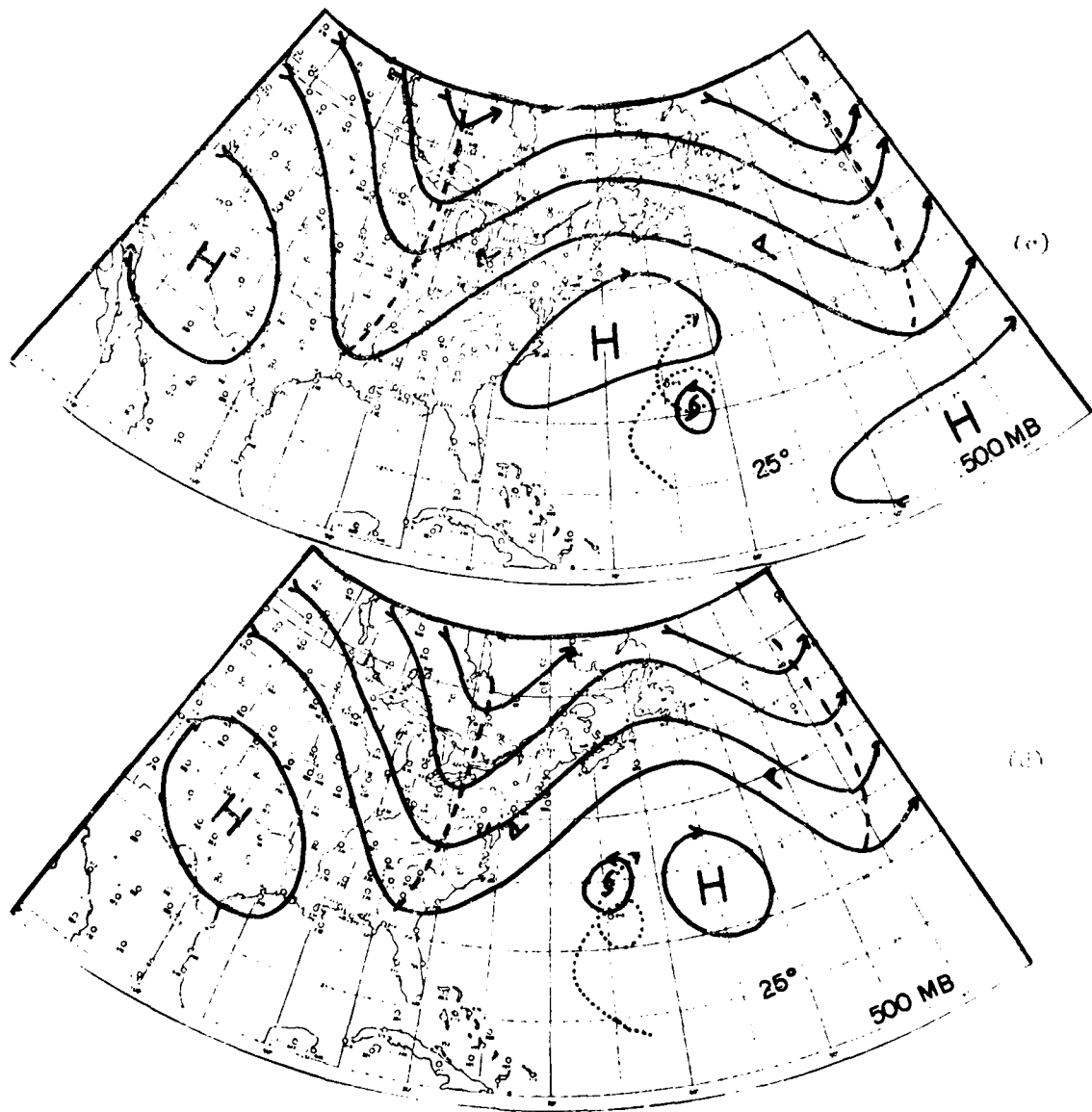
Fig. 92. Continued.

affected by the westerly air flow. In Fig. 90 the storm is very near to

a 500 mb trough to the west and an upper level westerly jet stream. Such

storms move very fast. Burroughs and Brand (1973) have also discussed

this special class of rapidly moving tropical cyclones to the east of

an upper trough. In both Figs. 91 and 92 there are large amplitude

westerly troughs to the east and west of the cyclone and the storm is

affected by the ridge pattern to the north. The synoptic scale flow

patterns of Fig. 91 are changing only very slowly. The surrounding

flow is weak. The storm moves only very slowly to the

north. In Fig. 92 the two troughs to the east and west are deepening.

The developing trough to the east initially steers the storm towards

the south. A high pressure cell then builds between the two troughs

and the storm moves to the west for a while until the deepening trough to

the west begins to influence the storm and drive it towards the northeast

again. It is to be noted that for the fast moving storms the 20 m/s

isotachs are very near to the storms (about $5-8^o$ latitude away). When

the storm is located in a deep easterly current and is headed westwards

the westerly jet stream is about $25-30^o$ away from the storm. For the

slow moving and looping storms this isotach is approximately $10-15^o$

away from the storm center. In the low index circulation flow pattern,

if the westerly trough is located to the north or northeast of the

storm, the storm will loop or move very slowly.

From these figures we can also see that when the directions of

500 mb and surface steering flows are the same, the storm moves quickly.

When these flow patterns come from opposite directions the storm moves

much slower.

The modification of the long-wave pattern is very important. We

can see that the situation of slow moving storms is very similar to
the one of looping storms. The difference is in the degree of short-
wave activity. In the looping situation there is more short-wave trough
activity than in the slow moving situation.

It is advantageous for a forecaster to be familiar with these
typical looping motion synoptic situations. With these flow patterns in
mind he can judge if the objective prediction is reasonable or not and
also he can make his estimates of looping potential. From these figures
we can also see that the large amplitude stationary longwave is one of
the most important factors which bring about looping. These long wave
patterns are of planetary scale. They are very closely related in the
hemisphere general circulation. The next section discusses the types of
typical long-wave general circulation patterns which are associated
with these various looping storm cases.

6.5 Association of Longwave Patterns with Storm Looping Motion

Figures 93-95 show composites of the westerly troughs distribution
occurring with storms looping to the North, South and near the subtro-
pical ridge. From these charts we can see that in the situations of
looping to the north and south of the subtropical ridge the longwave
pattern of number five is dominate. The relative wave length is about
70° longitude which happens to be the stationary wave length. Thus,
stationary and stable long waves are very important for looping motion.
When storms loop to the north of the subtropical ridge (Fig. 93) the
long wave troughs are located on both sides of the storm. When storms
loop to the south of the subtropical ridge (Fig. 94) the long wave
trough is located to the north of the storm with a slight bias to the
east. Figure 95 is for looping motion due to double vortex action. It

Fig. 93. Composite of 500 mb westerly wind trough positions (solid
curved lines) about the Northern Hemisphere relative to the
position of looping cyclones to the north of the subtropical
ridge. The symbol ∮ denotes the longitude of the looping cyclone.
Concentric circles denote latitude.
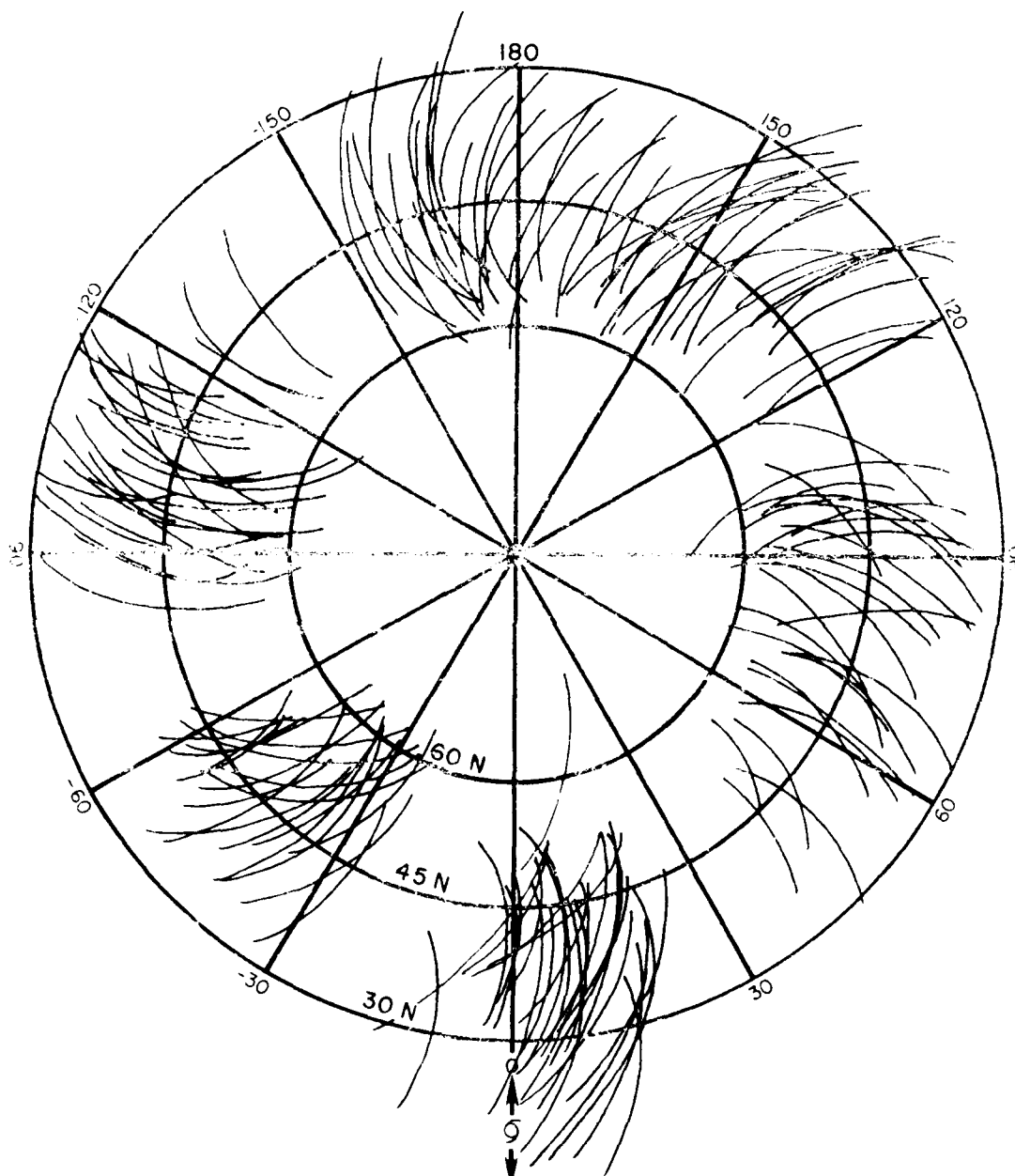
Fig. 94. Same as Fig. 93 but for looping tropical cyclones to the south
of the subtropical ridge.
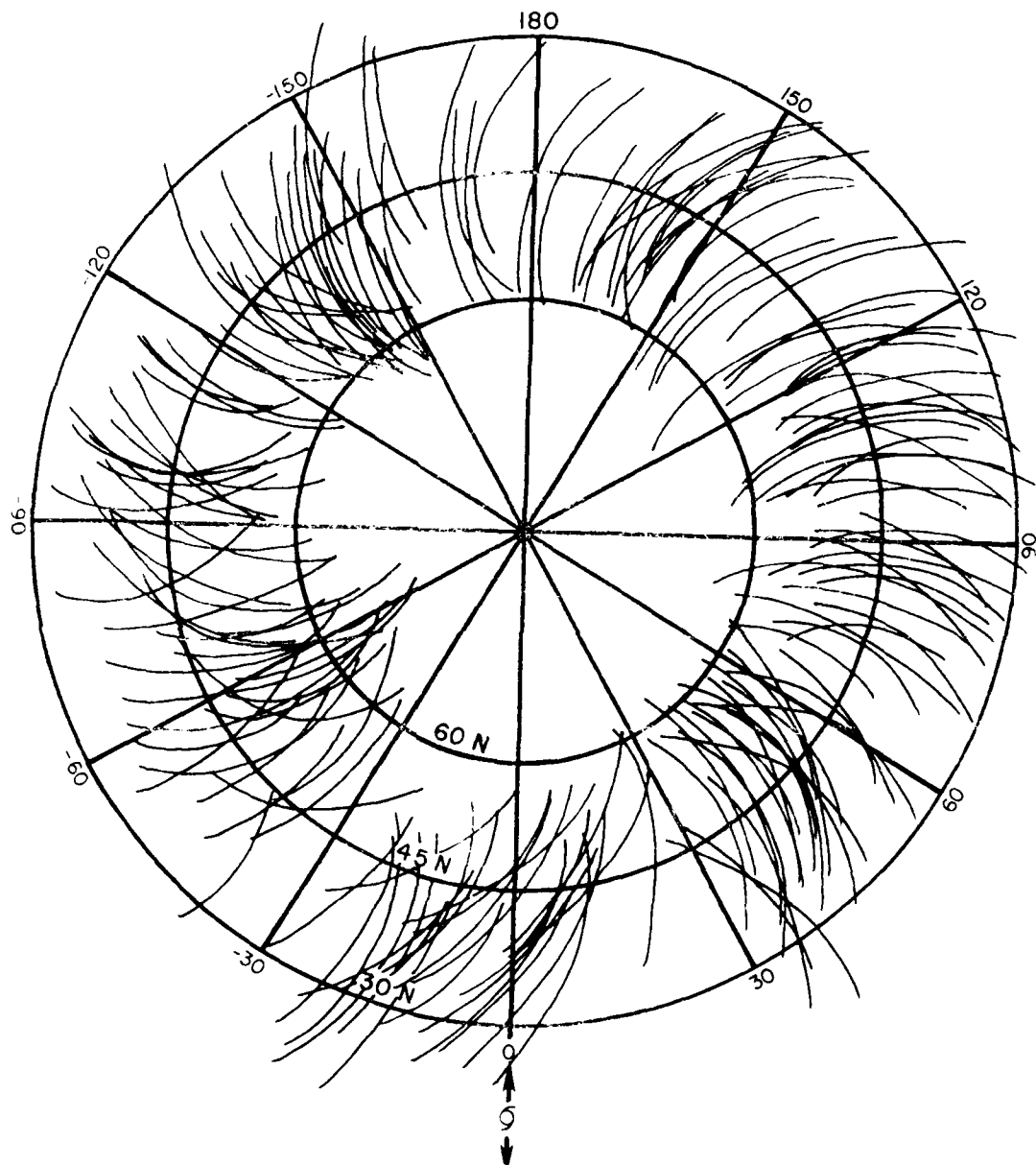
Fig. 95. Same as Fig. 93 but for the looping of tropical cyclones caused by double vortex cyclones.

is similar to Fig. 94 in showing the trough to be at the longitude of looping. Note how looping motion in these 3 figures is even correlated with long-wave trough activity at the opposite side of the globe. Such high correlations were not expected.

For comparison, Figs. 96 and 97 have been prepared. They show composite long wave trough patterns for storms moving very fast toward the west and for recurving storm patterns. In these cases the long wave troughs are not located at specific longitudes. The westerly winds are more zonal with higher wave numbers.

6.6 Looping Differences Between Atlantic and Pacific

Figures 98 and 99 show the geographic differences in the distribution of different types of looping motion in the two ocean basins. These figures should be compared with Fig. 83. We see that most of the loops to the north of the subtropical ridge are clockwise and located in the northeast part of the looping area. In the Atlantic almost all storm loops are of this type. Most of the loops caused by double storms are counterclockwise and occur in the most western part of the looping area. In the Atlantic there was only one loop in this type. This is because there are seldom storms existing simultaneously in the Atlantic. But in the Pacific it is very common that two or even three storms exist simultaneously. When they come close enough, usually the west storm takes on the looping tracks. This is one reason why double vortex looping occurs to the west part of the looping area. Most of the loops to the south of subtropical ridge are counterclockwise ones. They are located in the southwest part of the looping area. In the Pacific the counterclockwise looping is most prevalent. These are two types of
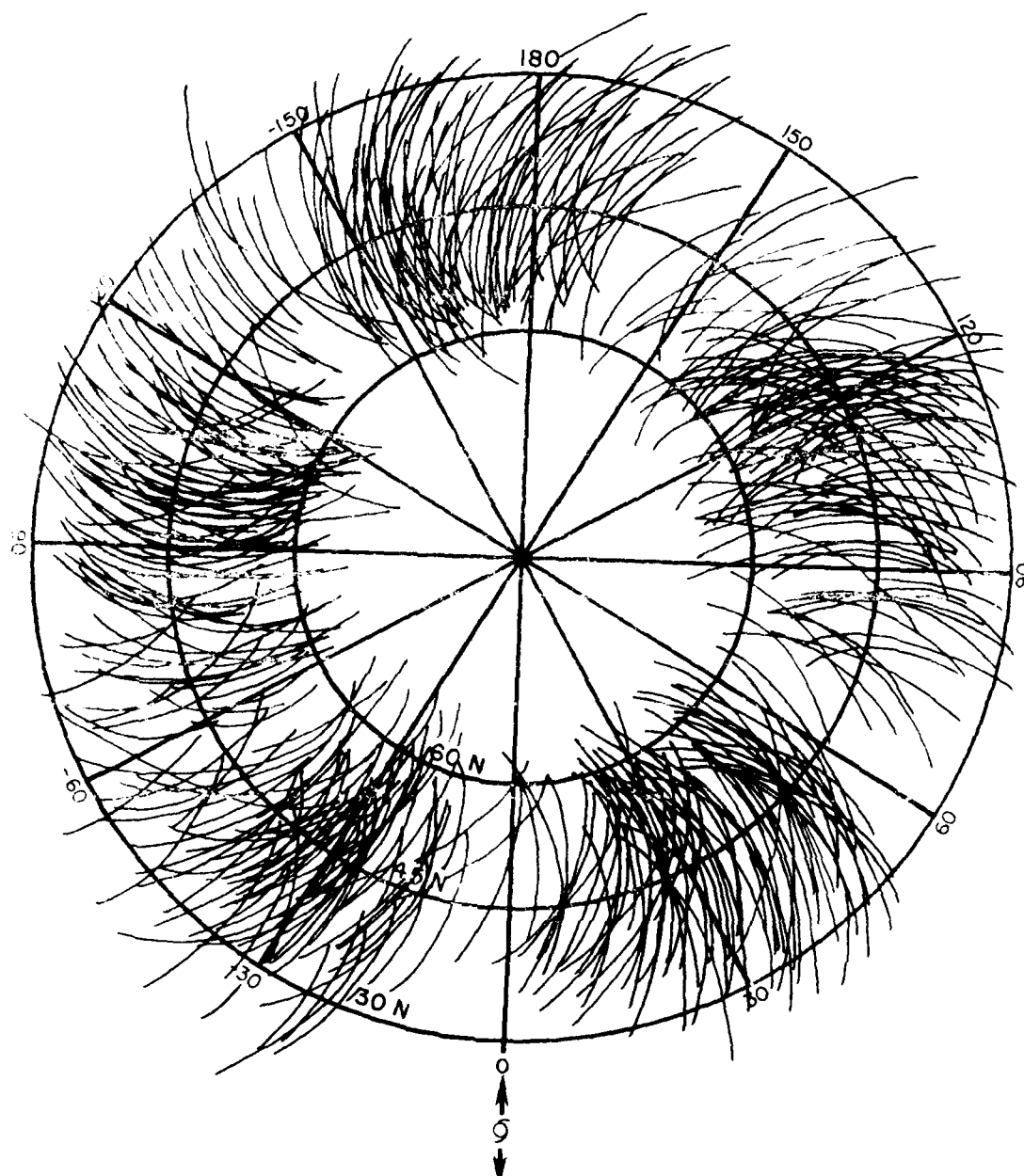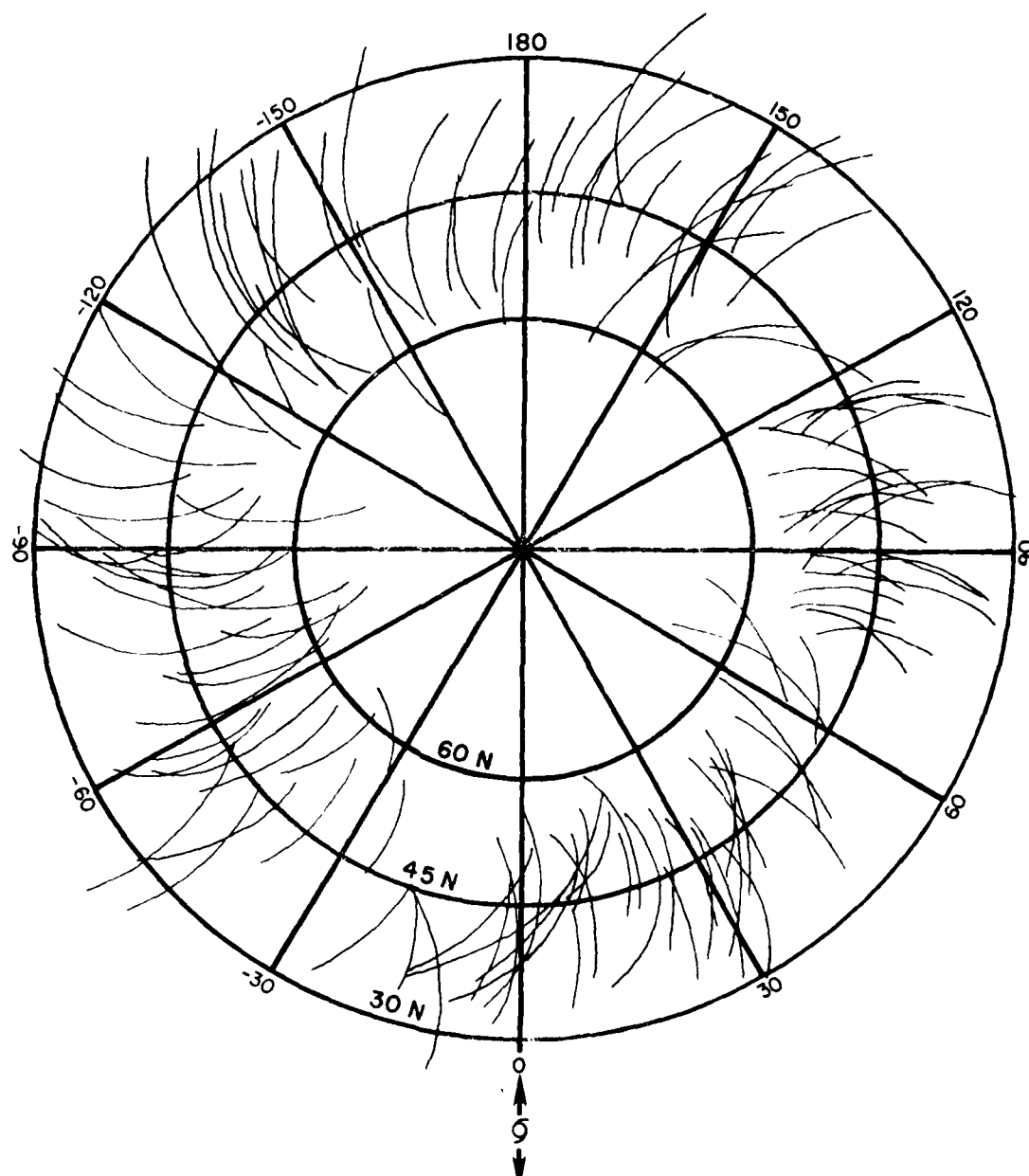
Fig. 96.   Composite of 500 mb westerly wind trough positions (solid
           curved lines) about the Northern Hemisphere relative to the
           position of tropical cyclones moving to the west. The symbol
           ⑨ denotes the longitude of the cyclone. Concentric circles
           denote latitude.
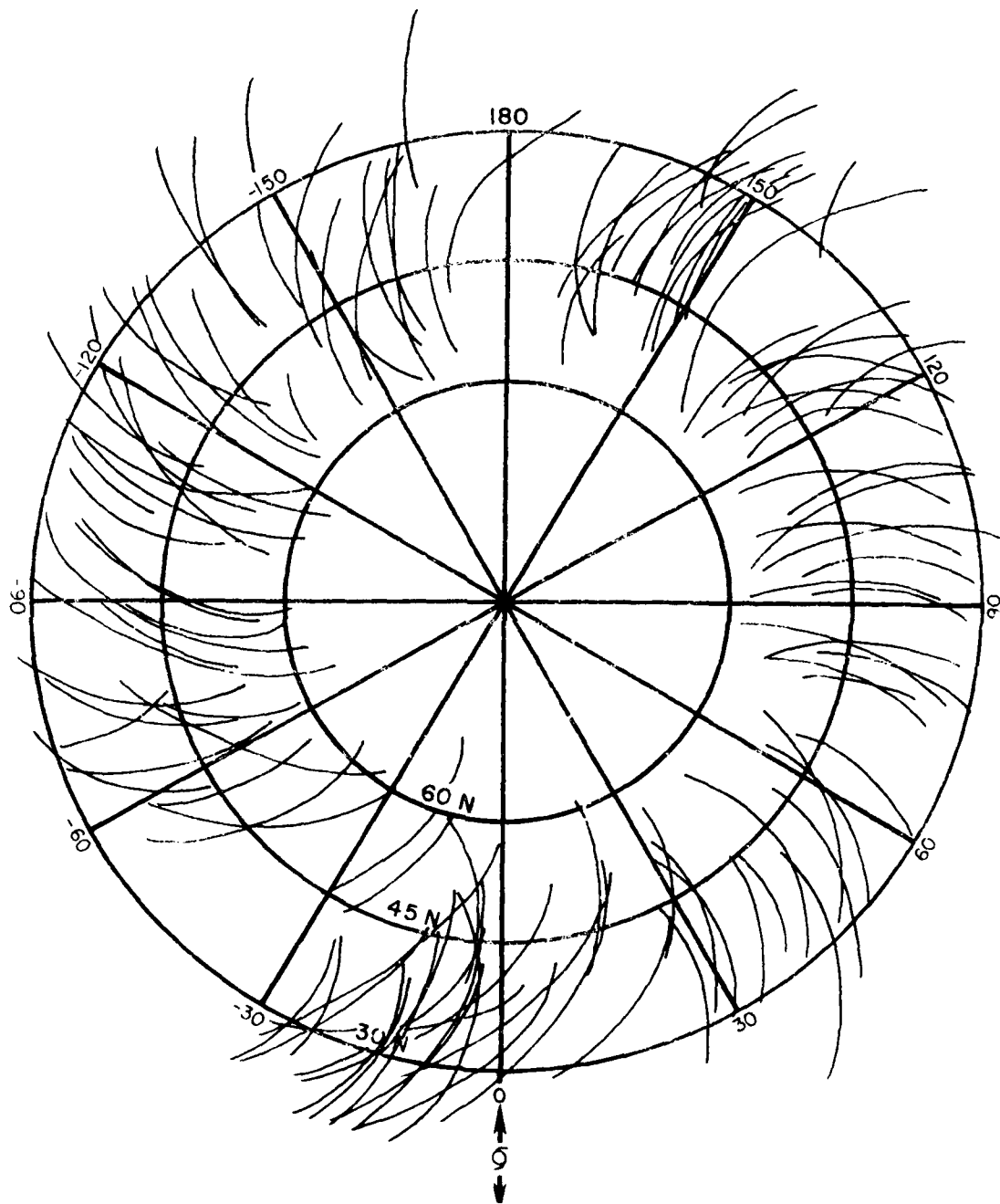
Fig. 97. Same as Fig. 96 but for tropical cyclones at recurvature.
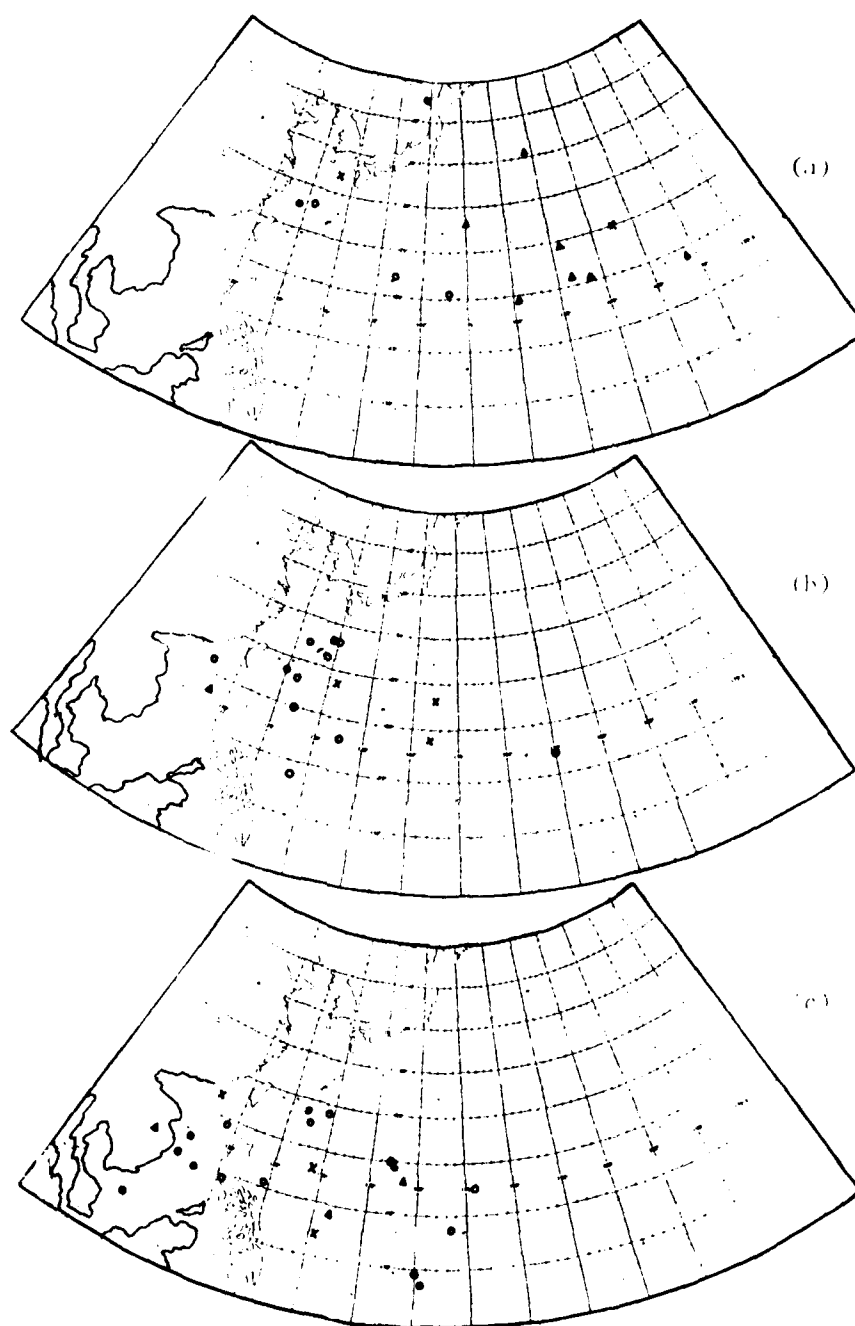
Fig. 98. Geographic distribution of west Pacific looping cyclones for
loopings to the north of the subtropical ridge (diagram a); looping
caused by double vortex cyclones (diagram b); and looping to
the south of the subtropical ridge (c). Triangles (Δ) denote
clockwise looping, open circles (o) counterclockwise (CC)
looping, and x's looping in both directions.
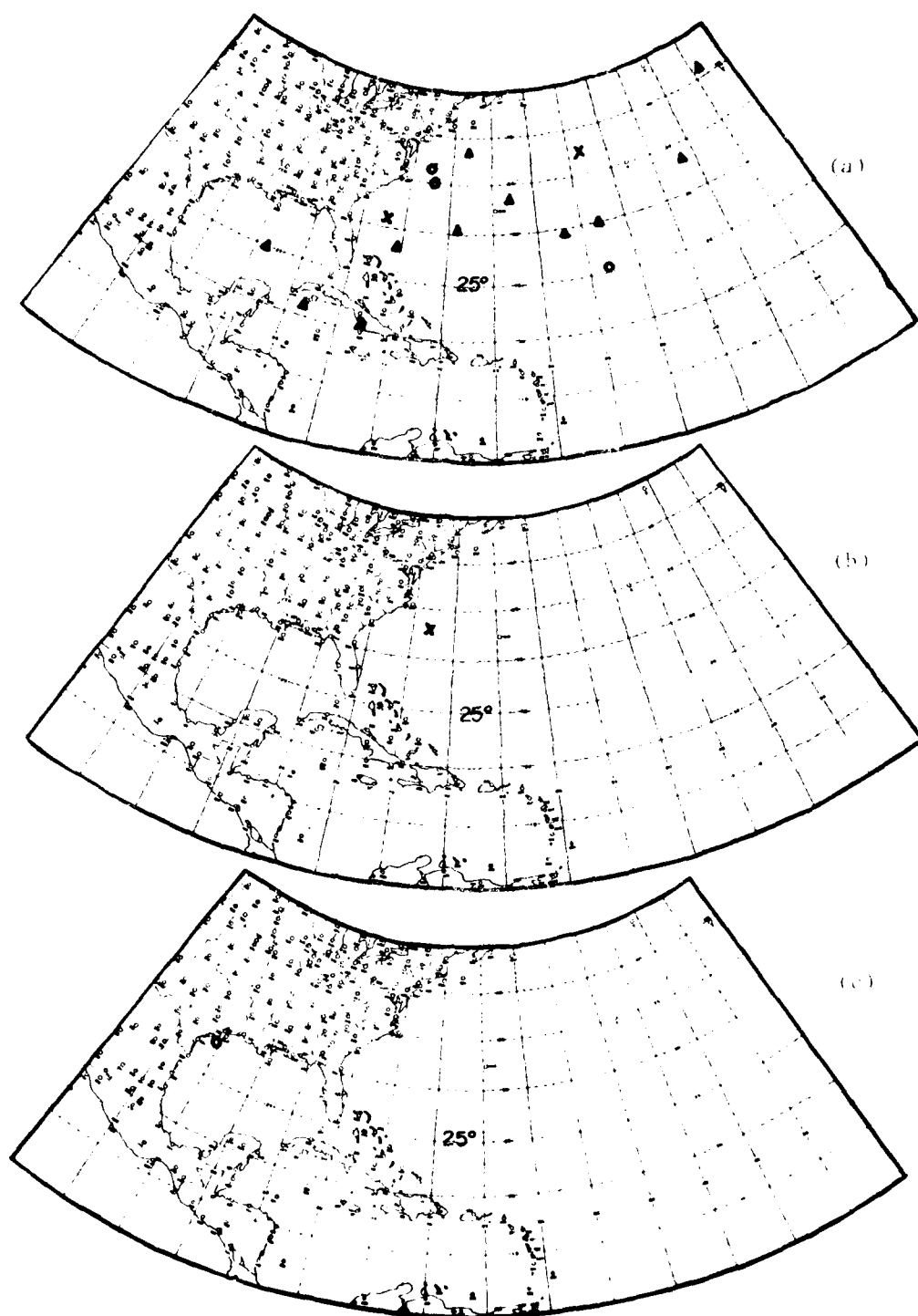
Fig. 99. Same as Fig. 98 but for Atlantic looping cyclones.

counterclockwise looping. By contrast, in the Atlantic there was only one counterclockwise loop. These differences are caused by the background circulation differences in the two regions. In the Pacific the lower tropospheric equatorial westerlies are quite strong. When the easterly winds to the north of storms weaken, the air currents to the north and south tends to balance each other and the storm can take on a looping track as its surrounding flow balance varies with time. In the Atlantic low-level equatorial westerly winds to the south of the cyclone are much rarer and weaker. When the easterly winds to the north of the storm weaken, the storms just move more slowly, they seldom go into a looping motion. The direction of steering is the same but weaker.

From the analyses shown above, we see that although there are significant differences between looping climatologies in the two ocean basins the basic cause of storm looping is directly related to the surrounding flow patterns.

REFERENCES

Arnold, C. P., 1977: Tropical cyclone cloud and intensity relationships. Dept. of Atmos. Sci. Paper No. 277, Colo. State Univ., Ft. Collins, CO, 155 pp.

Betts, A. K., et al., 1976: Structure and motion of tropical squall-lines over Venezuela. Quart. J. Roy. Meteor. Soc., 102, 395-404.

Brand, S., 1970: Interaction of binary tropical cyclones of the western north Pacific Ocean. J. Appl. Meteor., 3, 433-441.

Browner, S. P., W. L. Woodley and C. G. Griffith, 1977: Diurnal oscillation of the area of cloudiness associated with tropical storms. Mon. Wea. Rev., 105, 856-864.

Burroughs, L. D. and S. Brand, 1973: Speed of tropical storms and typhoons after recurvature in the western north Pacific Ocean. J. Appl. Meteor., 3, 452-453.

Chan, J. C. L., W. M. Gray and S. Q. Kidder, 1980: Forecasting tropical cyclone turning motion from surrounding wind and temperature fields. Mon. Wea. Rev., 108, 6, 778-792.

Dvorak, V. F., 1975: Tropical cyclone intensity analysis and forecasting from satellite imagery. Mon. Wea. Rev., 10?, 420-430.

Erickson, S. L., 1977: Comparison of developing vs. non-developing tropical disturbances. Dept. of Atmos. Sci. Paper No. 274, Colo. State Univ., Ft. Collins, CO, 81 pp.

Fingerhut, W. A., 1980: Tropical cyclone genesis - numerical modeling inferences. Dept. of Atmos. Sci. Ph.D. Thesis, Colo. State Univ., Ft. Collins, CO.

Frank, W. M., 1976: The structure and energetics of the tropical cyclone. Dept. of Atmos. Sci. Paper No. 258, Colo. State Univ., Ft. Collins, CO, 180 pp.

Frank, W. M., 1977a: The structure and energetics of the tropical cyclone, I: Storm structure. Mon. Wea. Rev., 105, 1119-1135.

Frank, W. M., 1977b: The structure and energetics of the tropical cyclone, II: Dynamics and energetics. Mon. Wea. Rev., 105, 1136-1150.

Frank, W. M., 1977c: Momentum and kinetic energy processes in the tropical cyclone. Volume of conference papers, 11th Technical Conference on Hurricanes and Tropical Meteorology, Dec. 13-16, Miami Beach, FL, Published by the AMS, Boston, MA, 535-542.

REFERENCES (cont'd)

Fujiwhara, S., 1913: Short note on the behavior of two vortices. _Proceedings of the Physico-Mathematical Society of Japan_, Third Series, vol. 13, 106-110.

George, J. E., 1975: Tropical cyclone motion and surrounding parameter relationships. Dept. of Atmos. Sci. Paper No. 241, Colo. State Univ., Ft. Collins, CO, 105 pp.

Gray, W. M., 1967: _Global view of the origin of tropical disturbances and storms._ Dept. of Atmos. Sci. Paper No. 114, Colo. State Univ., Ft. Collins, CO, 105 pp.

Gray, W. M., 1968: Global view of the origin of tropical disturbances and storms. _Mon. Wea. Rev._, 96, 669-700.

Gray, W. M., 1975a: Tropical cyclone genesis. Dept. of Atmos. Sci. Paper No. 234, Colo. State Univ., Ft. Collins, CO, 119 pp.

Gray, W. M. 1975b: Tropical cyclone genesis in the western North Pacific. ENVPREDRSCHFAC Technical Paper No. 16-75, Monterey, CA, 66 pp.

Gray, W. M., 1977a: Cyclone intensity determination through upper tropospheric reconnaissance. Paper prepared for the 11th Technical Conference on Hurricanes and Tropical Meteorology, Miami, FL, 6 pp.

Gray, W. M., 1977b: Tropical cyclone motion and steering flow relationships in the Western Atlantic and the Western Pacific. Paper prepared for the 11th Technical Conference on Hurricanes and Tropical Meteorlogy, Miami, FL, 6 pp.

Gray, W. M., 1977c: Tropical disturbance to cyclone transformation. Paper prepared for the 11th Technical Conference on Hurricanes and Tropical Meteorology, Miami, FL, 8 pp.

Gray, W. M., 1979: Hurricanes/their formation, structure and likely role in the tropical circulation. _Quart. J. Roy. Meteor. Soc._, 105, 155-218, supplement to _Meteorology Over the Tropical Oceans_.

Gray, W. M. and W. M. Frank, 1977: Tropical cyclone research by data compositing. NEPRF Technical Report TR-77-01, Naval Environmental Prediction Research Facility, Monterey, CA, 70 pp.

Gray, W. M. and W. M. Frank, 1978: New results of tropical cyclone research from observational analysis. NEPRF Technical Report TR-78-01, Naval Environmental Prediction Research Facility, Monterey, CA, 106 pp.

Gray, W. M. and R. W. Jacobson, Jr., 1977: Diurnal variation of deep cumulus convection. _Mon. Wea. Rev._, 105, 1171-1188.

REFERENCES (cont'd)

Haurwitz, B., 1951: The motion of binary tropical cyclones. Archiv
  fur Meteorologie, Geophysik und Bioklimatologie, Ser. A, vol. 4,
  73-86.

Hoover, E. W., 1961: Relative motion of hurricane pairs. Mon. Wea.
  Rev., 251-255.

McBride, J. L., 1979: Observational analysis of tropical cyclone
  formation. Dept. of Atmos. Sci. Paper No. 308, Colo. State Univ.,
  Ft. Collins, CO 230 pp.

McBride, J. L. and W. M. Gray, 1978: Mass divergence in tropical
  weather systems. Dept. of Atmos. Sci. Paper No. 299, Colo. State
  Univ., Ft. Collins, CO 109 pp.

Mielke, P. W., 1979a: Some parametric, nonparametric and permutation
  inference procedures resulting from weather modification experiments.
  Commun. Statist.-Theor. Meth., A8, 1083-1096.

Mielke, P. W., 1979b: On asymptotic non-normality of null distributions
  of MRPP statistics. Commun. Statist. -Theor. Meth., A8, 1541-1550.

Mielke, P. W., K. J. Berry and E. S. Johnson, 1976: Multi-response
  permutation procedures for a priori classifications. Commun.
  Statist.-Theor. Meth., A5, 1409-1424.

Morrison, D. F., 1967: Multivariate Statistical Methods. McGraw-Hill,
  New York, 338 pp.

Núñez, E., 1981: Tropical cyclone structure and intensity change. Ph.D.
  Thesis, Dept. of Atmos. Sci., Colo. State Univ., Ft. Collins, CO.

Núñez, E. and W. M. Gray, 1977: A comparison between West Indies hur-
  ricanes and Pacific typhoons. Vol. of Conference Papers, 11th
  Technical Conference on Hurricanes and Tropical Meteorology, Dec.
  13-16, Miami Beach, FL, Published by AMS, Boston, MA, 528-534.

O'Reilly, F. J. and P. W. Mielke, 1980: Asymptotic normality of MRPP
  statistics from invariance principles of U-statistics. Commun.
  Statist.-Theor. Meth., A9, 629-637.

Pearce, R., 1981: A dynamical analysis of hurricane intensification.
  Archives for Meteorology, FRG, (in press).

Puri, M. L. and P. K. Sen, 1971: Nonparametric Methods in Multivariate
  Analysis. Wiley, New York, 440 pp.

Riehl, H., 1954: Tropical Meteorology. McGraw-Hill, New York, 392 pp.

REFERENCES (cont'd)

Ruprecht, E. and W. M. Gray, 1974: Analysis of satellite observed tropical cloud clusters. Dept. of Atmos. Sci. Paper No. 219, Colo. State Univ., Ft. Collins, CO, 91 pp.

Ruprecht, E. and W. M. Gray, 1976a: Analysis of satellite-observed cloud clusters, Part I: Wind and dynamic fields. Tellus, 28, 391-413.

Ruprecht, E. and W. M. Gray, 1976b: Analysis of satellite-observed cloud clusters, Part II: Thermal, moisture and precipitation. Tellus, 28, 414-416.

Sadler, J. C., 1967: The tropical tropospheric trough as a secondary source of typhoons and a primary source of tradewind disturbances. Final Report, Cont. AF19 (628)3860, AF Cambridge Research Labs., Bedford, MA, Rept. 67-12. (Available from Inst. of Geophysics, Univ. of Hawaii.)

Sadler, J. C., 1976a: Tropical cyclone initiation by the tropical upper tropospheric trough. Tech. Paper No. 2-76, Ibid.

Sadler, J. C., 1976b: A role of the tropical upper tropospheric trough in early season typhoon development. Mon. Wea. Rev., 104, 1266-1278.

Silva Dias, P. L. and W. H. Schubert, 1979: The dynamics of equatorial mass-flow adjustment. Dept. of Atmos. Sci. Paper No. 312, Colo. State Univ., Ft. Collins, CO, 203 pp.

Wachtmann, R. F., 1968: Role of angular momentum transport in tropical storm dissipation over tropical oceans. Colorado State University, Ft. Collins, Atmospheric Science Research Paper, 46 pp.

Yanai, M., 1961: A detailed analysis of typhoon formation. J. Meteor. Soc. Japan, 39, 187-214.

Yanai, M., 1968: Evolution of a tropical disturbance in the Caribbean Sea region. J. Meteor. Soc. Japan, Series II, 46, 86-108.

Zehr, R., 1976: Tropical disturbance intensification. Dept. of Atmos. Sci. Paper No. 259, Colo. State Univ., Ft. Collins, CO, 91 pp.

COMMANDER IN CHIEF
U.S. ATLANTIC FLEET
NORFOLK, VA 23511

COMMANDER IN CHIEF
U.S. ATLANTIC FLEET
(N009/04E)
ATTN: NSAP SCIENCE ADVISOR
NORFOLK, VA 23511

COMMANDER IN CHIEF
U.S. PACIFIC FLEET
PEARL HARBOR, HI 96860

COMMANDER
THIRD FLEET
PEARL HARBOR, HI 96860

COMMANDER
SEVENTH FLEET (N30W,
ATTN: FLEET METEOROLOGIST
FPO SAN FRANCISCO 96601

COMTHIRDFLT
ATTN: NSAP SCIENCE ADVISOR
CODE N702/01T
PEARL HARBOR, HI 96860

COMSEVENTHFLT
ATTN: NSAP SCIENCE ADVISOR
BOX 167
FPO SEATTLE 98762

COMMANDER
AMPHIBIOUS GROUP 1
ATTN: METEOROLOGICAL OFFICER
FPO SAN FRANCISCO 96601

COMMANDING OFFICER
USS AMERICA (CV-66)
ATTN: MET. OFFICER
FPO NEW YORK 09531

COMMANDER
AMPHIBIOUS GROUP 2
ATTN: MET. OFFICER
FPO NEW YORK 09501

COMMANDING OFFICER
USS FORRESTAL (CV-59)
ATTN: MET. OFFICER
FPO MIAMI 34080

COMMANDING OFFICER
USS INDEPENDENCE (CV-62)
ATTN: MET. OFFICER
FPO NEW YORK 09537

COMMANDING OFFICER
USS J. F. KENNEDY (CV-67)
ATTN: MET. OFFICER
FPO NEW YORK 09538

COMMANDING OFFICER
USS NIMITZ (CVN-68)
ATTN: MET. OFFICER
FPO NEW YORK 09542

COMMANDING OFFICER
USS EISENHOWER (CVN-69)
ATTN: MET. OFFICER
FPO NEW YORK 09532

COMMANDING OFFICER
USS SARATOGA (CV-60)
ATTN: MET. OFFICER
FPO NEW YORK 09587

COMMANDING OFFICER
USS CONSTELLATION (CV-64)
ATTN: MET. OFFICER
FPO SAN FRANCISCO 96635

COMMANDING OFFICER
USS CORAL SEA (CV-43)
ATTN: MET. OFFICER
FPO SAN FRANCISCO 96632

COMMANDING OFFICER
USS ENTERPRISE (CVN-65)
ATTN: MET. OFFICER
FPO SAN FRANCISCO 96636

COMMANDING OFFICER
USS KITTY HAWK (CV-63)
ATTN: MET. OFFICER
FPO SAN FRANCISCO 96634

COMMANDING OFFICER
USS MIDWAY (CV-41)
ATTN: MET. OFFICER
FPO SAN FRANCISCO 96631

COMMANDING OFFICER
USS RANGER (CV-61)
ATTN: MET. OFFICER
FPO SAN FRANCISCO 96633

COMMANDING OFFICER
USS MOUNT WHITNEY (LCC-20)
ATTN: MET. OFFICER
FPO NEW YORK 09517

COMMANDING OFFICER
USS BLUE RIDGE (LCC-19)
ATTN: MET. OFFICER
FPO SAN FRANCISCO 96628

COMMANDING OFFICER
USS GUADALCANAL (LPH-7)
ATTN: MET. OFFICER
FPO NEW YORK 09562

COMMANDING OFFICER
USS GUAM (LPH-9)
ATTN: MET. OFFICER
FPO NEW YORK 09563

COMMANDING OFFICER
USS INCHON (LPH-12)
ATTN: MET. OFFICER
FPO NEW YORK 09529

COMMANDING OFFICER
USS IWO JIMA (LPH-2)
ATTN: MET. OFFICER
FPO NEW YORK 09561

COMMANDING OFFICER
USS NEW ORLEANS (LPH-11)
ATTN: MET. OFFICER
FPO SAN FRANCISCO 96627

COMMANDING OFFICER
USS OKINAWA (LPH-3)
ATTN: MET. OFFICER
FPO SAN FRANCISCO 96625

COMMANDING OFFICER
USS TRIPOLI (LPH-10)
ATTN: MET. OFFICER
FPO SAN FRANCISCO 96626

COMMANDING OFFICER
USS TARAWA (LHA-1)
ATTN: MET. OFFICER
FPO SAN FRANCISCO 96622

COMMANDING OFFICER
USS NASSAU (LHA-4)
ATTN: MET. OFFICER
FPO NEW YORK 09557

COMMANDING OFFICER
USS SAIPAN (LHA-2)
ATTN: MET OFFICER
FPO NEW YORK 09549

COMMANDING OFFICER
USS BELLEAU WOOD (LHA-3)
ATTN: MET. OFFICER
FPO SAN FRANCISCO 96623

COMMANDING OFFICER
USS PUGET SOUND (AD-38)
ATTN: MET. OFFICER
FPO NEW YORK 09544

COMMANDING OFFICER
USS LASALLE (AGF-3)
ATTN: MET. OFFICER
FPO NEW YORK 09577

COMMANDING OFFICER
USS LEXINGTON (AVT-16)
FPO MIAMI 34088

COMMANDING OFFICER
USS POINT LOMA (AGDS-2)
ATTN: MET. OFFICER
FPO SAN FRANCISCO 96677

COMMANDER IN CHIEF PACIFIC
BOX 13
STAFF CINCPAC J37
CAMP SMITH, HI 96861

SPECIAL ASST. TO THE ASST.
SECNAV (R&D)
ROOM 4E741
THE PENTAGON
WASHINGTON, DC 20360

CHIEF OF NAVAL RESEARCH
LIBRARY SERVICES, CODE 734
RM 633, BALLSTON TOWER #1
800 QUINCY STREET
ARLINGTON, VA 22217

OFFICE OF NAVAL RESEARCH
CODE 465
ARLINGTON, VA 22217

CHIEF OF NAVAL OPERATIONS
OP-952
NAVY DEPT.
WASHINGTON, DC 20350

CHIEF OF NAVAL OPERATIONS
OP-986
NAVY DEPT.
WASHINGTON, DC 20350

DEPUTY DIRECTOR FOR OPERATIONS
(ENVIRONMENTAL SERVICES)
OJCS, RM 1B679
THE PENTAGON
WASHINGTON, DC 20301

NAVAL DEPUTY TO THE ADMIN.
NOAA, RM 200, PAGE BLDG. #1
3300 WHITEHAVEN ST. NW
WASHINGTON, DC 20235

OFFICER IN CHARGE
NAVOCEANCOMDET, BOX 81
U.S. NAVAL AIR STATION
FPO SAN FRANCISCO 96637

OFFICER IN CHARGE
NAVOCEANCOMDET
U.S. NAVAL AIR FACILITY
FPO SEATTLE 98767

OFFICER IN CHARGE
NAVOCEANCOMDET
NAVAL AIR STATION
BARBERS PT., HI 96862

OFFICER IN CHARGE
NAVOCEANCOMDET
U.S. NAVAL AIR STATION
FPO NEW YORK 09560

OFFICER IN CHARGE
NAVOCEANCOMDET
NAVAL AIR STATION
CECIL FIELD, FL 32215

OFFICER IN CHARGE
NAVOCEANCOMDET
NAVAL STATION
CHARLESTON, SC 29408

OFFICER IN CHARGE
NAVOCEANCOMDET
NAVAL AIR STATION
CORPUS CHRISTI, TX 78419

OFFICER IN CHARGE
NAVOCEANCOMDET, BOX 63
U.S. NAVAL AIR STATION
FPO SAN FRANCISCO 96654

OFFICER IN CHARGE
US NAVOCEANCOMDET
BOX 16
FPO NEW YORK 09593

OFFICER IN CHARGE
NAVOCEANCOMDET
BOX 9048
NAVAL AIR STATION
KEY WEST, FL 33040

CPOIC
NAVOCEANCOMDET
NAVAL AIR STATION
KINGSVILLE, TX 78363

CPOIC
NAVOCEANCOMDET
NAVAL AIR STATION
MAYPORT, FL 32228

OFFICER IN CHARGE
NAVOCEANCOMDET
NAS, WHITING FIELD
MILTON, FL 32570

OFFICER IN CHARGE
NAVOCEANCOMDET
NAVAL AIR STATION
MERIDIAN, MS 39301

OFFICER IN CHARGE
US NAVOCEANCOMDET
APO SAN FRANCISCO 96519

OFFICER IN CHARGE
NAVOCEANCOMDET
AIR FORCE GLOBAL WEATHER CENTRAL
OFFUTT AFB, NE 68113

CPOIC
NAVOCEANCOMDET
NAVAL AIR STATION
NEW ORLEANS, LA 70116

OFFICER IN CHARGE
NAVOCEANCOMDET
NAVAL AIR STATION
PATUXENT RIVER, MD 2670

OFFICER IN CHARGE
NAVOCEANCOMDET
U.S. NAVAL STATION
FPO MIAMI 34051

OFFICER IN CHARGE
NAVOCEANCOMDET
NAS, OCEANA
VIRGINIA BEACH, VA 23460

OFFICER IN CHARGE
US NAVOCEANCOMDET
FPO SAN FRANCISCO 96685

OFFICER IN CHARGE
US NAVOCEANCOMDET
FLEET ACTIVITIES
FPO SEATTLE 98770

OFFICER IN CHARGE
NAVOCEANCOMDET
NAVAL AIR STATION
PENSACOLA, FL 32508

OFFICER IN CHARGE
NAVOCEANCOMDET
MONTEREY, CA 93941

COMMANDING OFFICER
NAVAL RESEARCH LAB
ATTN: LIBRARY, CODE 2620
WASHINGTON, DC 20390

COMMANDING OFFICER
OFFICE OF NAVAL RESEARCH
EASTERN/CENTRAL REGIONAL OFFICE
BLDG 114 SECT. D
666 SUMMER ST.
BOSTON, MA 02210

COMMANDING OFFICER
OFFICE OF NAVAL RESEARCH
1030 E. GREEN STREET
PASADENA, CA 91101

OFFICE OF NAVAL RESEARCH
SCRIPPS INSTITUTION OF OCEANO.
LA JOLLA, CA 92037

COMMANDING OFFICER
NORDA, CODE 101
NSTL STATION
BAY ST. LOUIS, MS 39529

COMMANDER
NAVAL OCEANOGRAPHY COMMAND
NSTL STATION
BAY ST. LOUIS, MS 39529

COMMANDER
NAVAL OCEANOGRAPHY COMMAND
ATTN: J. OWNBEY, CODE N542
NSTL STATION
BAY ST. LOUIS, MS 39522

COMMANDING OFFICER
NAVOCEANO, LIBRARY
NSTL STATION
BAY ST. LOUIS, MS 39522

COMMANDING OFFICER
FLENUMOCEANCEN
MONTEREY, CA 93940

COMMANDING OFFICER
NAVWESTOCEANCEN
BOX 113
PEARL HARBOR, HI 96860

COMMANDING OFFICER
NAVEASTOCEANCEN
MCADIE BLDG. (U-117)
NAVAL AIR STATION
NORFOLK, VA 23511

COMMANDING OFFICER
US NAVOCEANCOMCEN
BOX 12
COMNAVMARIANAS
FPO SAN FRANCISCO 96630

COMMANDING OFFICER
NAVOCEANCOMFAC
NAS, P.O. BOX 85
JACKSONVILLE, FL 32212

COMMANDING OFFICER
NAVOCEANCOMFAC
NAS, NORTH ISLAND
SAN DIEGO, CA 92135

COMMANDING OFFICER
US NAVOCEANCOMFAC
FPO SEATTLE 98762

SUPERINTENDENT
LIBRARY ACQUISITIONS
U.S. NAVAL ACADEMY
ANNAPOLIS, MD 21402

CHAIRMAN
OCEANOGRAPHY DEPT.
U.S. NAVAL ACADEMY
ANNAPOLIS, MD 21402

PRESIDENT
NAVAL WAR COLLEGE
ATTN: CDR M. E. GIBBS
NEWPORT, RI 02840

U.S. NAVAL OBSERVATORY
ATTN: DR. D. W. JAMES
OPNAV 952D1
34TH & MASSACHUSETTS AVE. NW
WASHINGTON, DC 20390

COMMANDER
NAVAIRSYSCOM
ATTN: LIBRARY, AIR-0004
WASHINGTON, DC 20361

COMMANDER
NAVAIRSYSCOM, AIR-370
WASHINGTON, DC 20361

COMMANDER
NAVAIRSYSCOM, AIR-553
MET. SYSTEMS DIVISION
WASHINGTON, DC 20360

DIRECTOR
NAVY SCIENCE ASST. PROGRAM
NAVSURFWEACEN, WHITE OAKS
SILVER SPRING, MD 20910

COMMANDER
PACMISTESTCEN
CODE 3250
PT. MUGU, CA 93042

CHIEF OF NAVAL EDUCATION & TRNG
NAVAL AIR STATION
PENSACOLA, FL 32508

NAVAL POSTGRADUATE SCHOOL
DEPT. OF METEOROLOGY
MONTEREY, CA 93940

NAVAL POSTGRADUATE SCHOOL
DEPT. OF OCEANOGRAPHY
MONTEREY, CA 93940

NAVAL POSTGRADUATE SCHOOL
LIBRARY
MONTEREY, CA 93940

COMMANDING OFFICER
U.S. MARINE CORPS AIR STATION
ATTN: WEATHER SERVICE OFFICE
(HELICOPTER)
FPO SEATTLE 98772

COMMANDING OFFICER
U.S. MARINE CORPS AIR STATION
ATTN: WEATHER SERVICE OFFICE
FPO SEATTLE 98764

COMMANDING OFFICER
MCAS (HELICOPTER)
HQRON OPERATIONS DEPT.
ATTN: WEATHER SERVICE DIV.
JACKSONVILLE, NC 28545

COMMANDER
AWS/DN
SCOTT AFB, IL 62225

USAFETAC/TS
SCOTT AFB, IL 62225

3350TH TECHNICAL TRNG GRP
TTGU-W/STOP 623
CHANUTE AFB, IL 61868

AFGL/LY
HANSCOM AFB, MA 01731

5WW/DN
LANGLEY AFB, VA 23665

OFFICER IN CHARGE
SERVICE SCHOOL COMMAND
DET. CHANUTE/STOP 62
CHANUTE AFB, IL 61868

1ST WEATHER WING (DON)
HICKAM AFB, HI 96853

DET 4 HQ AWS/CC
APO SAN FRANCISCO 96334

DET 5 1WW/CC
APO SAN FRANCISCO 96274

DET 8, 30 WS
APO SAN FRANCISCO 96239

DET 17, 30 WS
APO SAN FRANCISCO 96328

DET 18, 30 WS
APO SAN FRANCISCO 96301

AFOSR/NC
BOLLING AFB
WASHINGTON, DC 20312

COMMANDING OFFICER
U.S. ARMY RESEARCH OFFICE
ATTN: GEOPHYSICS DIV.
P.O. BOX 12211
RESEARCH TRIANGLE PARK, NC
27709

DIRECTOR
DEFENSE TECH. INFO. CENTER
CAMERON STATION
ALEXANDRIA, VA 22314

DIRECTOR
OFFICE OF ENV. & LIFE SCIENCES
OFFICE OF UNDERSECRETARY OF
DEFENSE FOR RSCH & ENG (E&LS)
RM 3D129, THE PENTAGON
WASHINGTON, DC 20301

DIRECTOR
TECHNICAL INFORMATION
DEFENSE ADVANCED RESEARCH
PROJECTS AGENCY

NATIONAL METEOROLOGICAL CENTER
DEVELOPMENT DIV., NWS/NOAA
WORLD WEATHER BLDG. W32, RM 204
WASHINGTON DC 20233

DIRECTOR
NATIONAL EARTH SAT. SERV./SEL
FB-4, S321B
SUITLAND, MD 20233

ACQUISITIONS SECTION IRDB-D823
LIBRARY & INFO SERV DIV NOAA
6009 EXECUTIVE BLVD
ROCKVILLE, MD 20852

FEDERAL COORDINATOR FOR
METEORO. SERVICES &
SUPPORTING RESEARCH
6010 EXECUTIVE BLVD.
ROCKVILLE, MD 20852

DIRECTOR
OFFICE OF PROGRAMS RX3
NOAA RESEARCH LAB
BOULDER, CO 80302

NATIONAL OCEANIC & ATMOS.
ADMINISTRATION
OCEANOGRAPHIC SERVICES DIV.
6010 EXECUTIVE BLVD.
ROCKVILLE, MD 20852

DIRECTOR
NATIONAL HURRICANE CENTER, NOAA
UNIV. OF MIAMI BRANCH
CORAL GABLES, FL 33124

CHIEF, SCIENTIFIC SERVICES
NWS, SOUTHERN REGION
NOAA, ROOM 10E09
819 TAYLOR STREET
FT. WORTH, TX 76102

CHIEF, SCIENTIFIC SERVICES
NWS, WESTERN REGION, NOAA
P.O. BOX 11188, FEDERAL BLDG.
SALT LAKE CITY, UT 84111

CHIEF, SCIENTIFIC SERVICES
NWS, PACIFIC REGION
P.O. BOX 50027
HONOLULU, HI 96850

DIRECTOR
ATLANTIC OCEANOGRAPHIC &
METEOR. LABS
15 RICKENBACKER CAUSEWAY
VIRGINIA KEY
MIAMI, FL 33149

DIRECTOR
INTERNATIONAL AFFAIRS OFFICE
ATTN: NELS JOHNSON, NOAA
6010 EXECUTIVE BLVD.
ROCKVILLE, MD 20852

METEOROLOGIST IN CHARGE
WEATHER SERVICE FORECAST
OFFICE, NOAA
660 PRICE AVE.
REDWOOD CITY, CA 94063

DIRECTOR
CENTRAL PACIFIC HURRICANE CENTER
NWS, NOAA
HONOLULU, HI 96819

DIRECTOR
NATIONAL SCIENCE FOUNDATION
DIV. OF ATMOS. SCIENCES, RM 644
1800 G. STREET, NW
WASHINGTON, DC 20550

LABORATORY FOR ATMOS. SCIENCES
NASA GODDARD SPACE FLIGHT CENTER
GREENBELT, MD 20771

EXECUTIVE SECRETARY
CAO SUBCOMMITTEE ON ATMOS. SCIENCES
NATIONAL SCIENCE FOUNDATION, RM 510
1800 G. STREET NW
WASHINGTON, DC 20550

NATIONAL CENTER FOR ATMOS. RSCH.
LIBRARY ACQUISITIONS
P.O. BOX 1470
BOULDER, CO 80302

DEPT. OF ATMOSPHERIC SCIENCES
ATTN: LIBRARIAN
COLORADO STATE UNIVERSITY
FORT COLLINS, CO 80521

CHAIRMAN
PENNSYLVANIA STATE UNIV.
503 DEIKE BLDG.
UNIVERSITY PARK, PA 16802

CHAIRMAN
MASSACHUSETTS INSTITUTE OF TECH.
DEPT. OF METEOROLOGY
CAMBRIDGE, MA 02139

ATMOSPHERIC SCIENCES DEPT.
UNIVERSITY OF CHICAGO
1100 E. 57TH STREET
CHICAGO, IL 60637

UNIVERSITY OF WASHINGTON
ATMOSPHERIC SCIENCES DEPT.
SEATTLE, WA 98195

FLORIDA STATE UNIVERSITY
ENVIRONMENTAL SCIENCES DEPT.
TALLAHASSEE, FL 32306

UNIVERSITY OF HAWAII
DEPT. OF METEOROLOGY
2525 CORREA ROAD
HONOLULU, HI 96822

CHAIRMAN
UNIV. OF WISCONSIN
DEPT. OF METEOROLOGY
1225 WEST DAYTON STREET
MADISON, WI 53706

CHAIRMAN
UNIVERSITY OF ARIZONA
INSTITUTE OF ATMOS. PHYSICS
TUSCON, AZ 85721

TEXAS A & M UNIVERSITY
DEPT. OF METEOROLOGY
COLLEGE STATION, TX 77843

CHAIRMAN
DEPT. OF METEOROLOGY
UNIVERSITY OF OKLAHOMA
NORMAN, OK 73069

CHAIRMAN
RUTGERS UNIVERSITY
DEPT. OF METEOROLOGY & PHYSICAL
OCEANO.
P.O. BOX 231
NEW BRUNSWICK, NJ 08903

DIRECTOR OF RESEARCH
INSTITUTE FOR STORM RESEARCH
UNIV. OF ST. THOMAS
3812 MONTROSE BLVD.
HOUSTON, TX 77006

CHAIRMAN
DEPT. OF METEOROLOGY
CALIFORNIA STATE UNIV. SAN JOSE
SAN JOSE, CA 95192

CHAIRMAN
DEPT. OF METEOROLOGY & PHYSICS
UNIV. OF FLORIDA
215 PHYSICS BLDG.
GAINESVILLE, FL 32601

SCRIPPS INSTITUTION OF OCEANO.
LIBRARY, DOCUMENTS/REPORTS SEC.
LA JOLLA, CA 92037

STATE UNIV. OF NEW YORK, ALBANY
ATMOS. SCIENCES DEPT., LIBRARY
1400 WASHINGTON AVE.
ALBANY, NY 12222

UNIVERSITY OF MIAMI
R.S.M.A.S. LIBRARY
4600 RICKENBACKER CAUSEWAY
VIRGINIA KEY
MIAMI, FL 33149

CHAIRMAN
DEPT. OF ATMOSPHERIC SCIENCES
UNIVERSITY OF VIRGINIA
CLARK HALL
CHARLOTTESVILLE, VA 22903

DEPT. OF ATMOS. SCIENCES LIBRARY
COLORADO STATE UNIVERSITY
FOOTHILLS CAMPUS
FT. COLLINS, CO 80523

THE EXECUTIVE DIRECTOR
AMERICAN MET. SOCIETY
45 BEACON STREET
BOSTON, MA 02108

AMERICAN MET. SOCIETY
METEORO. & GEOASTROPHYSICAL
ABSTRACTS
P.O. BOX 1736
WASHINGTON, DC 20013

DIRECTOR, JTWC
BOX 17
FPO SAN FRANCISCO 96630

WORLD METEOROLOGICAL ORG.
ATS DIV. (ATTN: N. SUZUKI)
CH-1211, GENEVA 20,
SWITZERLAND

LIBRARY, CSIRO DIV.
ATMOSPHERIC PHYSICS
STATION STREET
ASPENDALE, 3195
VICTORIA, AUSTRALIA

LIBRARIAN
METEOROLOGY DEPT.
UNIV. OF MELBOURNE
PARKVILLE, VICTORIA 3052
AUSTRALIA

BUREAU OF METEOROLOGY
ATTN: LIBRARY
BOX 1289K, GPO
MELBOURNE, VIC. 3001
AUSTRALIA

JAMES COOK UNIV. OF NORTH
QUEENSLAND
DEPT. OF GEOGRAPHY
TOWNSVILLE Q4811
AUSTRALIA

DIRECTOR OF NAVAL OCEANOGRAPHY &
METEOROLOGY
MINISTRY OF DEFENCE
OLD WAR OFFICE BLDG.
LONDON, S.W.1. ENGLAND

METEOROLOGICAL OFFICE LIBRARY
LONDON ROAD
BRACKNELL, BERKSHIRE
RG 12 2SZ
ENGLAND

DEPT. OF METEOROLOGY
UNIV. OF READING
2 EARLYGATE, WHITEKNIGHTS
READING RG6 2AU
ENGLAND

DIRECTOR, ROYAL OBSERVATORY
NATHAN ROAD, KOWLOON
HONG KONG, B.C.C.

THE DIRECTOR
INDIAN INSTITURE OF TROP. METEO.
RAMDURG HOUSE
PUNE 411-005
INDIA

DIRECTOR GENERAL
METEOROLOGICAL DEPT.
GOVERNMENT OF INDIA
NEW DELHI, 3 INDIA

LIBRARY
METEOROLOGICAL RESEARCH INSTITUTE
KOENJI-KITA, SUGINAMI
TOKYO 166, JAPAN

TYPHOON RESEARCH LAB
ATTN: LIBRARIAN
METEORO. RESEARCH INSTITUTE
1-1 NAGAMINE, YATABE-MACHI,
TSUKUBA-GUN.
IBARAKI-KEN, 305, JAPAN

MARITIME METEOROLOGY DIV.
JAPAN METEOROLOGICAL AGENCY
OTE-MACHI 1-3-4 CHIYODA-KU
TOKYO, JAPAN

JAPAN METEOROLOGICAL AGENCY
3-4, OTEMACHI 1-CHOME.
CHIYODA-KU
TOKYO 100, JAPAN

METEOROLOGICAL SATELLITE CENTER
235 NAKAKIYOT, 3-CHOME
KIYOSE, TOKYO, 180-04
JAPAN

CHAIRMAN
DEPT. OF EARTH SCIENCE
KONG JU NATIONAL TEACHERS
COLLEGE
KONG JU, KOREA

DIRECTOR GENERAL
MALAYSIAN METEOROLOGICAL SERVICE
JALAN SULTAN
PETALING JAYA
SELANGOR, WEST MALAYSIA

LIBRARIAN
NEW ZEALAND METEOROLOGICAL SERV.
P.O. BOX 722
WELLINGTON, NEW ZEALAND

COORDINATOR
ESCAP/WMO TYPHOON COMMITTEE
SECRETARIAT
C/O UNDP
MANILA, PHILIPPINES

DEPT. OF METEOROLOGY
COLLEGE OF ARTS & SCIENCES
UNIV. OF THE PHILIPPINES
DILMAN, QUEZON CITY 3004
PHILIPPINES

TECHNICAL LIBRARY
WEATHER BUREAU
DEPT. OF NATIONAL DEFENSE
LUNGSOD NG QUEZON
QUEZON, PHILIPPINES

NATIONAL WEATHER SERVICE
(PAGASA)
1424 QUEZON AVE.
QUEZON CITY, METRO MANILA
PHILIPPINES

DIRECTOR
TYPHOON MODERATION RSCH. &
DEVELOPMENT OFFICE (PAGASA)
MINISTRY OF NATIONAL DEFENSE
1424 QUEZON AVE.
QUEZON CITY, PHILIPPINES

COORDINATOR, NATIONAL ATMOSPHERIC
RESEARCH PROGRAM
INSTITUTE OF PHYSICS
ACADEMIA SINICA
TAIPEI, TAIWAN

CENTRAL WX BUREAU
64, KUNG YUAN RD.
TAIPEI, TAIWAN 100

DEPT. OF ATMOSPHERIC SCIENCE
NATIONAL TAIWAN UNIV.
TAIPEI, TAIWAN 107

DEPUTY DIRECTOR-GENERAL
THAILAND METEOROLOGICAL DEPT.
MINISTRY OF COMMUNICATIONS
BANGKOK, THAILAND